PREDICTION OF SUPERSONIC LAMINAR FLOW SEPARATION BY THE METHOD OF INTEGRAL RELATIONS WITH FREE INTERACTION

GARY D. KUHN

FREDERICK K. GOODWIN

JACK N. NIELSEN

FOREWORD

This report,[1] "Prediction of Supersonic Laminar Flow Separation by the Method of Integral Relations with Free Interaction," concerns the development of a predictive method for calculating separated laminar boundary layers on flat-plate-wedge and cylinder-flare configurations in supersonic flow. The work was carried out by Nielsen Engineering & Research, Inc., 850 Maude Avenue, Mountain View, California 94040, under Contract No. F33615-68-C-1499. The contract was initiated under Project 8219, Task 821902 of the Air Force Flight Dynamics Laboratory and was funded in part by Laboratory Director's Funds. The technical monitor of this contract was Mr. Eugene L. Fleeman, AFFDL, FDCC. The research documented in this report was started on May 20, 1968 and was effectively concluded with the submission of this report.

The authors wish to thank Mr. Fleeman for his assistance in solving some of the technical and administrative problems which arose during the course of the investigation and for his assistance in supervising the machine computations at AFFDL.

Requests for copies of the computer program and operating manual should be directed to the Air Force Flight Dynamics Laboratory (FDCC).

This manuscript was released by the authors in August 1969 as an AFFDL technical report.

This technical report has been reviewed and is approved.

C. B. Westbrook, Chief
Control Criteria Branch
Flight Control Division

[1]This is Nielsen Engineering & Research, Inc. Report TR 17.

ABSTRACT

This report describes the development of a predictive method for calculating separated laminar boundary layers on flat-plate-wedge and cylinder-flare configurations in supersonic flow and the application of the method to predicting the effects of Mach number, Reynolds number, and temperature ratio on the properties of the boundary layer. The purpose of this report is to extend previous analytical work employing the method of integral relations to the region downstream of reattachment and to describe an iterative technique developed to produce a unique solution. The theory is shown to produce good comparisons with pressure data on flat-plate-wedge configurations for both adiabatic and cold walls. Accounting for non-Blasius initial velocity profiles produced by favorable pressure gradients upstream of the beginning of interaction was shown to decrease the predicted extent of separation. For axisymmetric configurations the length of an equivalent cylinder must be calculated by an auxiliary method. Good to fair comparisons with experimental pressure distributions were produced by adjusting the equivalent cylinder length. Fair comparison was produced between the theory and experimental heat-transfer rate data on an ogive-cylinder-flare configuration. The theory is shown to predict an incipient separation wedge angle which agrees reasonably well with experimental results.

TABLE OF CONTENTS

ILLUSTRATIONS

ILLUSTRATIONS (CONTINUED)

ILLUSTRATIONS (CONCLUDED)

LIST OF SYMBOLS

a	local speed of sound
C	constant in viscous interaction parameter $\left(\frac{\mu}{\mu_\infty}\right)\Big/\left(\frac{T}{T_\infty}\right)$
c_o, c_1, c_2, c_3	coefficients specifying the velocity profile of the outer flow (eq. (48), ref. 4)
c_f	skin friction coefficient
E_o	coefficient in the temperature profile of the outer flow (eq. (49) and (52), ref. 4)
ℓ	reference length for a flat-plate-wedge configuration, taken equal to L_c
L	reference length for a cylinder-flare configuration, taken equal to L_{c_a}
L_b	overall length of configuration
L_c	distance from leading edge of the body to beginning of the compression surface, figs. 8 and 9
L_f	distance from leading edge of the body to the beginning of the flare, fig. 9
L_R	distance from end of flat plate to reattachment point, fig. 1
L_{sep}	distance from separation point to end of flat plate, fig. 1
L_t	total length of separated region, $L_{sep} + L_R$
L_w	distance from the leading edge of the flat plate to the beginning of the wedge, fig. 8
m	$\left(\frac{\gamma - 1}{2}\right) M^2$
M	local Mach number
p	local static pressure
p_t	local total pressure
$r(x_a)$	body radius in equivalent axisymmetric plane

r_o	cylinder radius
R	radius of fairing between flat plate and wedge or cylinder and flare
R_g	gas constant
R_o	Reynolds number, $u_o \ell/\nu_o = u_o L_c/\nu_o$
R_{∞_x}	Reynolds number, $u_\infty x/\nu_\infty$
R_{x_o}	Reynolds number, $u_o x_o/\nu_o$
R_∞/ft	free-stream unit Reynolds number, u_∞/ν_∞
S	temperature parameter, $S = (T_t/T_{t_o}) - 1$
T	local static temperature
T_t	local total temperature
T_w	wall temperature
u,v	velocities in physical plane
$\bar{u},\bar{v},\bar{w}$	velocities in Dorodnitsyn ξ,η plane given by equations (29) and (30) of ref. 4
U,V	velocities in Stewartson X,Y plane given by equations (16) and (17) of ref. 4
w(x)	y-coordinate of two-dimensional body
x,y	coordinate system in two-dimensional plane
x_a,y_a	coordinate system in equivalent axisymmetric plane
x',y'	coordinate system in axisymmetric plane
X,Y	coordinate system in Stewartson plane given by equation (15) of ref. 4
α	value of $\partial\bar{u}/\partial\eta$ at any η
$\bar{\alpha}_w$	value of $\partial\bar{u}/\partial\eta$ at the wall computed by equation (142) of ref. 4 when the inner velocity profile is a quadratic
γ	ratio of specific heats of the gas

δ^*	boundary-layer displacement thickness
δ^{**}	boundary-layer momentum thickness
θ_f	flare angle, see fig. 9
θ_w	wedge angle, see fig. 8
μ	absolute viscosity
ν	kinematic viscosity
ξ, η	coordinate system in Dorodnitsyn plane given by equation (28), ref. 4
ρ	mass density
ϕ	slope of streamline outside of boundary layer
$\overline{\chi}$	hypersonic viscous interaction parameter $M_\infty^3\sqrt{C/R_{\infty_x}}$

Subscripts

a	conditions in the equivalent axisymmetric plane
c	conditions at the beginning of the compression surface
F	conditions at downstream end of calculation
i	initial conditions at the beginning of interaction
P	conditions in the plateau region
R	conditions at the reattachment point
s	quantities evaluated at the $\overline{u} = 0$ line where $\eta = \eta_s$ in the separated region and at the wall in the attached flow region
S	conditions at the separation point
ST	quantities evaluated in the Stewartson plane
w	quantities evaluated at the wall
o	quantities evaluated at the outer edge of the boundary layer at the beginning of interaction
1	quantities evaluated at the outer edge of the boundary layer at any point downstream of the beginning of interaction

∞	free-stream conditions

Special Notation

$\dot{(\ )}$	differentiation with respect to ξ
$(\ )'$	quantities evaluated in the axisymmetric plane

PREDICTION OF SUPERSONIC LAMINAR FLOW SEPARATION BY THE METHOD OF INTEGRAL RELATIONS WITH FREE INTERACTION

1. INTRODUCTION

In the design of high-speed aircraft and missiles, it is necessary that aerodynamic forces and moments and heat loads be predictable when control surfaces are deflected. Methods of doing this are available when boundary-layer separation does not occur. However, when the control surface deflections are sufficient to cause boundary-layer separation, the prediction of these quantities is more difficult without prior knowledge of the separated flow, such as information concerning the beginning of the separation interaction, the separation point, or the pressure distribution. It has been demonstrated in references 1 through 4 that if the position of the separation point or the beginning of interaction is known, the Dorodnitsyn method of integral relations, reference 5, can be used to calculate quite accurately, for laminar boundary layers, the separated flow pressure distribution from the beginning of interaction to the reattachment point under the assumption of free interaction between the boundary layer and the outer inviscid flow. The methods of references 1 through 4, however, do not allow a separated flow to be predicted uniquely. In order to be able to extend the methods of these references to a prediction technique, it is necessary that the calculation be extended downstream of the reattachment point and that a downstream boundary condition be developed such that a unique solution can be obtained for a specified set of flow conditions at the edge of the boundary layer at the beginning of interaction.

Under a contract with NASA, Ames Research Center, the results of which are partially reported in reference 6, the method of integral relations with free-interaction was applied to the calculation of separated flows caused by the interaction of a shock wave with a laminar boundary layer. In that investigation it was found that by extending the calculation downstream of reattachment and imposing a suitable downstream boundary condition, a unique solution could be found for a specified beginning of interaction, flow conditions at the edge of the boundary layer at this point, and the shock impingement point.

The purpose of the present investigation is to extend the work of references 1 through 4 to the calculation of the boundary layer

downstream of reattachment and to calculate a unique solution for a given configuration and set of flow conditions by imposing a downstream boundary condition. The configurations to be treated are a flat plate followed by a wedge and a cylinder followed by a flare. The method can then be used as a prediction technique in that no prior knowledge of the separated flow pattern is required.

This report will first describe the separated flows to be treated and then present the analysis. The analysis will be presented principally by reference to the work of reference 4 since the analysis developed in that reference is applicable almost unchanged to the present work. The equations used downstream of the reattachment point are the same as the preseparation equations of reference 4 except for the free-interaction equation as will be shown.

The next section of this report will discuss the investigation of the downstream boundary condition. This investigation was performed by computer, and results are presented which describe the criterion selected in order to determine the unique solution.

The computer program is described next. Comparisons are then presented showing the accuracy of the prediction method when compared with experimental data. At high Mach numbers on flat plates and at almost all Mach numbers on axisymmetric configurations, favorable pressure gradients exist upstream of the beginning of interaction. The present calculations have been largely carried out on the assumption that the boundary layer velocity profile at the beginning of interaction is of the Blasius type. Since a boundary layer subjected to a favorable pressure gradient would not have a Blasius profile at the beginning of interaction, an investigation was carried out to study the effects of a non-Blasius initial profile on the unique solution.

The last section of the report presents the results of a set of parametric runs which have been made with the present computer program for the flat-plate-wedge configuration. Mach number, Reynolds number based on flat-plate length, the ratio of wall temperature to free-stream stagnation temperature, and wedge angle have been varied parametrically.

2. DESCRIPTION OF MATHEMATICAL PROBLEM

2.1 Description of Two-Dimensional and Axisymmetric Problems

The problems to be treated in the present investigation are those of predicting two-dimensional and axisymmetric laminar boundary-layer separation on surfaces of arbitrary but uniform temperature. The type of separation to be treated is that of the free-interaction type. By free interaction we mean that the pressure distribution on a body immersed in a viscous flow is the same as that on an equivalent body in an inviscid flow where the shape of the original body has been augmented by the displacement thickness of the boundary layer.

The two flow models to be treated are shown in figures 1 and 2. In both cases, a compression surface induces a free interaction between the boundary layer and the outer inviscid flow. The interaction begins at the beginning of interaction, x_o in figure 1 and x_{a_o} in figure 2. At this point, the Mach number, unit Reynolds number, and total temperature at the edge of the boundary layer are assumed known. The boundary-layer velocity profile is assumed to be of the zero pressure gradient Blasius type and the temperature profile is assumed to be given by the Crocco relationship which is valid for zero pressure gradient. The surfaces are assumed to be at arbitrary but uniform wall temperature. The interaction causes the boundary layer to thicken and separate at x_S or x_{a_S} depending on the configuration. At some point downstream, x_c or x_{a_c}, a compression surface begins and the boundary layer reattaches to it at x_R or x_{a_R}. Between the separation and reattachment points, the boundary layer is divided into two regions by the $u = 0$ or $u_a = 0$ line. The flow below this line, the reversed flow as shown by the velocity profiles sketched in figures 1 and 2, is termed the inner flow and that above this line is called the outer flow. Downstream of the reattachment point, the boundary layer is again an attached boundary layer.

The two problems just described are the same as those treated in references 1 through 4 except that, in those works, the region downstream of reattachment was not considered. The analyses and computer programs only covered the region from the beginning of interaction to the reattachment point. It was found there that, for a particular configuration, wall temperature, and set of flow conditions, separated flows could be calculated for a range of values of the beginning of

interaction. Thus, prior knowledge of the separated flow pattern was required in order to select the correct beginning of interaction. In this context, the method was a data matching technique.

Work performed for NASA, Ames Research Center, and partially reported in reference 6, showed that it was possible to calculate a unique separated flow in the case of an interaction between a laminar boundary layer and an oblique shock wave without prior knowledge of the separated flow. This was done with an iterative solution by imposing a suitable boundary condition downstream of the reattachment point. This boundary condition was that both the first and second derivatives of the pressure at the edge of the boundary layer with respect to axial distance go to zero simultaneously. This boundary condition was applied to the same problem by Reyhner and Flügge-Lotz, reference 7, using finite difference techniques.

This section of the present report will describe the extension of the analysis of reference 4 to the region downstream of reattachment in order that a suitable downstream boundary condition can be developed for the two problems being treated. In this way the method of reference 4 can be made a prediction method.

2.2 Assumptions

In the analysis made in reference 4, certain assumptions were made. The same assumptions apply to the present work since the analysis is the same. They are:

(1) The governing equations are those for a compressible laminar boundary layer.

(2) The Prandtl number is unity.

(3) The fluid behaves as an ideal gas with constant specific heats.

(4) The wall is at a uniform arbitrary temperature.

(5) The viscosity varies linearly with temperature.

(6) The flow at the outer edge of the boundary layer is isentropic and the pressure is given by the Prandtl-Meyer relationship.

(7) The pressure across the boundary layer is constant.

(8) In the axisymmetric case, the boundary layer thickness is small compared to the cylinder radius.

2.3 Ordinary Differential Equations

The derivations of the ordinary differential equations will not be repeated in this report since they are presented in detail in reference 4. The derivations are presented in sections 2 and 3 of that report for the two-dimensional and axisymmetric configurations, respectively. The only difference is in the equations used in the post-reattachment region. In this region the equations are the same as in the preseparation region except for the free-interaction equation. The change in this equation downstream of reattachment will be shown.

2.3.1 Preseparation equations

The equations which are solved in the preseparation region for the two-dimensional configuration are derived in section 2 of reference 4 with the ordinary differential equations being given by equations (59) through (62), equation (70), and equation (98). This set allows the axial variations of the four unknowns in the velocity profile, c_o, c_1, c_2, and c_3 in equation (48) of reference 4, the unknown in the temperature profile, E_o in equation (49) of that reference, and the velocity at the edge of the boundary layer, U_1/U_o, to be found. Note that the "second-order coupling" type of temperature profile developed in reference 4 is retained in the present work. The integration of these differential equations thus calculates the boundary layer from the beginning of interaction to the separation point for the two-dimensional configuration. For the axisymmetric configuration, equation (98) of reference 4 is replaced by equation (134) of that reference, the axisymmetric free-interaction equation. One change made in the present work which will be discussed later is a change in the definition of the reference length, ℓ in the two-dimensional case and L in the axisymmetric case. In the work of reference 4 these lengths were defined to be the distance from the leading edge of the flat plate or the hollow cylinder, respectively, to the beginning of interaction. In the present work they are defined to be the flat-plate length or hollow-cylinder length, x_c or x_{a_c} of figures 1 and 2. This change in the definition of the reference lengths does not change the differential equations but only the initial conditions of the variables. The initial conditions will be discussed later.

2.3.2 Separated region equations

In the separated region, the differential equations to be solved are also the same as those derived in reference 4. The profiles which are assumed in this region are given in reference 4 by equations (48) and (52) for the outer flow and equations (55) and (58) for the inner flow. These profiles contain nine unknown coefficients whose variations with axial distance must be determined. These coefficients are c_o, c_1, c_2, c_3, E_o, S_s, α_w, α_s, and η_s. For both configurations the differential equations are given by equations (74) through (77), equation (79), equations (85) and (86), equation (90), and equation (93) of reference 4.

In addition to these equations, a pressure boundary condition must be imposed such that the variation of velocity at the edge of the boundary layer, and thus the pressure, can be determined. As is discussed in Section 2.7 of reference 4, two different conditions are imposed in the separated region. Free interaction is imposed from the separation point to the beginning of the constant pressure plateau region, if one is developed, and also from the beginning of the compression surface to the reattachment point. The free-interaction equation is given by equation (103) of reference 4 for the two-dimensional configuration and equation (138) of that reference for the axisymmetric configuration. In the constant pressure plateau region, equation (94) of reference 4 is used for both configurations.

2.3.3 Post-reattachment region equations

In the post-reattachment region the equations which are solved are the same as those solved in the preseparation region with the exception of the free-interaction equation. For both the two-dimensional and axisymmetric cases the differences in this equation occur on the right-hand side. For the two-dimensional case the preseparation free-interaction equation is given by equation (98) of reference 4. In the post-reattachment region, the term

$$\frac{-\sqrt{R_o}}{1 + m_o} \frac{dw}{dx}$$

is added to the right-hand side. The preseparation free-interaction equation for the axisymmetric case is given by equation (134) of

reference 4. In the post-reattachment region the term

$$\frac{\sqrt{R_o}}{r(1 + m_o)} \frac{dr}{dx_a}\left(\frac{\delta^*}{r^2} - 1\right)$$

is added to the right-hand side with

$$\delta^* = \frac{(1 + m_o)}{\sqrt{R_o}} \left(\frac{1 + m_1}{1 + m_o}\right)^{\frac{s\gamma-1}{2(\gamma-1)}} \frac{U_o \ell}{U_1} \left[(\bar{H}_1 - E_o \bar{N}_o + \bar{f}_1) + \frac{m_1}{1 + m_1} \bar{f}_2\right]$$

The quantities appearing in this equation are defined in reference 4.

3. DETERMINATION OF DOWNSTREAM BOUNDARY CONDITION

The principal purpose of the present report is to extend the work of reference 4 to the region downstream of reattachment and to find a downstream boundary condition such that the work of that reference can be made a prediction method rather than a data matching method. In this way no prior knowledge of the separated flow would be required in order to compute a separated flow pattern for a particular configuration. To determine a suitable downstream boundary condition, the method of reference 4 has been extended to the calculation of the boundary layer downstream of reattachment and the results of computer runs have been compared with data. One possible condition is that the flow make a smooth transition to a constant pressure downstream of reattachment to the extent that both the first and second derivatives of the pressure with respect to distance be zero simultaneously. This is the condition imposed in the work of reference 6 for the shock-wave, boundary-layer interaction problem. Another possible condition is that the first derivative of pressure with respect to distance be zero when the pressure equals the inviscid value given by the local geometry.

For the solution to be unique, the solution which satisfies a particular downstream boundary condition must either yield a particular value of the wedge angle, θ_w,[1] if the beginning of interaction is specified,

[1]The discussion in this section applies equally to both the two-dimensional and axisymmetric configurations. The two-dimensional case is used for illustration.

or it must yield the beginning of interaction, x_o, if the wedge angle is specified. Typical solutions for the pressure distribution for different wedge angles, with the beginning of interaction fixed, on a flat-plate-wedge configuration are shown in figure 3. Similarly, in figure 4 are shown solutions for two values of the location of the beginning of interaction, with the wedge angle fixed. For given flow conditions at the beginning of interaction, the solutions fall into two classes. For a value of the wedge angle, θ_w, or the location of the beginning of interaction measured from the leading edge of the flat plate, x_o, which is too small, the boundary layer either does not reattach or the solutions, if continued, develop an inflection and would result in a second separation point downstream of reattachment. These conditions are unallowable since the boundary layer must reattach, and no mechanism is present to induce a second separation. For larger values of θ_w or x_o the pressure reaches a maximum and then decreases. Thus, there appears to be a unique solution for which the pressure reaches a final, constant value for a value of the wedge angle or the beginning of interaction between those shown in the figures.

The portions of the curves shown in figures 3 and 4 downstream of the pressure maximum or downstream of an inflection are represented by dotted curves because the numerical calculations were not actually carried out beyond those points. They are shown to indicate the behavior of the solution had the calculation been continued. The reasons for terminating the calculations at those points will be discussed subsequently.

The inviscid wedge pressures for the wedge angles used are also shown in figures 3 and 4. It is apparent that the condition that the first derivative of the pressure with distance be zero when the pressure reaches the inviscid value for a particular wedge angle could not be satisfied. Such a boundary condition would not account for the displacement effect of the boundary layer. The slope of the δ^* line at the beginning of interaction causes the effective turning angle of the flow to be less than the geometrical angle between the plate and the ramp. Thus, the inviscid pressure corresponding to the ramp angle would be expected to be higher than that for which the calculated pressure would make a smooth transition to a constant value. The experimental data to be presented in section 5 of this report tend to support this conclusion, since the inviscid pressure is usually higher than the experimental final pressure.

More detailed information on the behavior of the solutions for several wedge angles is provided by figure 5, where the pressure gradient, $d(p_1/p_o)/d(x/L_c)$, for a calculation like that of figure 3, is plotted as a function of x/L_c downstream of the reattachment point for several values of the wedge angle with a fixed location of the beginning of interaction. In the figure, the two classes of solutions mentioned above apparently are those for which either dp/dx becomes zero with d^2p/dx^2 negative or d^2p/dx^2 becomes zero with dp/dx positive. The solution which would satisfy the downstream condition $dp/dx = d^2p/dx^2 = 0$ appears to separate the two classes of solutions. The pressure distributions corresponding to the iterations shown in figure 5 are plotted in figure 6. The calculation in each case was terminated when a certain condition as discussed below was encountered. The curves shown in figure 6 are shown dashed after the particular condition for each curve was encountered in order to show the behavior had they been continued. For the cases where dp/dx became zero with d^2p/dx^2 negative, the pressure reaches a maximum and then decreases. For the cases where d^2p/dx^2 became zero for positive values of dp/dx, the pressure distribution has an inflection.

The computer runs discussed above indicated that certain behaviors of several parameters in the solution could be used to determine the correct value of the wedge angle or beginning of interaction to determine the unique solution. The conditions encountered in the calculations of figures 5 and 6 are listed in figure 6.

A value of θ_w or x_o which is too small results in a solution for which d^2p/dx^2 becomes zero for a positive value of dp/dx. This is always accompanied by a negative derivative, $\dot{c}_3$, of the velocity profile parameter, c_3. If the angle is too large or the beginning of interaction is too near the beginning of the wedge or flare, the pressure attains a maximum downstream of the reattachment point and begins to fall. In the computer program, this is indicated by the first derivative of the boundary-layer edge velocity, $\dot{U}_1$, becoming positive.

Another criterion for terminating an iteration was found by examining the behavior of the velocity gradient profile parameter c_3. The two classes of solutions mentioned above are characterized by two families of curves representing the variation of c_3 with x. This is illustrated by figure 7 where the variation of c_3 is plotted for the

same iterations shown in figures 5 and 6. For wedge angles larger than the value for $dp/dx = d_2p/dx_2 = 0$, c_3 appears to increase without bound as the calculation proceeds downstream, while for smaller angles, c_3 reaches a maximum. The iteration procedure tends to converge to the solution which separates the two families of curves. As mentioned above, the solutions for wedge angles larger than the unique value correspond to the pressure distribution reaching a maximum ($\dot{U}_1$ becoming positive). This pressure maximum is usually reached for reasonably low values of c_3, whereas, as the unique solution is approached very high values of c_3 and $\dot{c}_3$ are produced before the maximum pressure is attained. Since large values of $\dot{c}_3$ result in a divergent solution, a maximum value of 200.0 was used in the computer program to limit the value of c_3. When this limit is reached, the wedge angle is decreased for the next iteration.

The iterations shown in figures 5, 6, and 7 determine the wedge angle within 0.004°. Subsequent iterations showed that for angles sufficiently close to the exact value, the numerical solution became indeterminate as the final pressure plateau was approached. This behavior was due to the determinant of the coefficients of the simultaneous equations approaching zero. Thus the present computer program cannot integrate all the way to the exact final pressure plateau. If a combination of values of the wedge angle and the location of the beginning of interaction is reached for which the indeterminacy mentioned above is encountered, the calculation is terminated. The resulting solution is very close to the solution which satisfies the downstream boundary condition but will terminate slightly upstream of the pressure plateau. The final solution at the downstream end is then determined by examination of the iterations which produced bracketing solutions.

Another condition which may be encountered is failure of the solution to predict reattachment. If the $\bar{u} = 0$ line diverges from the surface as the calculation proceeds up the wedge or flare, the boundary layer will not reattach. This failure to reattach is manifested by the slope of the $\bar{u} = 0$ line in the Dorodnitsyn plane, $\dot{\eta}_s$, becoming positive. This condition indicates that the wedge angle is too small or the location of the beginning of interaction is too near the leading edge of the configuration. This condition was not encountered in the cases shown in figures 5, 6, and 7.

4. COMPUTER PROGRAM

The computer program written on the basis of the preceding discussion will not be described in detail, since it is fully documented in an operating manual which accompanies the program. However, the basic information necessary for understanding the program is now presented.

4.1 Configurations Treated

The program calculates the laminar boundary layer from the beginning of interaction through the entire interaction region to approximately the final pressure downstream of reattachment for the two families of configurations shown in figures 8 and 9. The first of these families is a two-dimensional body consisting of a flat plate of length L_c followed by a wedge of angle θ_w. A circular arc of radius R, beginning at L_c and ending at L_w, fairs the flat plate into the wedge. The beginning of interaction is at x_o. As the radius, R, is decreased, a flat-plate-wedge configuration is approached.

The second family of configurations is shown in figure 9. A typical axisymmetric body is shown in figure 9(a). It is made up of a nose of any shape (a hemispherical nose is shown in the sketch), a cylinder of radius r_o, and a circular arc of radius R, beginning at L_c' and ending at L_f', which fairs the cylinder smoothly into the flare of angle θ_f. The axisymmetric body which the analysis and the computer program treat is shown in figure 9(b). It is made up of a hollow, sharp-leading-edge cylinder followed by a circular arc of radius R which fairs the cylinder smoothly into the flare of angle θ_f. The method of applying the computer program to the configuration of figure 9(a) will now be described. At the beginning of interaction on the equivalent body, x_{a_o}, the velocity profile is assumed to be of the Blasius type, and the unit Reynolds number and Mach number at the edge of the boundary layer are taken to be the same as they are at the beginning of interaction, x_o', on the real body. If at x_o' the displacement thickness is known then x_{a_o} is taken to be the length of boundary-layer run on the equivalent body at constant edge conditions, equal to those at x_o', which matches the displacement thickness at that point. Some other quantity such as momentum thickness could be used to determine x_{a_o}. In any event, some knowledge of the boundary-layer characteristics at x_o' on the blunt body is needed to determine x_{a_o}. Once this is known then

$$\left.\begin{aligned} x_a &= x' + \left(x_{a_o} - x'_o\right) \\ L_{c_a} &= L'_c + \left(x_{a_o} - x'_o\right) \\ L_{f_a} &= L'_f + \left(x_{a_o} - x'_o\right) \end{aligned}\right\} \qquad (1)$$

The determination of the equivalent lengths must be done by the user and provided as input to the program, as the program treats only the sharp-edged cylinder configuration.

4.2 Method of Solution

From the mathematical point of view, the computer program solves a set of simultaneous ordinary differential equations starting at the beginning of interaction and ending at the point at which an iteration is terminated. The program then proceeds through a series of iterations until the unique solution is determined as nearly as possible. The unknowns in the equations are the coefficients in the assumed velocity and temperature profiles and the pressure distribution. The solution is started at the beginning of interaction by assuming the profiles are those given by the present solution for zero pressure gradient.

4.2.1 Preseparation region

In the preseparation region there are four unknown parameters in the velocity profile (eq. (48), ref. 4), c_o, c_1, c_2, and c_3, one unknown quantity in the temperature profile (eq. (49), ref. 4), E_o, and the unknown pressure distribution. Thus, between the beginning of interaction and the separation point six equations are required. These equations are given by equations (59) through (62), equation (70), and equation (98) of reference 4 for the two-dimensional configuration. For the axisymmetric configuration, equation (134) of reference 4 replaces equation (98).

Integration of these equations proceeds step by step until the separation point is reached. Since at separation $\partial u/\partial \eta$ at the wall must be zero, c_3 in the profile must be zero. Thus, a check of c_3 is made at the end of each integration step to see if it is zero or negative. A negative c_3 is not possible. However, because of numerical accuracy, it is possible to compute a very small negative value.

Since c_3 must be positive and becomes zero at separation, the derivative of c_3, $\dot{c}_3$, must also be zero at separation.

Once a zero or negative value of c_3 has been computed, conditions at separation are determined by backing up one step in the integration and extrapolating $\dot{c}_3$ to zero linearly to determine the separation point. The other quantities are then extrapolated linearly to this point.

The next step in the program is to extrapolate downstream of the separation point in order to begin the solution in the post-separation region. The length of this extrapolation is equal to the length of the extrapolation to reach separation. All of the quantities are again extrapolated linearly except for c_3. This quantity varies nearly parabolically in the region of separation so that $(c_3)_{x_S+\Delta x}$ is set equal to $(c_3)_{x_S-\Delta x}$.

4.2.2 Separated region

In the separated region the velocity profiles are given by equations (55) and (48) of reference 4 for the inner and the outer flow, respectively. The temperature profiles are given by equations (58) and (52) of reference 4 for the inner and outer flow, respectively. There are nine unknown parameters in these profiles, c_0, c_1, c_2, c_3, α_w, α_s, η_s, E_0, and S_s, so that nine equations, in addition to that specifying the pressure, are required. These nine equations are equations (74) through (77), (79), (85), (86), (90), and (93) of reference 4. The pressure distribution except in the plateau region is given by the free-interaction equation which for the two-dimensional case is equation (103) of reference 4 and for the axisymmetric case is equation (138) of reference 4. In the plateau pressure region, the free-interaction equation is replaced by equation (94) of reference 4 for both configurations. The plateau pressure boundary condition is relaxed and free interaction again imposed at the beginning of the compression surface.

In the work of references 1 and 2, it was found that if the inner velocity profile was represented as a cubic, the integration immediately downstream of separation became unstable. It was found necessary to start the integration with the inner layer velocity profile represented as a quadratic, $\alpha_w = -\alpha_s$ in equation (55) of reference 4, and integrate a short distance downstream before switching to the cubic profile.

In this region the differential equation

$$\dot{\alpha}_w = -\dot{\alpha}_s \tag{2}$$

replaces the momentum equation applied at the wall, equation (93) of reference 4. The criterion used to make the switch to the cubic profile is

$$\alpha_s - |\alpha_w| \geq 10^{-3} \tag{3}$$

where, from equation (93), reference 4

$$\bar{\alpha}_w = \frac{1}{2}\left[\frac{1}{2}(S_w + 1)\eta_s \frac{\dot{U}_1}{U_1} - \alpha_s\right] \tag{4}$$

Approaching reattachment the quadratic inner layer velocity profile is again used. The switch back to the quadratic is made when

$$\alpha_s - |\alpha_w| \leq 10^{-3} \tag{5}$$

where α_w is one of the variables being integrated.

The extrapolation procedure used to determine the reattachment point is the same as that described earlier for determining the separation point.

4.2.3 Post-reattachment region

In the post-reattachment region, the velocity and temperature profiles are given by the same relations as in the preseparation region. The solution downstream of the reattachment point is begun by extrapolating in the same manner as described before in beginning the solution downstream of separation.

Integration of the equations proceeds step by step until a condition is reached for which an iteration is to be terminated. At that point, the wedge angle, or beginning of interaction is changed in accordance with the iteration procedure, and the calculation is reinitialized to perform the next iteration. This procedure continues until the wedge angle, or the beginning of interaction has been determined within a tolerance predetermined by the user of the program.

4.3 Iteration Options

The iteration for a unique solution can be done on either the wedge (flare) angle or the beginning of interaction. The iteration on the wedge (flare) angle makes use of the fact that the solution upstream of the wedge (flare) is independent of the angle. Thus, the calculation of the boundary layer upstream of the wedge or flare is performed only once. When the end of the flat plate or cylinder is reached on the first iteration step, the values of the profile coefficients and their derivatives needed to continue the calculation from that point downstream are saved. Then, when an iteration is completed, those values are recalled to begin a new iteration starting at the beginning of the wedge. In the iteration on the beginning of interaction, the complete calculation is always repeated starting with the same Mach number, unit Reynolds number, and temperature ratio, at the value of x_o or x_{a_o} determined by the iteration.

4.4 Initial Conditions

4.4.1 Two-dimensional case

To begin the integration of the differential equations at the beginning of interaction initial values of c_o, c_1, c_2, c_3, and E_o, the coefficients in the assumed velocity and temperature profiles, must be specified. As in reference 4, the initial velocity profile is assumed to be a Blasius profile which is independent of wall temperature and the temperature profile is the Crocco relationship.

It was shown in reference 1 that for a Blasius velocity profile the values of c_o, c_1, and c_2 are proportional to $\sqrt{\xi}$, and c_3 is a constant. If the reference length, ℓ, is taken equal to the length of the flat plate, L_c, and x_o is the beginning of interaction then, from the transformations of reference 4,

$$\frac{x_o}{\ell} = \frac{X_o}{\ell} = \xi_o \tag{6}$$

and the initial values of the coefficients in the velocity profile are (ref. 2)

$$\left.\begin{aligned} c_o &= 3.157\sqrt{\xi_o} \\ c_1 &= -1.923\sqrt{\xi_o} \\ c_2 &= -0.3133\sqrt{\xi_o} \\ c_3 &= 1.1000 \end{aligned}\right\} \tag{7}$$

Again, as in reference 4

$$E_o = 0 \tag{8}$$

so the initial temperature profile reduces to the Crocco relationship

$$S = S_w(1 - \bar{u}) \tag{9}$$

In the free-interaction equation, (eq. (98), ref. 4) an initial value of U_1/U_o is required. It was found in reference 1 that perturbing the pressure by 0.1 percent from the value ahead of the beginning of interaction was sufficient to start the interaction. From the isentropic relationship

$$\frac{p}{p_t} = \left(1 + \frac{\gamma - 1}{2} M^2\right)^{-\gamma/(\gamma-1)} \tag{10}$$

and since $p_{t_o} = p_{t_1}$

$$\frac{U_1}{U_o} = \frac{M_1}{M_o} = \left\{ \frac{1}{\frac{\gamma - 1}{2} M_o^2} \left[\frac{1 + \frac{\gamma - 1}{2} M_o^2}{(1.001)^{(\gamma-1)/\gamma}} - 1 \right] \right\}^{1/2} \tag{11}$$

Since the Mach number is defined parallel to the δ^* line it has been assumed that

$$\frac{U_1}{U_o} = \frac{M_1 \cos \phi_1}{M_o \cos \phi_o} = \frac{M_1}{M_o} \tag{12}$$

In order to evaluate ϕ_1 in the free-interaction equation, using equations (101) and (102), reference 4, an initial value of ϕ, ϕ_o, is required. Equation (96), reference 4, says that

$$\left.\frac{d\delta^*}{dx}\right|_{x_o} = \tan \phi_o \tag{13}$$

The compressible displacement thickness

$$\delta^* = \int_o^\infty \left(1 - \frac{\rho u}{\rho_1 u_1}\right) dy \tag{14}$$

becomes after transforming to the Stewartson plane with zero pressure gradient

$$\delta^* = (1 + m_o)\left[\int_o^\infty S\, dY + \int_o^\infty \left(1 - \frac{U}{U_1}\right) dY\right] + m_o \int_o^\infty \frac{U}{U_1}\left(1 - \frac{U}{U_1}\right) dY \tag{15}$$

In the Stewartson plane the Blasius expressions for displacement thickness and momentum thickness are, respectively, (ref. 4)

$$\left.\begin{aligned} \delta^*_{ST} &= \int_o^\infty \left(1 - \frac{U}{U_1}\right) dY = 1.73\sqrt{\frac{\nu_o X}{U_o}} \\ \delta^{**}_{ST} &= \int_o^\infty \frac{U}{U_1}\left(1 - \frac{U}{U_1}\right) dY = 0.664\sqrt{\frac{\nu_o X}{U_o}} \end{aligned}\right\} \tag{16}$$

so that equation (15) becomes

$$\delta^* = (1 + m_o)(S_w + 1)\delta^*_{ST} + m_o \delta^{**}_{ST} \tag{17}$$

since from equation (9)

$$\int_o^\infty S\, dY = S_w \int_o^\infty (1 - \bar{u})\, dY = S_w \int_o^\infty \left(1 - \frac{U}{U_1}\right) dY \tag{18}$$

Differentiation of equation (17) yields

$$\left.\frac{d\delta^*}{dx}\right|_{x_o} = \left.\left(\frac{d\delta^*}{dX}\frac{dX}{dx}\right)\right|_{x_o} = \tan \phi_o$$

$$= \frac{1}{\sqrt{R_{x_o}}}\left[0.865(1 + m_o)(1 + S_w) + 0.332\, m_o\right] \qquad (19)$$

To begin the calculation downstream of the separation point after extrapolating c_o, c_1, c_2, c_3, U_1, and E_o through separation, initial values of α_s, η_s, and S_s are needed. These are obtained from equations (83), (84), and (89) of reference 4, with $\alpha_w = -\alpha_s$.

4.4.2 Axisymmetric case

The initial profiles for the axisymmetric configuration are taken to be those on a hollow cylinder or a flat plate with zero pressure gradient, a Blasius profile for the velocity profile and the Crocco relationship for the temperature profile. The Mangler, Stewartson, and Dorodnitsyn transformations (see ref. 4) give the following relationships between the axial coordinates in the various planes for zero pressure gradient.

$$x_a = \frac{x}{r_o^2} = \frac{X}{r_o^2} = \frac{\xi \ell}{r_o^2} \qquad (20)$$

Taking the reference length L in the equivalent axisymmetric plane equal to the length of the hollow cylinder, figure 9, it is found that

$$\frac{x_{a_o}}{L} = \frac{x_o}{\ell} = \frac{X_o}{\ell} = \xi_o \qquad (21)$$

Thus, the initial conditions for the parameters in the velocity profile and the temperature profile are the same as those for the two-dimensional case, equations (7) and (8). The initial condition on U_1/U_o is again determined from equation (11).

The initial value of ϕ_{a_o} which is used in equation (132), reference 4, is found in the following way. On the cylinder

$$\delta_a^* = \frac{\delta^*}{r_o} \tag{22}$$

from equation (128), reference 4. Thus,

$$\frac{d\delta^*}{dx_a} = \frac{1}{r_o} \frac{d\delta^*}{dx} \frac{dx}{dx_a} = r_o \frac{d\delta^*}{dx} \tag{23}$$

and from equation (133), reference 4

$$\tan \phi_{a_o} = r_o \left.\frac{d\delta^*}{dx}\right|_{x_o} = r_o \tan \phi_o \tag{24}$$

where $\tan \phi_o$ is given by equation (19).

5. COMPARISON WITH EXPERIMENTAL DATA

Several comparisons have been made between experimental pressure distributions and those calculated by the theory described in this report in order to study the adequacy of the theory. In all of the comparisons the theoretical solution has been found by iterating on the beginning of interaction until it converged to within at least 0.1 percent of the flat plate or hollow cylinder length. Examples are presented first for two-dimensional flows and then for axisymmetric flows. In each figure, theoretical curves are shown for the final iteration from the beginning of interaction through the reattachment point. Downstream of the reattachment point, two calculated curves are shown, for a value of x_o larger and one smaller than the value for the unique solution. Nearly all of the comparisons to be presented are for nonadiabatic flows.

The first sets of data, shown in figure 10, are taken from the work of Lewis, Kubota, and Lees, reference 8. These data were taken on a highly cooled flat-plate-wedge configuration. The ratio of wall temperature to free-stream stagnation temperature was 0.204. The configuration was a flat plate followed by a 10.25^o wedge. Considerable care was taken in the experiment to assure that the flow was two-dimensional and laminar throughout the entire interaction region.

Shown on the plots are the free-stream test conditions as well as the flow conditions at the edge of the boundary layer at the beginning of interaction used in the theoretical calculations. In most cases these conditions have been calculated from the available experimental data. The data of figure 19 of reference 8 show that the pressure at the edge of the boundary layer at the beginning of interaction is not equal to the free-stream static pressure. The conditions at the edge of the boundary layer used in the theoretical calculations at the beginning of interaction have been computed by assuming that the total pressure at the edge of the boundary layer is the same as that in the free stream, but that the static pressure at the beginning of interaction is that given by the data. Thus, since this pressure is higher than that of the free stream, the Mach number is lower and the unit Reynolds number is higher.

The theoretical calculation based on the calculated conditions at the beginning of interaction is compared with the experimental data in figure 10(a). The theory predicts a slightly longer separated region and steeper pressure gradients than are indicated by the experimental data. Also, it appears the predicted final pressure, if the plateau could be reached, would be slightly higher than the experimental value. The entire pressure distribution is shifted upstream. Figure 10(b) shows a comparison with the same experimental data as figure 10(a), but with the theoretical prediction based on the experimental free-stream Mach number and unit Reynolds number. Again, the pressure distribution is shifted upstream and it appears the final pressure would be slightly overpredicted if the unique solution could be found exactly. The effect of the different initial boundary-layer edge conditions appears to be negligible.

The experimental data indicate a slightly favorable pressure gradient upstream of the beginning of interaction. The significance of such a favorable gradient regarding the comparison of theoretical predictions with experimental data will be discussed in section 6 of this report.

Figure 11 shows a comparison between experiment and theory for a set of adiabatic data also presented in reference 8. The free-stream conditions at which these data were taken are the same as those at which the cold wall data shown in figure 10(a) were taken. Comparison

of these figures shows the large effect which wall cooling has on the extent of separation. Since the theory has assumed that the Prandtl number is unity, all of the computations made for comparison with adiabatic data have been made with $T_w/T_{t_o} = 1.0$; that is, the recovery factor has been taken as unity. The nature of the agreement between the experimental data and the theory in figure 11 is about the same as in figure 10. The final pressure appears to be slightly overpredicted by the theory and the entire pressure distribution appears to be slightly shifted upstream of the data. As in the comparison in figure 10, the discrepancies may be explained in part by neglect of an accelerating flow behind the leading edge. The final pressure appears to be predicted more accurately in figure 11 since the pressure gradients are not as steep as for the data of figure 10. The steepness of the pressure rise in the cold wall case (fig. 10) causes the calculated pressure distributions to diverge more sharply, thus making the definition of the final pressure plateau less certain than for the adiabatic case. Tighter tolerance on the iteration is thus required for nonadiabatic cases in order to obtain good definition of the final plateau pressure.

Figure 12 presents a comparison for another set of data from reference 8. In this case, the wall was cooled so the temperature ratio was the same as for the data of figure 10, but the unit Reynolds number at the beginning of interaction was higher. The Mach number at the beginning of interaction, calculated in the manner described when discussing figure 10(a), was only slightly different for the two runs. The experimental data indicates a longer separated region than in the previous data. This effect is also predicted by the theory, although the predicted separation is more extensive than the data indicate. As mentioned above, the calculations were performed until the location of the beginning of interaction was determined within 0.1 percent of the flat-plate length, L_c. In this case, the theoretical solution was determined within approximately 0.05 percent of the flat-plate length. The solutions for values of x_o above and below the value for the unique solution show that the unique final pressure would be very close to the experimental value.

Also shown in figures 10, 11, and 12 are the inviscid wedge pressure ratios calculated for Mach number M_o. In all cases, the

experimental data and the theoretical solution are below the inviscid pressure. The agreement seems to improve as the wall is cooled or the Reynolds number increased. Either of these tends to thin the boundary layer, indicating that the lack of agreement may be due to boundary-layer displacement thickness effects. The displacement thickness effectively changes the shape of the configuration. The effective turning angle of the flow is the change in the slope of the δ^* line between the beginning of interaction and the point where the final pressure plateau is reached and is smaller than the wedge angle. The theoretical calculation appears to account for the effect quite well.

Comparison with some adiabatic data from figure 21 of reference 1 taken on a flat-plate-wedge configuration at a Mach number of 2.3 is shown in figure 13. The model was inclined at an angle of attack of 6° in order to obtain a Mach number on the flat plate higher than that of the free stream. The Mach number at the beginning of interaction was found to be 2.5. The calculated pressure distribution is in excellent agreement with the experimental data up to the leading edge of the ramp. The experimental pressure then rises more slowly than the calculated pressure and finally reaches a maximum that is higher than the inviscid value. This behavior is different from the other cases examined in that the experimental data usually rises to a value lower than the inviscid value. The discrepancy may be explained in part by the indicated favorable pressure gradient upstream of the beginning of interaction. Also, the separated region develops a very long pressure plateau. This appears to affect the response of the boundary layer to the ramp in a way which cannot be predicted by the present theory. There is also reason to believe that the experimental data shown in figure 13 may be transitional since examination of figures 20 and 21 of reference 1 reveals that as the free-stream Reynolds number was increased, the extent of the separated region decreased as would be expected for a transitional boundary layer.

Figure 14 presents a comparison with the adiabatic data of Ko and Kubota presented in reference 9. The static pressure ratio at the beginning of interaction was taken to be that indicated in figure 3 of reference 9. As in the previous cases, this pressure is not the same as the free-stream static pressure. This is accounted for in part by a favorable gradient which is apparent ahead of the beginning of

interaction. The difference is also explained by the authors of reference 9 as due to nonisentropic effects introduced by the shock wave at the leading edge of the model. They state that the total pressure at the boundary-layer edge could be as little as half of that upstream of the shock wave on the model.

The conditions used for the theoretical calculation are shown on the figure. The Mach number was 5.69, the unit Reynolds number was 8.2×10^5 per foot and the temperature ratio was taken to be 1.0. The configuration was a sharp-leading-edge flat plate, 2 inches long, faired into a 10.15° wedge by a circular arc of 2-inch radius. The agreement in this case is quite good. The discrepancy between the experiment and the theoretical pressure distribution (fig. 14(a)) and displacement thickness (fig. 14(b)) downstream of reattachment may be due to the favorable upstream pressure gradient and the nonisentropic nature of the flow.

The remaining comparisons between the theory and experimental data are for axisymmetric configurations. As described in section 4 of this report, calculations for axisymmetric configurations require the determination of the length of an equivalent hollow cylinder on which the conditions at the beginning of interaction are the same as those on the particular configuration being considered. Such a match requires either experimental data on the boundary-layer properties on the body of revolution at the beginning of interaction or an accurate method for calculating these properties. It is necessary to account for the existence of a non-Blasius velocity profile at the beginning of interaction for blunt-nosed bodies followed by short slender cylinders where favorable pressure gradients may be strong and nonisentropic conditions may exist at the edge of the boundary layer.

A complete investigation of methods for predicting the initial conditions for axisymmetric bodies was not undertaken in this study. The data comparisons to be discussed in this section were obtained by adjusting the length of the equivalent hollow cylinder until the theoretical and experimental separation points approximately coincided. An example is also given of a calculation of the equivalent cylinder length by an approximate technique. That example indicates that such approximate techniques are inadequate and that the initial conditions must be computed more accurately.

Comparisons between the theory and experimental data taken by Kuehn, reference 10, are presented in figure 15. The data were taken on the axisymmetric configuration shown in figure 15. It consists of a hemispherical nose followed by a cylinder one cylinder diameter in length and a 10° flare. The free-stream test conditions are shown on the figure. The flow conditions at the edge of the boundary layer were calculated in the following manner. The free-stream flow was assumed to go through a normal shock in order to obtain the stagnation pressure behind the shock wave. The flow was then assumed to go through an isentropic expansion around the body from the stagnation point to the experimentally measured pressure on the cylinder at the beginning of interaction. This pressure ratio determines the Mach number, M_o. The unit Reynolds number, R_o/L_{c_a}, at the beginning of interaction was calculated in the following way. The Reynolds number ratio can be written

$$\frac{R_o/L_{c_a}}{R_\infty/ft} = \frac{\rho_o}{\rho_\infty}\,\frac{u_o}{u_\infty}\,\frac{\mu_\infty}{\mu_o} = \frac{\rho_o}{\rho_\infty}\,\frac{M_o}{M_\infty}\,\frac{a_o}{a_\infty}\,\frac{\mu_\infty}{\mu_o}$$

Since

$$p = \rho RT \quad , \quad a = \sqrt{\gamma R_g T}$$

and, in the present work,

$$\frac{\mu_\infty}{\mu_o} = \frac{T_\infty}{T_o}$$

then

$$\frac{R_o/L_{c_a}}{R_\infty/ft} = \frac{p_o}{p_\infty}\,\frac{M_o}{M_\infty}\left(\frac{T_\infty}{T_o}\right)^{3/2}$$

Some explanation of the quantities x_o' and x_{a_o} is required. The first quantity, x_o', (see fig. 9) is the location of the beginning of interaction on the actual body whereas x_{a_o} is an equivalent hollow-cylinder boundary-layer run to match some quantity such as momentum or displacement thickness at the beginning of interaction. Since in the

present case the momentum and displacement thicknesses on the cylinder are not known, the length of the cylinder, L_{C_a}, on the equivalent body has been adjusted until the location of the experimental and theoretical separation points coincide as mentioned above.

The results shown in figure 15 indicate that the theory overpredicts the plateau pressure and the final pressure and predicts a longer separated region than the experimental data. Calculations performed using different equivalent cylinder lengths showed that the plateau and final pressures were only slightly affected by changes in the cylinder length even though the length of the plateau and separated regions was significantly changed. The difference between the theory and the experimental data is influenced by nonisentropic effects introduced by the blunt nose, or by the fact that the boundary layer velocity profile may not have achieved a Blasius form at the beginning of interaction because of the short cylinder.

In figure 16, comparisons of the present theory with experimental data of Becker and Korycinski, reference 11, are presented. The model tested is made up of a von Kármán minimum-drag shape tangent-ogive nose of fineness ratio 5 with a 10° half-angle cone at the tip. Following this is a cylinder 5 diameters in length and a 10° flare. Shown on the figure are the free-stream test conditions. The ratio of wall temperature to stagnation temperature is 0.5. The flow conditions at the edge of the boundary layer at the beginning of interaction have been calculated as follows. Cone tables were used to find the ratio of the free-stream pressure to surface pressure behind the nose shock and the surface Mach number on the nose. The flow was then assumed to go through an isentropic expansion around the body from the vertex of the ogive to the experimentally measured pressure on the cylinder at the beginning of interaction as has just been described for the hemisphere-cylinder-flare model of Kuehn presented in figure 15.

Figure 16(a) shows the comparison between the experimental and theoretical pressure distributions. There are few data points from figure 5(a) of reference 11 which fall in the interaction region. The agreement between experiment and theory appears to be good. Figure 16(b) shows comparison between heat-transfer data, taken at the same test conditions, and the theory. As can be seen, the agreement between the calculated distribution and the experimental data is only fair. The

lack of agreement may be due to the degree of approximation used in the formulation of the temperature profile. The degree of approximation was discussed in references 2 and 4. For first-order coupling, the relation between the velocity and temperature fields is just the Crocco relationship for which the heat-transfer rate at the separation point is zero. For second-order coupling, a second parameter is included in the temperature profile representation. This produces a nonzero heat-transfer rate at the separation point as seen in figure 16(b), but the heat-transfer rate distribution undergoes cusp-like changes in direction at the separation and reattachment points. A minimum is produced in the distribution at the cylinder-flare juncture as for the experimental data, although the heat-transfer rate is in general lower than that shown by the data. It was shown in reference 4 that the heat transfer prediction in the preseparation region could be improved by including third or higher-order coupling in the formulation. No attempts to evaluate the effect of higher-order coupling were made in this work.

Comparison with three sets of data obtained on an ogive-cylinder-flare configuration are shown in figure 17. The data were obtained in hypersonic flow with the model highly cooled (ref. 12). The cylindrical part of the body was very long, resulting in a nearly constant pressure for a substantial distance ahead of the beginning of the separation interaction.

The test conditions are shown in the figures. The free-stream Mach number was 8.0 for all three cases. The stagnation conditions were varied to produce different test Reynolds numbers. The temperature ratios were approximately 0.2 for the first two cases and 0.4 for the third case. The conditions at the beginning of interaction were obtained as described previously for the comparison in figure 16. In the calculation of conditions behind the nose shock, the angle of the vertex of the ogive nose was used. Comparisons shown in figure 17 were obtained in the same manner as for the previous axisymmetric cases; that is, the equivalent sharp leading-edged hollow cylinder length was adjusted until the theoretical and experimental separation points approximately coincided.

The agreement in these cases is seen to be considerably better through the separated region than in the previous axisymmetric cases. This is possibly due to the fact that the long constant pressure region

ahead of the beginning of interaction allows the boundary-layer velocity profile to more nearly approach the Blasius form.

In order to illustrate the importance of accurate knowledge of the initial conditions on the prediction of axisymmetric separated boundary layers, an approximate technique described in reference 13 was employed to compute the equivalent cylinder length for the conditions of figure 17(c). In that technique an equivalent flat plate boundary-layer distance to the beginning of interaction, x_o, is determined by assuming the momentum thickness on the axisymmetric body at the beginning of interaction is equal to that on a flat plate. The momentum thickness at the beginning of interaction on the axisymmetric body is computed by integration of a suitable form of the boundary-layer equations along the surface of the body from the nose to the beginning of interaction. Equating the resulting value of momentum thickness to the Blasius value for a flat plate yields an equivalent value of x_o.

When the equivalent flat plate value of x_o is known, the cylinder length is calculated by adding the distance from the beginning of interaction to the flare, as determined from the experimental pressure distribution, to the calculated equivalent flat plate value of x_o. The calculated cylinder length is then used with the experimental flare angle and flow conditions at the beginning of interaction calculated as described above to compute a unique boundary-layer solution by iterating on the location of the beginning of interaction.

The results of a calculation based on the above procedure are shown in figure 18. The configuration and flow conditions are the same as shown in figure 17(c). The agreement with the experimental data is only fair compared to the agreement shown in figure 17(c). The approximate technique used to compute initial conditions for figure 18 apparently does not account accurately for the effects of the pressure gradient on the nose and nonisentropic boundary-layer edge conditions which may result from the interaction between the boundary layer and the shock at the nose of the body.

6. INVESTIGATION OF FAVORABLE UPSTREAM PRESSURE GRADIENTS

As described in section 4 of this report, the computer program is based on the assumption of a constant pressure and a Blasius velocity profile up to the point of the beginning of the separation interaction. Near the leading edge of a sharp-leading-edge flat plate in supersonic flow this assumption may not be valid. Near the leading edge is a region of strong interaction between the viscous boundary layer and the inviscid outer flow in which the flow is displacement dominated. Also, the total pressure at the boundary-layer edge may not be constant along the plate due to nonisentropic effects induced by curvature of the leading edge shock in the displacement-dominated region. The attainment of a constant pressure for which the Blasius theory applies is only achieved at a long distance from where the value of the hypersonic interaction parameter $\overline{\chi} = M_\infty^3\sqrt{C/R_\infty x}$ approaches zero. In a hypersonic flow, a favorable pressure gradient may exist for a significant distance downstream of the leading edge of sharp flat plates. For flat-plate-wedge configurations with short plates, the beginning of the separation interaction may occur at some point in the favorable pressure gradient region where the boundary layer has not yet achieved the Blasius form. Such a non-Blasius condition is possible in the data of figures 10, 11, 12, and 14 where the values of $\overline{\chi}$ at the beginning of interaction are approximately 0.63, 0.63, 0.37, and 0.89, respectively, with the constant C in the expression for $\overline{\chi}$ taken equal to unity. Another effect of favorable upstream pressure gradients is to cause the effective run length to the beginning of interaction to be lower than for a constant pressure distribution corresponding to the pressure at the beginning of interaction, with the result that the values of the displacement thickness, momentum thickness, and skin friction coefficient are different from the values predicted by the Blasius theory.

An attempt was made to study the effect of favorable upstream pressure gradients by applying a prescribed pressure gradient upstream of the beginning of the separation interaction. The computational method used in the preseparation region was modified by deleting the free-interaction equation from the set of simultaneous ordinary differential equations and prescribing the pressure distribution as a polynomial. This modified computational scheme was programmed, and

attempts were made to obtain solutions for favorable pressure gradients which would provide a set of coefficients c_o, c_1, c_2, c_3, and E_o for the velocity and temperature profiles. These coefficients would then be used as initial conditions in lieu of the Blasius initial conditions, for the program employing free interaction. That program was modified for the investigation of favorable upstream pressure gradients to accept initial non-Blasius velocity gradient profiles, and iteration on the wedge angle was used to develop a unique solution. The pressure distribution was represented by a segmented polynomial with zero pressure gradient at the beginning of the calculation and at a point selected as the beginning of a separation interaction. Several attempts were made to develop solutions with the prescribed pressure gradient program. However, the program would not integrate the equations with significant negative pressure gradients. Rapidly divergent solutions were produced. This behavior is similar to that noted by Bethel (ref. 14), and is believed to be due to an instability of the mathematical equations in the presence of negative pressure gradients when a variable coefficient is used in the square root term of the following boundary-layer velocity-gradient formulation.

$$\frac{\partial \bar{u}}{\partial \eta} = \frac{(1 - \bar{u})\sqrt{\bar{u} + c_3}}{c_o + c_1 \bar{u} + c_2 \bar{u}^2}$$

It is probable that the solution in the presence of a favorable pressure gradient develops a large positive eigenvalue which dominates the numerical solution. In particular cases it may be possible to suppress such eigenvalues. One possible method might be to suppress the variation of the parameter c_3. Comprehensive study of this problem to adapt the "root" formulation to allow solutions with negative pressure gradients was beyond the scope of the present work and was not undertaken.

Previous experience (ref. 15) has shown that calculations for favorable upstream pressure gradients are possible using a computer program employing the velocity-gradient formulation

$$\frac{\partial \bar{u}}{\partial \eta} = \frac{1 - \bar{u}}{c_o + c_1 \bar{u} + c_2 \bar{u}^2}$$

Since separation does not usually occur with favorable pressure gradients, the square root term in the previous formulation is unnecessary. This formulation will subsequently be referred to as the "no root" formulation since the square root term in the numerator is omitted. The present investigation of upstream pressure gradient effects is limited to adiabatic boundary layers by the fact that the existing no-root program employs first-order temperature coupling and is not accurate for highly cooled walls.

The use of the no-root program over the region of negative pressure gradients required an intermediate step in developing initial conditions for the free-interaction program. To obtain values of c_0, c_1, c_2, and c_3 for the square root formulation, the velocity-gradient profiles produced by the no-root program were fitted by a technique based on the method of least squares.

Several non-Blasius velocity gradient profiles were obtained using the no-root program and various favorable pressure gradient distributions. Pressure gradients of the weak-interaction type as described in reference 16 as well as arbitrary pressure gradients were used. The velocity gradient profiles were then fitted to obtain initial conditions for the free-interaction program. The free-interaction calculations were found to be very sensitive to the initial profiles. In most cases, divergent solutions were produced. The determination of the exact reasons for this divergent behavior was not undertaken in the present effort. The initial velocity gradient profile for which a nondivergent solution was obtained is compared with a Blasius profile in figure 19. The pressure gradient which produced the non-Blasius profile was a hypothetical one shown in figure 20. The non-Blasius profile shown in figure 19 represents both the profile obtained from the no-root program and the profile obtained from least-squares fitting. The difference between the original curve and the fitted curve was insignificant compared to the difference between the Blasius and non-Blasius profile. A boundary-layer calculation was made using both the Blasius and the non-Blasius profiles shown in figure 19. The effect of the non-Blasius profile can be seen in figure 20. The results of calculations started at the same value of x_o but with the two different velocity profiles are shown. Even though the initial velocity profiles were only slightly different, the wedge angle and consequently the pressure distribution

are significantly affected. The calculation which started with a Blasius profile converged to a wedge angle of 8.12° while the calculation started with the non-Blasius profile converged to a wedge angle of 10.56°. The Mach number, temperature ratio and unit Reynolds number at the beginning of interaction in the two cases were the same as for the data of figure 14. The beginning of interaction was obtained from the experimental data. The actual wedge angle was 10.15°. The values of displacement thickness at the beginning of interaction were the same in the two theoretical cases shown in figure 20 within 2 percent. The initial values of momentum thickness were within 4 percent in the two cases, while a difference of 5 percent was noted in the initial values of the skin friction coefficient.

The errors in the initial boundary-layer properties mentioned above correspond to errors in the Reynolds number for Blasius conditions of less than 10 percent. Parametric studies to be discussed in section 7 of this report indicate that this amount of error in Reynolds number would account for less than 1 degree change in the wedge angle. The wedge angle for the unique solution was changed by 2.4° in the example shown in figure 20, indicating that the use of a non-Blasius initial velocity profile has a significant effect on the boundary-layer calculation. That accounting for the non-Blasius initial velocity profile improves the comparison with data can be seen by comparing the locations of the separation point predicted for Blasius and for non-Blasius initial conditions. In the calculation shown in figure 14 for Blasius initial conditions, the separation point is located at $x_s = 0.137$ foot from the leading edge, while if the calculation for non-Blasius initial conditions shown in figure 20 is adjusted to an angle, $\theta_w = 10.15^{\circ}$, by assuming the same type of relationship between θ_w, x_o, and x_s as for Blasius initial conditions, the separation point would be at approximately $x_s = 0.149$ foot from the leading edge. The experimental value is approximately $x_s = 0.15$ foot. Thus, accounting for the non-Blasius initial conditions tends to decrease the predicted upstream extent of separation, and improve the comparison with data.

These results indicate that in cases where a favorable pressure gradient may exist upstream of the separation interaction, as in many of the data comparisons discussed in section 5 of this report, the effect of the pressure gradient on the velocity profile must be accounted for to obtain very accurate results.

7. PARAMETRIC DATA

Systematic calculations were made for the purpose of evaluating the effects of Mach number, Reynolds number, temperature ratio, and ramp angle on the characteristics of separated two-dimensional laminar boundary layers. The calculations also provided valuable insight into the nature of solutions produced by the present theory and helped to establish ranges of applicability of the computer program.

The systematic calculations were performed for a flat-plate-wedge configuration in which a flat plate was faired into a wedge of arbitrary angle, θ_w, by a circular arc of radius R. The radius was chosen so that the transition from the plate to the wedge required a few integration steps, thus avoiding a discontinuity in the right-hand side of the free-interaction equation as mentioned in section 4.

Axisymmetric configurations were not treated in the systematic calculations. Parametric data supplied by the calculations on a flat-plate-wedge configuration can be used as a first approximation for calculations on axisymmetric configurations. In the axisymmetric case, the cylinder radius must be included as an additional parameter.

To perform boundary-layer calculations for a specific configuration, the Mach number, unit Reynolds number, and temperature ratio must be specified. The present computer program requires either the value of the wedge angle, or the location of the beginning of interaction, depending on the iteration scheme to be employed. In the calculations to be described here, the location of the beginning of interaction was specified, an estimated initial value of the wedge angle was provided, and the wedge angle was iterated to within 0.1° of the value for the unique solution. This procedure was chosen since the iteration on the wedge angle requires calculating the boundary layer ahead of the wedge only once as described in section 4.3, whereas if the beginning of interaction was iterated, the entire boundary layer from the beginning of interaction would be calculated on each iteration. Thus, when a large number of computer runs are to be made, iteration on the wedge angle requires a significantly lesser amount of computer time.

As mentioned above, four parameters are required to specify a certain boundary-layer calculation. The parameters are the value of the Mach number, M_o, at the beginning of interaction, the Reynolds number based on flat-plate length and conditions at the beginning of interaction,

R_o, and the temperature ratio, T_w/T_{t_o} and, for iteration on the wedge angle, the location of the beginning of interaction. A comprehensive set of parametric data was developed in the following manner. First, all combinations of the following values of the parameters were used to establish a basic matrix of boundary-layer data.

M_o	R_o	T_w/T_{t_o}	x_o/L_c
2.0	10^5	0.2	0.25
6.0	10^6	0.6	0.5
10.0	10^7	1.0	0.75

Then, Mach numbers of 4.0 and 8.0, a Reynolds number of 10^4, and temperature ratio of 0.4 and 0.8 were used where necessary to clarify trends in the calculated results. The relationship between the location of the beginning of interaction and the wedge angle was found to be quite nonlinear. Therefore, in order to establish a more detailed graph between x_o/L_c and θ_w for each set of values of M_o, R_o, and T_w/T_{t_o}, calculations were made for additional values of x_o/L_c.

The Mach number range used in the calculations provides a wide range of data in the supersonic and hypersonic flow regimes where isentropic flow can reasonably be expected and real-gas effects can be neglected. The Reynolds number range used in the calculations covers the range in which laminar separated flows can be expected to occur for wedge angles below about 20^o for the Mach number range considered.

The results of the systematic calculations are presented in two forms. The results of all computer runs made in the parametric study are tabulated in Table I. Results for some specific characteristics of the solution are presented for illustration in graphical form in figures 21-29.

In Table I, the values of θ_w and x_o/L_c are listed for different values of M_o, R_o, and T_w/T_{t_o}. This provides enough information to obtain the approximate values of θ_w and x_o/L_c for any other values of M_o, R_o, and T_w/T_{t_o} in the range of the calculations. The calculated values of some of the other important boundary-layer parameters are also presented in Table I. All lengths are presented in nondimensional form, normalized with respect to the length of the flat plate. The pressures are presented in nondimensional form, normalized by the pressure at the beginning of interaction. In this table the pressure ratios

at various characteristic points in the boundary layer, the separation point, p_S/p_o, the plateau region, p_P/p_o, the beginning of the wedge, p_C/p_o, and the reattachment point, p_R/p_o, are presented. Dashed lines in table I signify that no plateau was achieved in the separated region. The pressure ratio at the end of the final iteration, p_F/p_o, is also tabulated. This pressure ratio is not necessarily the value of the final plateau pressure ratio, but is the pressure at the end of the iteration for which the wedge angle had converged to within 0.1° of the unique value. In addition, the values of displacement thickness, momentum thickness, and skin friction coefficient at the beginning of interaction are tabulated.

The present effort and previous work using the method of integral relations on separation of laminar boundary layers have shown certain limiting boundaries occurring in the calculative method. These boundaries are associated with critical temperature ratio, minimum Reynolds number, and incipient separation.

Previous work on separation of laminar boundary layers (refs. 2, 3, and 4) has shown the existence in the theory of a critical temperature ratio, below which the laminar boundary layer will not separate under the type of free interaction used in the present theory. The critical temperature ratio corresponding to the second-order coupling theory used here is shown in figure 21. The critical temperature ratio is a function of the Mach number, but not of the Reynolds number. The temperature ratios used in the present parametric study are greater than the critical value for all Mach numbers used.

A minimum value of the Reynolds number at the beginning of interaction, R_{x_o}, was imposed on the computer program after the numerical integration scheme was found to produce divergent solutions for small values of R_{x_o}. The present calculative technique does not apply near the leading edge of a flat plate. It was found that for a beginning of interaction too close to the leading edge, the value of the ratio $(\delta^*/x)_o$ became very large, and the iteration on the wedge angle either would not converge or would converge to a high angle incompatible with the assumptions of the theory. A limiting value of the Reynolds number, R_{x_o}, was then defined as that for which the value of the ratio $(\delta^*/x)_o$ is equal to 0.1. This minimum Reynolds number represents a limit imposed on the computer program to avoid unduly thick boundary

layers. The variation of this minimum Reynolds number with temperature ratio and Mach number is shown in figure 22.

The present theory also predicts an incipient separation wedge angle. Comprehensive calculations were made at a Mach number of 2.0, Reynolds number of 10^6, and temperature ratios of 0.2 and 1.0. In figure 23 are shown the variations with wedge angle of the separation pressure ratio and the reattachment pressure ratio for the unique solutions. It is noted that for small angles the two pressure ratios are approximately linear functions of the wedge angle and that there is a value of θ_w for which the two pressures are equal. This is the value of θ_w for which both the separation point and the reattachment point occur at the juncture of the flat plate and the wedge. This value of θ_w is defined in this report as the incipient separation angle. For angles above this value, the separation point is upstream of the beginning of the wedge and for angles below this value, separation would not occur on the flat plate. The present computer program will not compute a unique solution if separation occurs beyond the end of the flat plate. Therefore, the incipient separation angle is an effective limit on the range of applicability of the program.

The results of figure 23 indicate that the wedge angle for incipient separation is a weak function of temperature ratio, at least for the Mach number and Reynolds number of the figure. The incipient separation angle exists for other Mach numbers and Reynolds numbers but was not calculated in the present investigation. The calculation presented here is shown to indicate how the incipient separation angle might be determined.

The value of the parameter $\theta_{w_i}/\sqrt{M_o}$ obtained from the results of figure 23 is approximately 30 percent lower than the value obtained from the experimental correlation of reference 17. In interpreting this result, several factors must be considered. First, the result is not surprising in view of the difficulty of exactly determining the onset of separation from experimental data. That is, it is to be expected that the theory should predict a smaller incipient separation wedge angle than one obtained from an experimental correlation. Also, the correlation of reference 17 was obtained from experiments at hypersonic Mach numbers, on highly cooled plates whereas the Mach number used in figure 23 is not hypersonic. Furthermore, some of the data used for the correlation

of reference 17 was transitional while the rest of the data was obtained in a nonuniform (conical) flow field. Finally, the hypersonic interaction parameter at the beginning of interaction varied from 0.25 to 13.4 for the correlation data suggesting the existence of non-Blasius conditions at the beginning of interaction.

The location of the beginning of interaction corresponding to the incipient separation angle can be found by examining the variation of x_s/L_c with x_o/L_c shown in figure 24. The variation is approximately linear so that the value of x_o/L_c for incipient separation can be determined by extrapolating the curves of x_s/L_c versus x_o/L_c to $x_s/L_c = 1.0$. Thus at incipient separation the value of x_o/L_c for the adiabatic wall is about 0.77 and for the highly cooled wall is 0.94.

In the remainder of this section, the effect of Mach number, Reynolds number, and temperature ratio on the extent of the upstream influence of the ramp, the length and characteristics of the separation region and the overall boundary-layer pressure distribution will be discussed. Certain results of the systematic boundary-layer calculations will be shown graphically to illustrate the basic trends of the data. Data for constructing the curves to be presented were obtained by cross plotting and interpolating the data from the systematic calculations which are presented in table I.

The relationship between the wedge angle and the location of the beginning of interaction for a unique solution is illustrated in figure 25. The effect of wall temperature is shown in figure 25(a), the effect of Mach number is shown in figure 25(b), and the effect of Reynolds number is shown in figure 25(c). The relationship between θ_w and x_o/L_c is nonlinear, yielding high values of the wedge angle when the beginning of interaction is near the leading edge of the plate, becoming approximately linear over the middle of the range and curving sharply downward as incipient separation is approached. For a given set of values of M_o, R_o, and T_w/T_{t_o}, an increase in θ_w is accompanied by a decrease in x_o/L_c. For a given angle, decreasing the temperature results in an increase in x_o/L_c (fig. 25(a)). Conversely, an increase in Mach number, M_o, for given values of T_w/T_{t_o} and R_o and θ_w results in an increase in x_o/L_c (fig. 25(b)). Finally, for a given Mach number and temperature ratio, an increase in flat-plate Reynolds number for a given wedge angle results in moving the location

of the beginning of interaction toward the leading edge of the plate (fig. 25(c)). These results agree with the observed experimental behavior for pure laminar separation.

The effect of wedge angle, temperature ratio, Reynolds number, and Mach number on the upstream influence of the wedge as indicated by the upstream extent of separation is shown in figure 26. In figure 26(a) the effect of wedge angle on the distance of the separation point from the wedge, L_{sep}, is shown for a Mach number of 2.0, a Reynolds number of 10^6, and temperature ratios of 1.0, 0.6, and 0.2. This figure clearly illustrates the incipient separation angle as it was defined previously. For small wedge angles, no separation is predicted. At a certain angle, approximately 2.0°, the separation point occurs at the end of the flat plate. That angle was defined previously as the incipient separation angle. As the angle is increased above the incipient separation angle, the extent of separation ahead of the wedge increases nonlinearly until the separation point approaches the leading edge of the plate for large values of the wedge angle.

Figure 26(b) shows that the upstream extent of separation increases with increasing flat-plate Reynolds number for fixed values of the wedge angle, Mach number, and temperature ratio.

The effect of Mach number on the upstream extent of separation is shown in figure 26(c) for a wedge angle of 10°, a Reynolds number of 10^6, and temperature ratios of 0.2, 0.6, and 1.0. At the wedge angle of 10°, the extent of separation appears to approach a constant value at high Mach numbers, and to increase nonlinearly as the Mach number decreases for fixed θ_w, R_o, and T_w/T_{t_o}.

The effect of the various parameters on the total length of the separated region is shown in figure 27. The nature of the relationships between the length of separation and the parameters is basically the same as for the extent of the upstream influence of the wedge as discussed previously. The variation of the length of separation with wedge angle for a fixed Mach number and Reynolds number is shown in figure 27(a). The variation with Reynolds number, for a fixed Mach number and wedge angle, shown in figure 27(b), when compared with the upstream extent of separation shown in figure 26(b), indicates that the extent of the separated region downstream of the beginning of the wedge approaches zero for high Reynolds numbers even though the upstream

extent of separation is nearly equal to the flat-plate length for a wedge angle of 10°. This can be explained by the fact that the boundary-layer thickness decreases with increasing Reynolds number so that the slope of the dividing streamline is small compared to the wedge angle. For small Reynolds numbers the separation and reattachment points are close to the corner. As the Reynolds number is increased, the separation point moves forward as indicated by figure 26(b). At the same time, the slope of the dividing streamline decreases due to the thinning boundary layer. The forward movement of the separation point and the decrease in the slope of the dividing streamline are compensating effects. For a certain range of Reynolds numbers, the forward movement of the separation point dominates and the reattachment point moves away from the corner. Then for a higher range of Reynolds numbers, the decrease in the slope of the dividing streamline dominates and the reattachment point moves toward the corner as the Reynolds number increases.

In figure 27(c) is shown the variation with Mach number of the length of the separated region for $\theta_w = 10^{\circ}$ and $R_o = 10^6$. As the Mach number is increased, L_t/L_c decreases nonlinearly, approaching a constant value at high Mach numbers for a given temperature ratio.

In figure 28 the variations of the separation pressure and the plateau pressure with Reynolds number are shown for Mach numbers of 2.0, 6.0, and 10.0 and temperature ratios of 0.2, 0.6, and 1.0. The variations are presented in terms of the quantities $\left[(p_s/p_o) - 1\right]$ and $\left[(p_p/p_o) - 1\right]$ respectively. These data show that the theory predicts the typical logarithmic variations of the pressure rise quantities as discussed in reference 18. The data are slightly dependent on the wall temperature, with the dependence increasing at high Mach numbers. The quantities decrease with increasing Reynolds number for given values of T_w/T_{t_o} and M_o. For fixed R_o and T_w/T_{t_o}, the quantities increase with increasing Mach number. Both quantities exhibit non-monotonic behavior and slight dependence on T_w/T_{t_o} for fixed M_o and R_o.

In figure 29, the effects of Mach number, Reynolds number, and temperature ratio on the entire boundary-layer pressure distribution are shown for a wedge angle of 10°. In figure 29(a), the effect of Mach number is shown for a temperature ratio of 0.6 and Reynolds number of 10^6. For low Mach numbers, a long pressure plateau is produced which

shortens and finally disappears at high Mach numbers, whereas, the total length of the separated region approaches a constant value at high Mach numbers as shown in figure 27(c). The final pressure increases with increasing Mach number. For the low Mach number case, $M_o = 2.0$, shown in figure 29, the calculated final pressure is nearly equal to the inviscid pressure for $M_o = 2.0$, while the difference between the calculated and inviscid pressures increases with increasing Mach number. The same temperature ratio is used in figure 29(b) where the effect of Reynolds number is shown for a Mach number of 6.0. In this case, the length of the plateau region increases with increasing R_o as does the steepness of the pressure rise on the wedge. The effect of increasing Reynolds number on the reattachment location, as discussed in conjunction with figure 27(b), can also be noted in figure 29(b). As R_o increases, the reattachment point first moves away from the corner, then as the pressure rise steepens, the reattachment is forced to move back toward the corner. The separation point moves toward the leading edge of the plate monotonically as the Reynolds number increases. Finally, the effect of temperature ratio is shown in figure 29(c) for a Mach number of 6.0 and Reynolds number of 10^6. As the temperature ratio decreases, the separation point moves toward the corner, thus shortening the extent of separation. This clearly shows the significance of cooled walls for reducing the extent of separation.

The pressure distributions shown in figure 29 were obtained by interpolating the systematic computer runs to obtain data at a wedge angle of 10^o. An approximate pressure distribution for any set of conditions in the range covered by this study can be plotted by interpolating from table I to obtain values of x_o/L_c, x_s/L_c, x_p/L_c, x_R/L_c, and x_F/L_c and the pressure ratios at those points. Knowing the general shape of a boundary layer pressure distribution, one can obtain a reasonable representation of the pressure distribution with the data at those five points for any flow conditions.

8. CONCLUDING REMARKS

This report extends the analysis of references 1 through 4 to the calculation of the boundary layer downstream of reattachment and the development of a unique solution through application of a downstream boundary condition. A predictive method is thus developed for calculating separated laminar flows with no prior knowledge of the flow pattern.

Several comparisons are presented showing good agreement between the theoretical pressure distributions and those measured experimentally on both flat-plate-wedge and axisymmetric cylinder-flare configurations. On the flat-plate-wedge configuration, a non-Blasius initial velocity profile resulting from a favorable pressure gradient upstream of the beginning of interaction was found to decrease the predicted extent of separation from that predicted with a Blasius initial profile. This result is consistent with the fact that the theory using a Blasius initial profile predicts a longer separated region than indicated by the data for cases where significant favorable pressure gradients existed near the leading edge of the plate.

For axisymmetric configurations, the length of an equivalent hollow cylinder is required as an additional parameter. This parameter must be determined by an auxiliary calculation. In the work described in this report, the cylinder length was determined such that the experimental and theoretical separation points approximately coincided. This procedure produced good comparisons with data for the pressure distributions on ogive-cylinder-flare bodies and fair comparisons for a blunt-nosed cylinder-flare configuration. The theory produced fair agreement between predicted and experimental heat transfer rates. It is possible to improve the prediction of heat-transfer rates by increasing the order of coupling between the velocity and temperature fields.

Systematic variation of the Mach number, temperature ratio and unit Reynolds number at the beginning of interaction as well as the location of the beginning of interaction provided general information as to the effect of the flow conditions on the extent of separation, and on the pressure distribution. A wedge angle for incipient separation is predicted for both the two-dimensional and axisymmetric case as determined by the simultaneous occurrence of the separation and reattachment points at the end of the flat plate or cylinder.

Table I.- Calculated boundary-layer properties.

M_o	R_o	$\frac{T_w}{T_{t_o}}$	$\frac{x_o}{L_c}$	θ_w	$\frac{\delta_o^*}{L_c}$ $\times 10^3$	$\frac{\delta_o^{**}}{L_c}$ $\times 10^3$	c_{f_o} $\times 10^3$	$\frac{x_S}{L_c}$	$\frac{p_S}{p_o}$	$\frac{x_P}{L_c}$	$\frac{p_P}{p_o}$	$\frac{p_c}{p_o}$	$\frac{x_R}{L_c}$	$\frac{p_R}{p_o}$	$\frac{x_F}{L_c}$	$\frac{p_F}{p_o}$
2.0	10^4	0.2	0.25	16.25	5.76	3.33	13.30	0.380	1.38	0.470	1.51	1.51	1.34	2.10	1.53	2.19
			.40	14.39	7.28	4.21	10.50	.576	1.34	.682	1.46	1.46	1.30	1.94	1.55	2.06
			.50	13.25	8.14	4.71	9.40	.703	1.32	.821	1.43	1.43	1.25	1.82	1.42	1.91
		1.0	.15	14.69	14.10	2.58	17.20	.386	1.24	.981	1.43	1.43	2.03	1.79	2.97	1.91
			.25	12.19	18.10	3.33	13.30	.596	1.23	-----	-----	1.38	1.64	1.62	2.41	1.75
			.30	11.06	19.90	3.65	12.10	.697	1.22	-----	-----	1.35	1.43	1.52	2.05	1.62
			.40	8.36	23.00	4.21	10.50	.892	1.21	-----	-----	1.26	1.13	1.32	1.71	1.43
	10^5	0.2	.25	12.91	1.82	1.05	4.20	.307	1.21	.351	1.29	1.29	1.18	1.90	1.25	1.97
			.35	12.01	2.15	1.25	3.55	.421	1.19	.472	1.27	1.27	1.16	1.79	1.27	1.87
			.50	10.54	2.58	1.49	2.98	.589	1.17	.642	1.24	1.24	1.15	1.68	1.22	1.76
		0.6	.20	11.56	3.38	.940	4.70	.309	1.18	.420	1.28	1.28	1.34	1.71	1.47	1.76
			.40	9.38	4.78	1.33	3.23	.577	1.15	.740	1.24	1.24	1.31	1.54	1.48	1.60
			.50	8.31	5.35	1.48	2.97	.707	1.15	.888	1.23	1.23	1.29	1.48	1.47	1.55
		1.0	.10	11.94	3.63	.666	6.65	.197	1.18	.365	1.30	1.30	1.58	1.72	1.87	1.80
			.25	9.69	5.74	1.05	4.20	.404	1.15	.710	1.25	1.25	1.52	1.55	1.83	1.61
			.35	8.56	6.79	1.25	3.55	.593	1.14	.910	1.23	1.23	1.46	1.47	1.74	1.52
			.50	6.51	8.11	1.49	2.97	.815	1.13	-----	-----	1.20	1.24	1.31	1.54	1.38
	10^6	0.2	.025	13.81	.182	.105	4.20	.031	1.21	.045	1.29	1.29	1.08	1.98	1.10	1.99
			.15	11.94	.446	.258	1.72	.168	1.13	.191	1.18	1.18	1.08	1.82	1.10	1.84
			.25	10.81	.576	.333	1.33	.275	1.11	.291	1.16	1.16	1.08	1.73	1.12	1.78
			.35	10.00	.680	.393	1.13	.380	1.10	.553	1.14	1.14	1.08	1.66	1.14	1.70
			.50	8.79	.814	.471	.940	.539	1.09	.560	1.13	1.13	1.07	1.56	1.11	1.59
			.75	6.56	.997	.576	.767	.801	1.08	.831	1.11	1.11	1.05	1.38	1.07	1.39
			.85	5.26	1.06	.614	.721	.905	1.08	.931	1.11	1.11	1.04	1.29	1.07	1.32
			.92	3.66	1.10	.638	.693	.978	1.08	-----	-----	1.11	1.02	1.19	1.05	1.23
			.93	3.26	1.11	.642	.689	.989	1.08	-----	-----	1.11	1.01	1.15	1.03	1.17
			.94	2.19	1.12	.645	.686	.999	1.08	-----	-----	1.08	1.00	1.09	1.03	1.13
		0.4	.025	13.06	.280	.105	4.20	.034	1.18	.045	1.28	1.28	1.13	1.92	1.17	1.97
			.25	9.69	.885	.333	1.33	.295	1.10	.330	1.16	1.16	1.11	1.62	1.16	1.65
			.50	7.56	1.25	.471	.940	.572	1.09	.621	1.13	1.13	1.11	1.47	1.16	1.51
			.75	5.36	1.53	.576	.767	.844	1.08	.891	1.12	1.12	1.08	1.29	1.11	1.31
			.87	3.34	1.65	.621	.713	.974	1.08	-----	-----	1.13	1.02	1.15	1.10	1.20
		0.6	.025	12.56	.378	.105	4.20	.038	1.17	.066	1.27	1.27	1.16	1.86	1.23	1.90
			.25	8.89	1.20	.333	1.33	.314	1.10	.371	1.15	1.15	1.16	1.56	1.23	1.61
			.50	6.74	1.69	.471	.940	.604	1.08	.681	1.13	1.13	1.14	1.39	1.21	1.42
			.75	4.49	2.07	.576	.767	.887	1.08	.971	1.12	1.12	1.10	1.23	1.21	1.27
			.83	2.86	2.18	.606	.730	.978	1.07	-----	-----	1.11	1.02	1.13	1.12	1.16
		0.8	.025	11.89	.476	.105	4.20	.041	1.16	.066	1.26	1.26	1.20	1.79	1.28	1.83
			.25	8.19	1.51	.333	1.33	.333	1.10	.412	1.15	1.15	1.21	1.52	1.28	1.55
			.50	6.06	2.13	.471	.940	.635	1.08	.740	1.13	1.13	1.19	1.34	1.33	1.39
			.75	3.64	2.61	.576	.767	.930	1.07	-----	-----	1.11	1.08	1.17	1.19	1.21
			.79	2.69	2.68	.592	.748	.977	1.07	-----	-----	1.10	1.02	1.11	1.16	1.15

Table I.- Continued.

M_o	R_o	$\frac{T_w}{T_{t_o}}$	$\frac{x_o}{L_c}$	θ_w	$\frac{\delta_o^*}{L_c}$ $\times 10^3$	$\frac{\delta_o^{**}}{L_c}$ $\times 10^3$	c_{f_o} $\times 10^3$	$\frac{x_S}{L_c}$	$\frac{p_S}{p_o}$	$\frac{x_P}{L_c}$	$\frac{p_P}{p_o}$	$\frac{p_c}{p_o}$	$\frac{x_R}{L_c}$	$\frac{p_R}{p_o}$	$\frac{x_F}{L_c}$	$\frac{p_F}{p_o}$
2.0	10^6	1.0	.025	11.71	.574	.105	4.20	.044	1.15	.086	1.25	1.25	1.24	1.77	1.31	1.82
			.050	10.41	.811	.149	2.97	.082	1.13	.131	1.21	1.21	1.26	1.69	1.32	1.72
			.077	10.00	1.01	.185	2.39	.120	1.12	.283	1.19	1.19	1.26	1.64	1.35	1.69
			.10	9.56	1.15	.211	2.10	.152	1.11	.211	1.18	1.18	1.25	1.60	1.40	1.63
			.25	7.56	1.81	.333	1.33	.351	1.09	.450	1.15	1.15	1.26	1.46	1.35	1.50
			.40	6.34	2.30	.421	1.05	.542	1.08	.666	1.13	1.13	1.24	1.36	1.30	1.40
			.50	5.64	2.57	.471	.940	.666	1.08	.805	1.13	1.13	1.22	1.30	1.30	1.32
			.60	4.84	2.81	.516	.858	.789	1.08	.940	1.12	1.12	1.20	1.25	1.30	1.28
			.70	3.59	3.04	.557	.794	.912	1.07	-----	-----	1.11	1.11	1.18	1.22	1.22
			.75	2.71	3.14	.576	.767	.972	1.07	-----	-----	1.09	1.03	1.11	1.13	1.14
			.76	2.41	3.16	.580	.762	.984	1.07	-----	-----	1.08	1.02	1.09	1.16	1.13
	10^7	0.2	.10	10.69	.115	.067	.665	.106	1.08	.121	1.11	1.11	1.04	1.74	1.05	1.77
			.25	9.44	.182	.105	.420	.261	1.06	.270	1.08	1.08	1.04	1.64	1.05	1.66
			.50	7.64	.258	.149	.297	.517	1.05	.541	1.07	1.07	1.03	1.49	1.05	1.51
			.75	5.56	.315	.182	.243	.772	1.05	.791	1.06	1.06	1.02	1.33	1.03	1.33
			.85	4.39	.336	.194	.228	.873	1.05	.891	1.06	1.06	1.02	1.26	1.03	1.28
		0.6	.25	7.81	.378	.105	.420	.282	1.06	.310	1.08	1.08	1.06	1.48	1.07	1.48
			.50	5.69	.535	.149	.297	.551	1.05	.580	1.07	1.07	1.06	1.33	1.07	1.34
			.75	3.69	.655	.182	.243	.818	1.04	.850	1.06	1.06	1.06	1.21	1.09	1.23
		1.0	.10	7.69	.363	.067	.665	.127	1.07	.162	1.11	1.11	1.10	1.48	1.14	1.50
			.25	6.31	.584	.105	.420	.302	1.05	.352	1.09	1.09	1.11	1.38	1.14	1.40
			.50	4.54	.811	.149	.297	.586	1.05	.640	1.07	1.07	1.11	1.26	1.20	1.28
			.75	2.99	.994	.182	.243	.864	1.04	.931	1.06	1.06	1.09	1.15	1.12	1.16
4.0	10^4	0.2	.25	22.50	17.90	3.33	13.30	.310	1.71	.472	2.41	2.41	1.49	4.89	1.77	5.49
			.35	21.31	21.10	3.94	11.20	.427	1.65	.610	2.29	2.29	1.46	4.52	1.67	5.03
			.50	19.38	25.30	4.71	9.40	.599	1.60	.825	2.17	2.17	1.38	3.93	1.60	4.44
	10^5	1.0	.25	13.19	14.80	1.05	4.20	.438	1.32	.902	1.65	1.65	1.74	2.59	2.16	2.90
			.50	8.69	21.00	1.50	2.97	.828	1.28	-----	-----	1.46	1.24	1.73	1.63	1.97
	10^6	0.2	.25	13.31	1.89	.333	1.33	.268	1.22	.290	1.40	1.40	1.12	3.04	1.17	3.20
			.50	10.96	2.53	.471	.940	.531	1.19	.561	1.33	1.33	1.11	2.49	1.14	2.61
			.61	10.00	2.79	.519	.852	.644	1.18	-----	-----	1.31	1.11	2.33	1.15	2.50
			.75	8.54	3.10	.576	.767	.791	1.17	.830	1.30	1.30	1.09	2.01	1.12	2.11
			.85	7.14	3.30	.614	.721	.895	1.17	.951	1.29	1.29	1.07	1.77	1.10	1.87
		1.0	.025	14.56	1.78	.105	4.20	.044	1.00	.105	1.65	1.65	1.39	3.10	1.48	3.26
			.23	10.00	4.50	.320	1.38	.342	1.21	.635	1.40	1.40	1.44	2.27	1.58	2.43
			.25	9.79	4.67	.333	1.33	.367	1.21	.541	1.39	1.39	1.38	2.20	1.57	2.34
			.50	7.26	6.61	.471	.940	.701	1.18	.973	1.33	1.33	1.32	1.76	1.49	1.87
			.70	3.94	7.83	.557	.794	.961	1.17	-----	-----	1.22	1.05	1.27	1.25	1.39

Table I.- Continued.

M_o	R_o	$\frac{T_w}{T_{t_o}}$	$\frac{x_o}{L_c}$	θ_w	$\frac{\delta_o^*}{L_c}$ $\times 10^3$	$\frac{\delta_o^{**}}{L_c}$ $\times 10^3$	c_{f_o} $\times 10^3$	$\frac{x_S}{L_c}$	$\frac{p_S}{p_o}$	$\frac{x_P}{L_c}$	$\frac{p_P}{p_o}$	$\frac{p_c}{p_o}$	$\frac{x_R}{L_c}$	$\frac{p_R}{p_o}$	$\frac{x_F}{L_c}$	$\frac{p_F}{p_o}$
6.0	10^5	0.2	.25	18.19	12.00	1.05	4.20	.270	1.41	.391	2.36	2.36	1.39	6.54	1.54	7.48
			.50	15.81	17.00	1.49	2.97	.535	1.36	.720	2.13	2.13	1.33	5.17	1.49	6.24
			.60	14.94	18.60	1.63	2.71	.640	1.35	.850	2.08	2.08	1.30	4.62	1.44	5.44
		0.6	.25	16.50	20.95	1.05	4.20	.366	1.50	.772	2.26	2.26	1.72	4.90	1.99	5.55
			.50	12.75	29.60	1.49	2.97	.709	1.45	-----	----	2.00	1.40	3.26	1.67	4.08
			.60	10.63	32.50	1.63	2.71	.884	1.44	-----	----	1.80	1.23	2.44	1.44	2.86
		1.0	.40	11.94	37.80	1.33	3.32	.693	1.40	-----	----	1.84	1.52	2.74	2.13	3.51
			.50	9.69	42.30	1.49	2.97	.858	1.39	-----	----	1.61	1.24	1.99	1.81	2.56
	10^6	0.2	.25	13.56	3.81	.333	1.33	.263	1.27	.314	1.73	1.73	1.20	4.75	1.27	5.33
			.50	11.46	5.38	.471	.940	.524	1.24	.600	1.61	1.61	1.18	3.71	1.27	4.84
			.67	10.00	6.25	.547	.809	.705	1.23	.878	1.56	1.56	1.15	3.09	1.22	3.46
			.75	9.29	6.59	.576	.767	.783	1.22	.871	1.54	1.54	1.14	2.82	1.21	3.19
			.85	7.94	7.02	.614	.721	.886	1.22	.990	1.52	1.52	1.10	2.34	1.15	2.57
			.90	6.69	7.22	.631	.700	.938	1.22	-----	----	1.50	1.07	1.99	1.13	2.25
		0.6	.25	11.81	6.63	.333	1.33	.331	1.35	.501	1.74	1.74	1.38	3.66	1.47	3.92
			.50	9.31	9.37	.471	.940	.642	1.30	.892	1.62	1.62	1.34	2.79	1.56	3.23
			.70	6.44	11.10	.557	.794	.887	1.29	-----	----	1.51	1.15	1.90	1.31	2.25
		1.0	.05	14.44	4.23	.149	2.97	.058	1.39	.230	1.97	1.97	1.61	4.22	1.74	4.50
			.25	10.54	9.45	.333	1.33	.390	1.32	.733	1.69	1.69	1.59	3.07	1.78	3.34
			.29	10.00	10.20	.360	1.23	.453	1.31	.908	1.67	1.67	1.57	2.91	1.81	3.20
			.50	7.39	13.40	.471	.940	.750	1.28	-----	----	1.55	1.35	2.14	1.61	2.49
			.60	5.69	14.60	.516	.858	.890	1.27	-----	----	1.43	1.15	1.66	1.60	2.03
	10^7	0.2	.10	12.19	.761	.067	.665	.104	1.21	.121	1.50	1.50	1.10	4.37	1.12	4.58
			.50	8.69	1.70	.149	.297	.515	1.16	.541	1.32	1.32	1.09	2.91	1.13	3.16
			.75	6.69	2.08	.182	.243	.770	1.14	.811	1.28	1.28	1.08	2.27	1.10	2.47
		0.6	.25	8.94	2.10	.105	.420	.302	1.22	.370	1.42	1.42	1.19	2.98	1.25	3.23
			.50	6.88	2.97	.149	.297	.589	1.19	.702	1.35	1.35	1.19	2.29	1.25	2.48
			.75	4.69	3.63	.182	.243	.872	1.17	.993	1.32	1.32	1.13	1.69	1.20	1.80
		1.0	.10	9.56	1.89	.067	.665	.144	1.25	.222	1.51	1.51	1.28	3.07	1.33	3.20
			.50	5.69	4.23	.149	.297	.660	1.18	.862	1.34	1.34	1.28	1.95	1.46	2.14
			.75	2.69	5.18	.182	.243	.969	1.17	-----	----	1.23	1.04	1.27	1.21	1.43
8.0	10^6	0.2	.25	13.74	6.63	.333	1.33	.260	1.27	.350	2.12	2.12	1.29	6.84	1.37	7.82
			.50	11.91	9.38	.471	.940	.519	1.26	.660	1.93	1.93	1.25	5.25	1.32	5.98
			.73	10.00	11.30	.569	.778	.756	1.24	.931	1.84	1.84	1.19	3.88	1.27	4.53
			.75	9.71	11.50	.576	.767	.776	1.24	.950	1.83	1.83	1.19	3.78	1.27	4.63
			.85	8.29	12.20	.614	.721	.880	1.24	-----	----	1.80	1.13	2.91	1.22	3.71
		1.0	.15	12.64	12.50	.258	1.72	.250	1.41	.671	1.97	1.97	1.61	4.22	1.74	4.50
			.25	11.16	16.10	.333	1.33	.406	1.39	.986	1.69	1.69	1.59	3.07	1.78	3.34
			.34	10.00	18.70	.385	1.15	.538	1.38	-----	----	1.93	1.63	3.45	1.92	3.93
			.50	7.54	22.80	.471	.940	.787	1.36	-----	----	1.55	1.35	2.14	1.61	2.49
			.55	6.69	24.00	.494	.896	.861	1.36	-----	----	1.59	1.22	1.99	1.64	2.51

Table I.- Concluded.

M_o	R_o	$\frac{T_w}{T_{t_o}}$	$\frac{x_o}{L_c}$	θ_w	$\frac{\delta_o^*}{L_c}$ $\times 10^3$	$\frac{\delta_o^{**}}{L_c}$ $\times 10^3$	c_{f_o} $\times 10^3$	$\frac{x_s}{L_c}$	$\frac{p_s}{p_o}$	$\frac{x_p}{L_c}$	$\frac{p_p}{p_o}$	$\frac{p_c}{p_o}$	$\frac{x_R}{L_c}$	$\frac{p_R}{p_o}$	$\frac{x_F}{L_c}$	$\frac{p_F}{p_o}$
10.0	10^5	0.2	.50	17.94	45.90	1.49	2.97	.519	1.29	-----	----	3.36	1.57	11.99	1.75	16.50
			.60	17.06	50.30	1.63	2.71	.623	1.29	-----	----	3.16	1.45	9.82	1.73	15.00
			.80	14.63	58.10	1.88	2.35	.830	1.29	-----	----	2.44	1.24	5.28	1.39	7.39
	10^6	0.2	.25	14.06	10.30	.333	1.33	.256	1.27	.410	2.57	2.57	1.40	9.81	1.51	12.16
			.50	12.19	14.50	.471	.940	.516	1.25	.745	2.30	2.30	1.34	7.28	1.45	9.22
			.75	10.19	17.80	.576	.767	.772	1.24	-----	----	2.16	1.23	4.89	1.33	6.43
			.77	10.00	18.00	.584	.758	.792	1.24	-----	----	2.11	1.21	4.60	1.35	6.32
			.85	8.82	18.90	.614	.721	.875	1.24	-----	----	2.01	1.14	3.38	1.21	4.07
		0.6	.25	12.81	17.49	.333	1.33	.342	1.49	.774	2.52	2.52	1.73	6.95	1.98	8.29
			.50	10.06	24.70	.471	.940	.671	1.45	-----	----	2.21	1.45	4.40	1.85	6.07
			.70	6.69	29.30	.570	.790	.931	1.44	-----	----	1.65	1.11	2.01	1.50	3.03
		1.0	.25	11.69	24.70	.333	1.33	.417	1.44	-----	----	2.32	1.99	5.18	2.42	6.49
			.37	10.00	30.02	.404	1.09	.606	1.43	-----	----	2.07	1.68	3.88	2.29	5.25
			.50	7.99	35.00	.471	.940	.811	1.42	-----	----	1.76	1.35	2.52	1.85	3.35
			.55	7.06	36.70	.494	.896	.889	1.41	-----	----	1.63	1.21	2.03	1.75	2.83
	10^7	0.2	.50	8.69	4.59	.149	.297	.512	1.20	.600	1.70	1.70	1.18	4.79	1.22	5.33
			.75	6.94	5.62	.182	.243	.767	1.20	.878	1.63	1.63	1.15	3.46	1.20	4.12
		0.6	.25	8.81	5.53	.105	.420	.321	1.37	.511	1.89	1.89	1.40	4.80	1.55	5.65
			.50	6.94	7.82	.149	.297	.628	1.33	.915	1.75	1.75	1.36	3.44	1.47	4.04
			.60	6.19	8.57	.163	.271	.749	1.32	-----	----	1.71	1.27	2.82	1.38	3.19
		1.0	.25	7.81	7.82	.105	.420	.379	1.34	.753	1.84	1.84	1.63	3.89	1.83	4.50
			.50	5.56	11.10	.149	.297	.734	1.31	-----	----	1.67	1.37	2.49	1.62	3.00

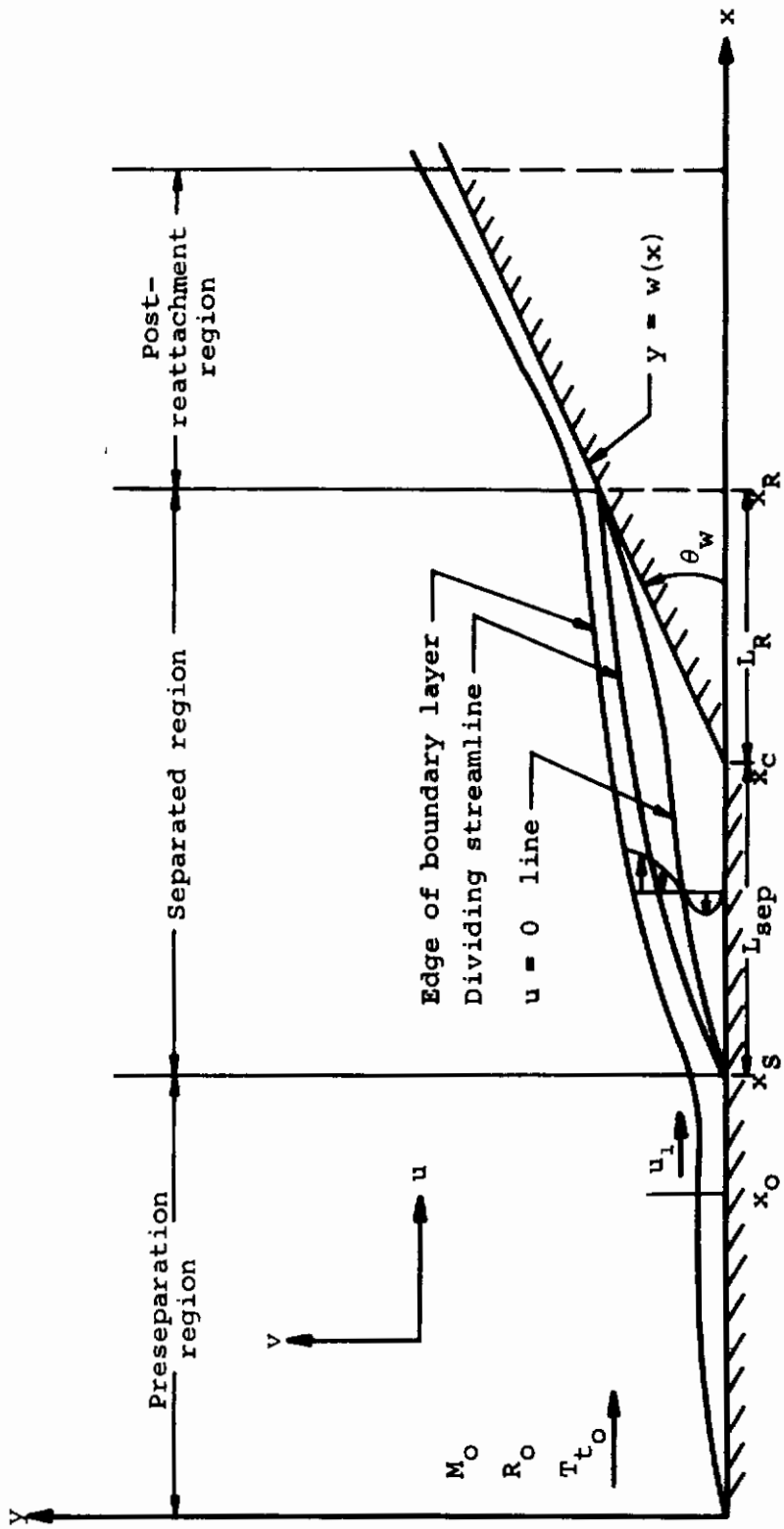

Figure 1.- Separated flow over a flat plate followed by a wedge.

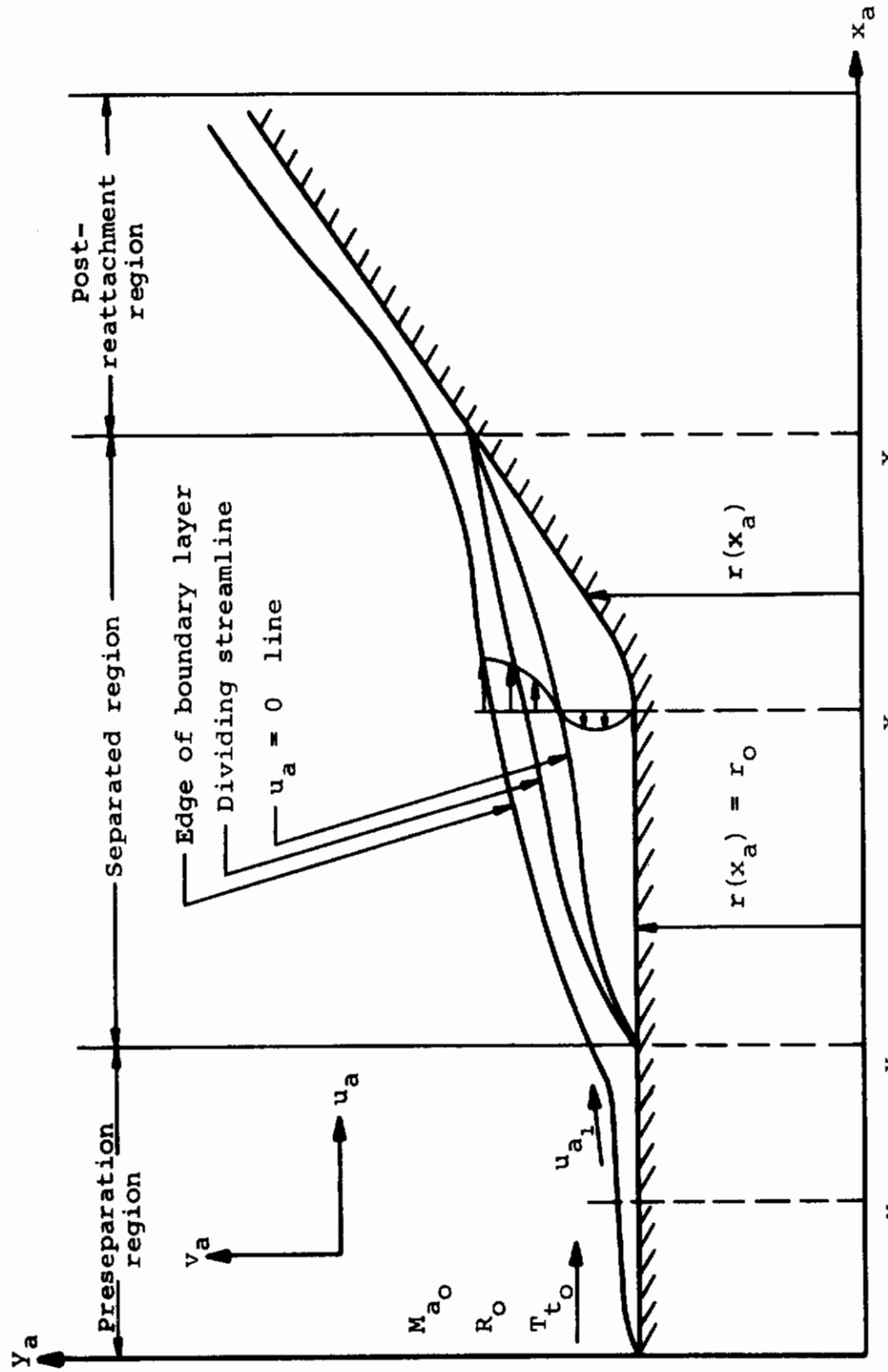

Figure 2.- Separated flow over an axisymmetric body.

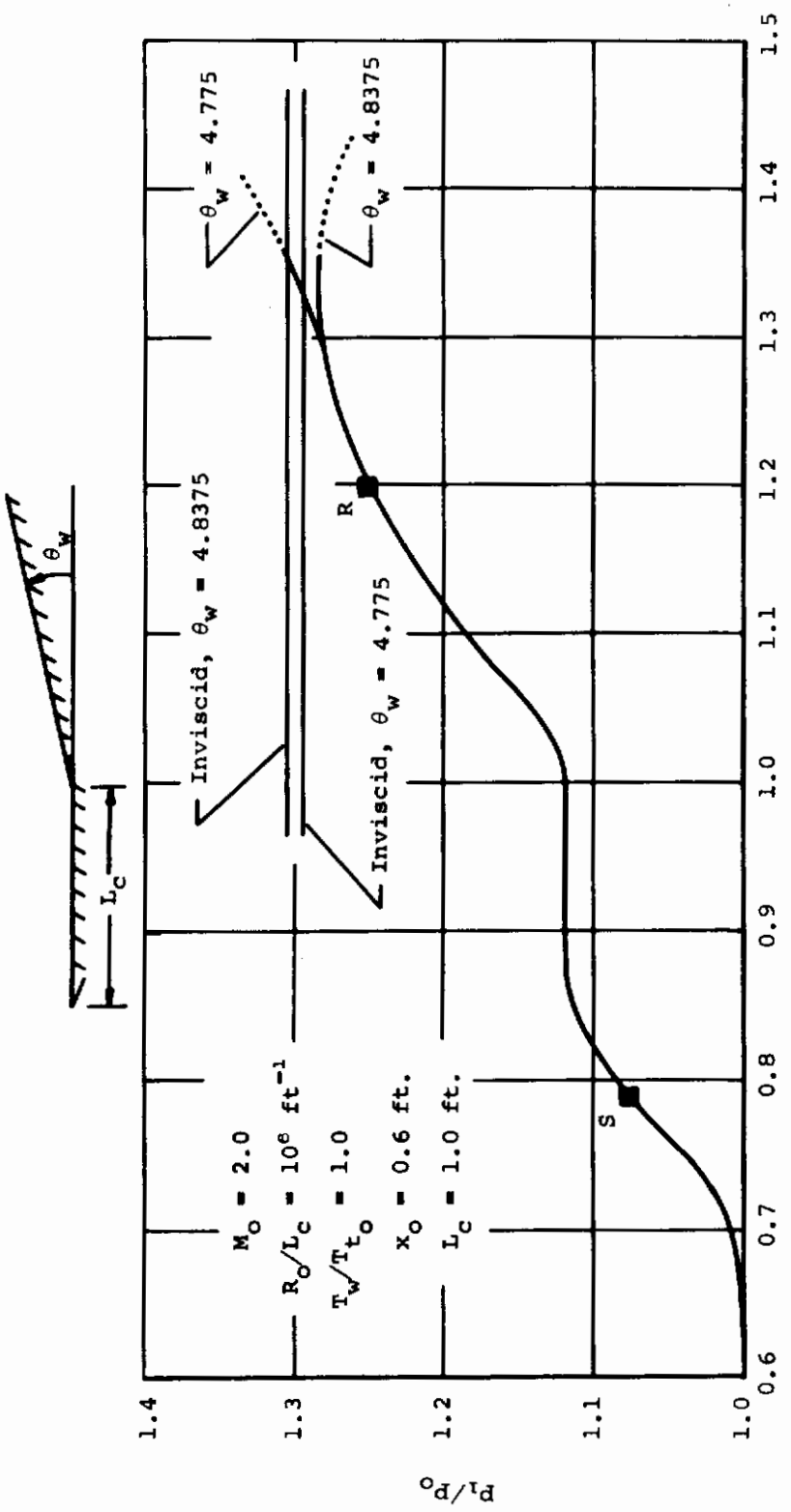

Figure 3.- Typical boundary-layer pressure distributions on a flat-plate-wedge for two wedge angles.

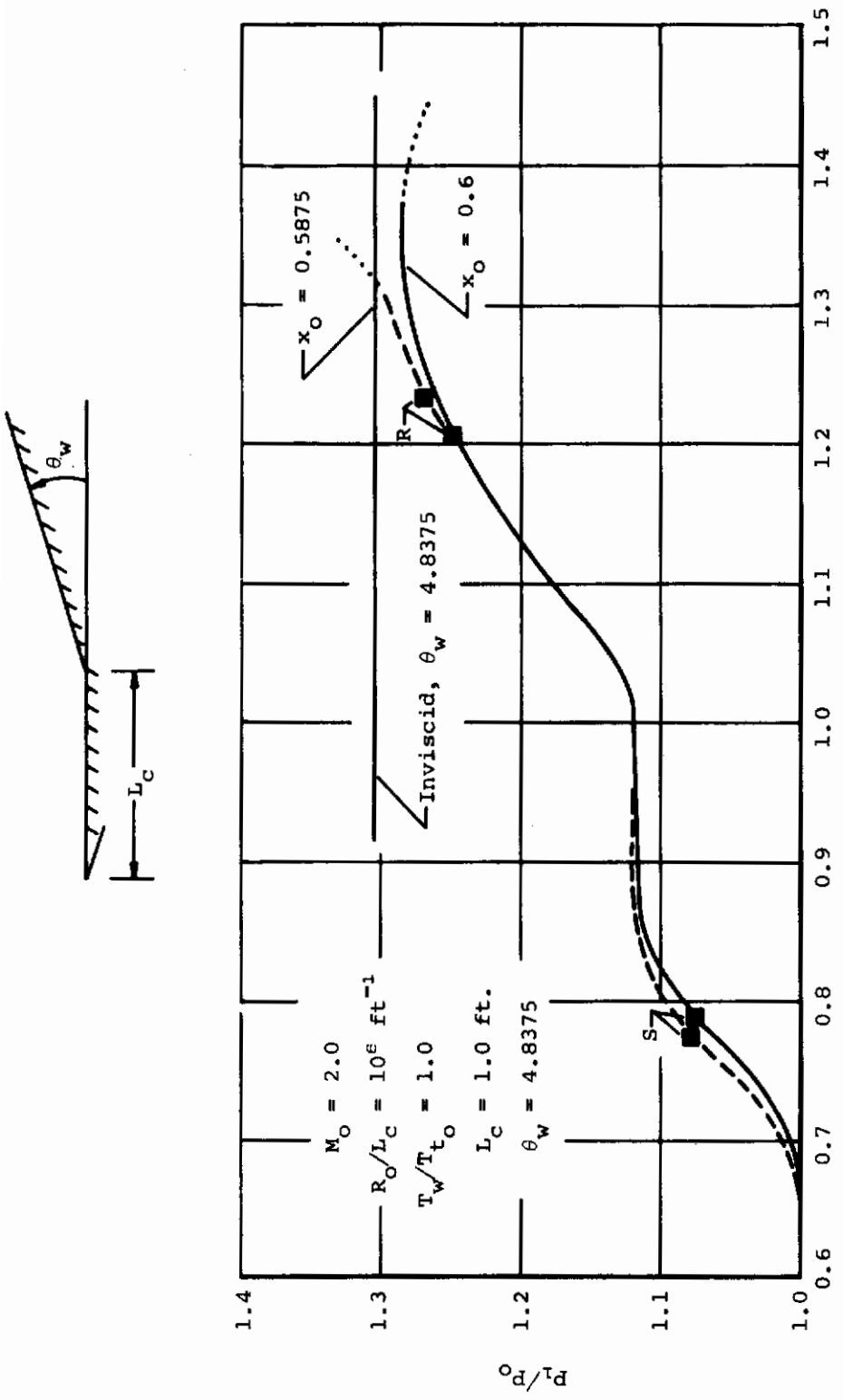

Figure 4.- Typical boundary-layer pressure distributions on a flat-plate-wedge for two locations of the beginning of interaction.

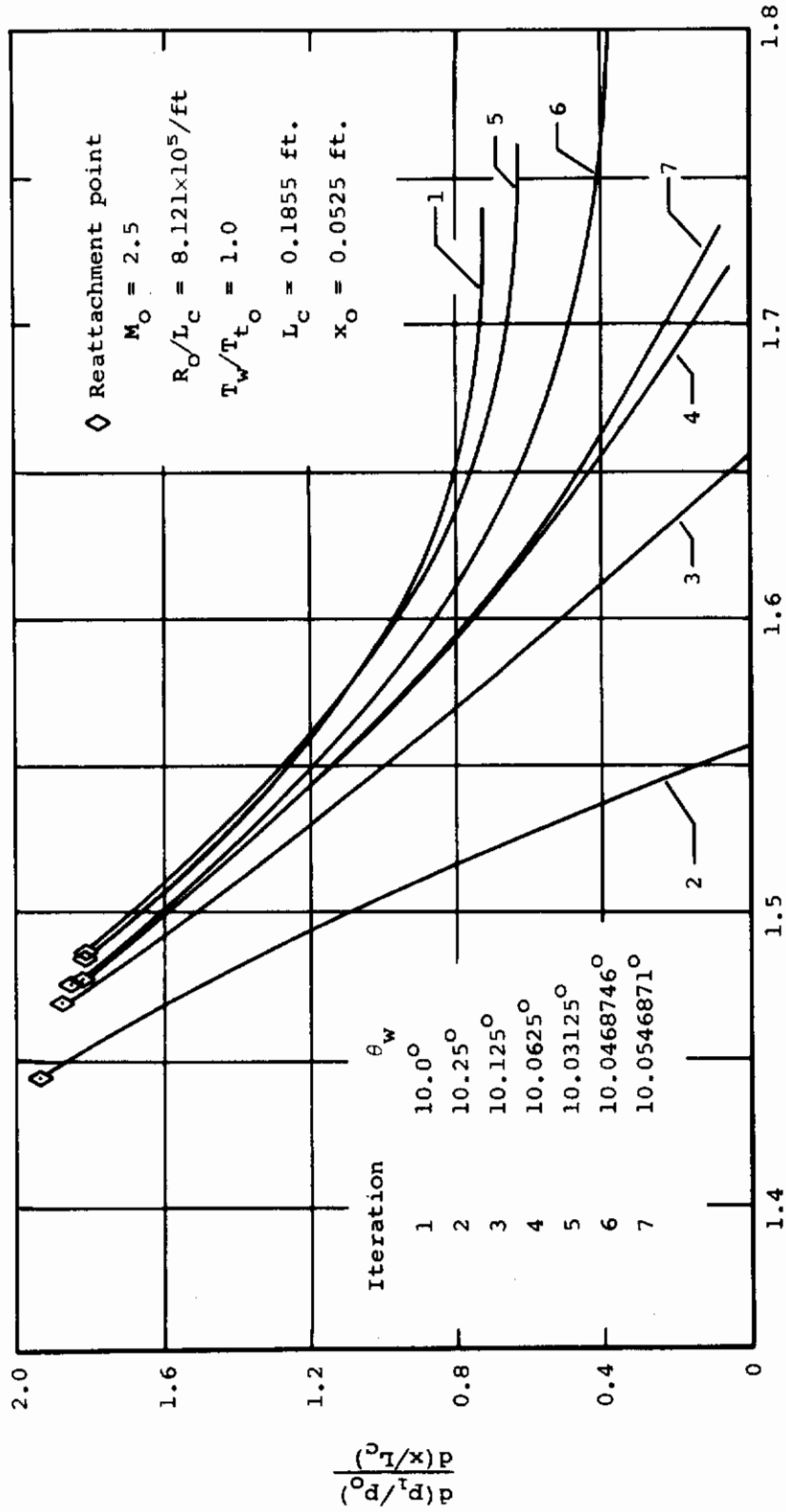

Figure 5.- Pressure gradient in vicinity of downstream end of interaction region.

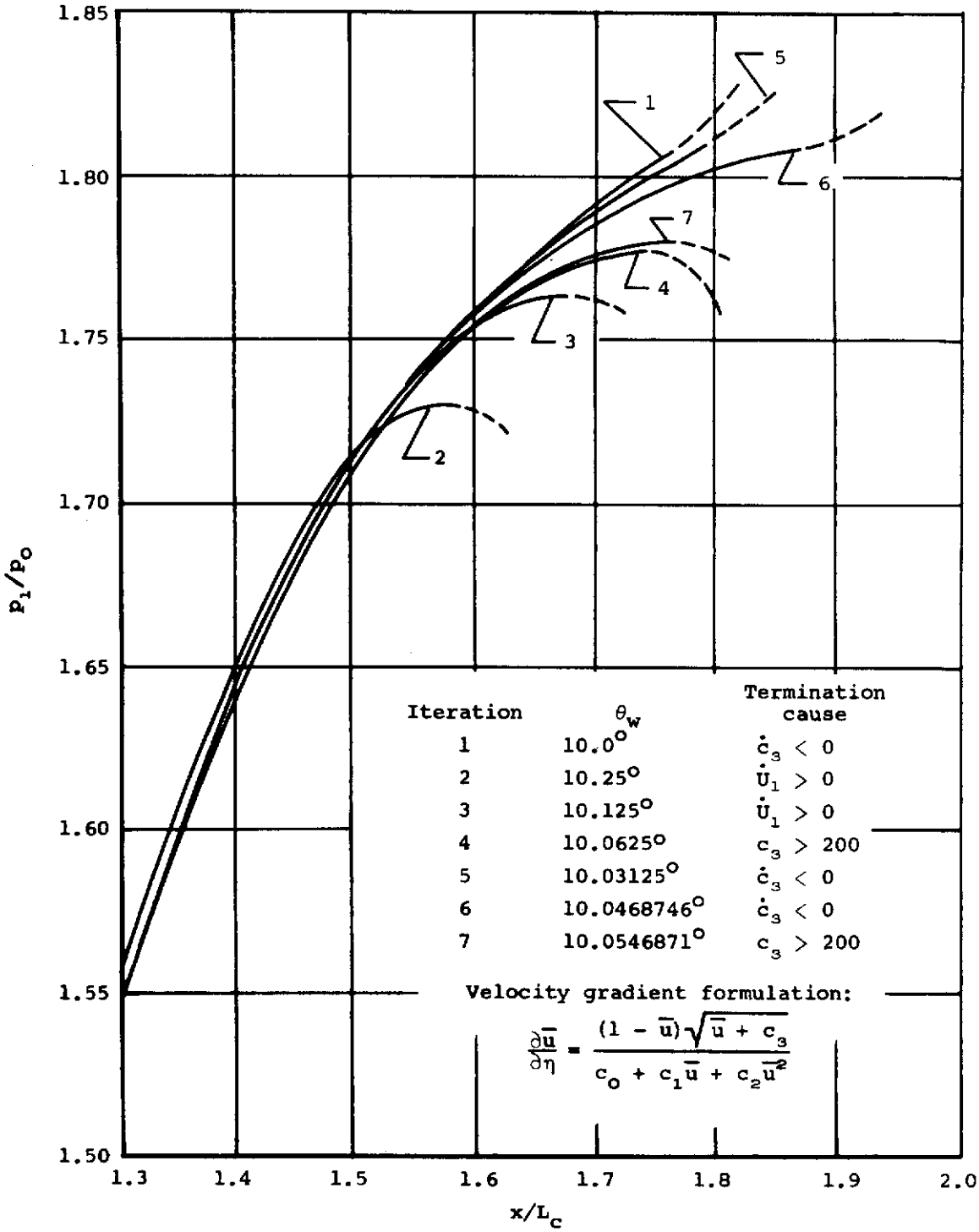

Figure 6.- Pressure distributions at downstream end of interaction region.

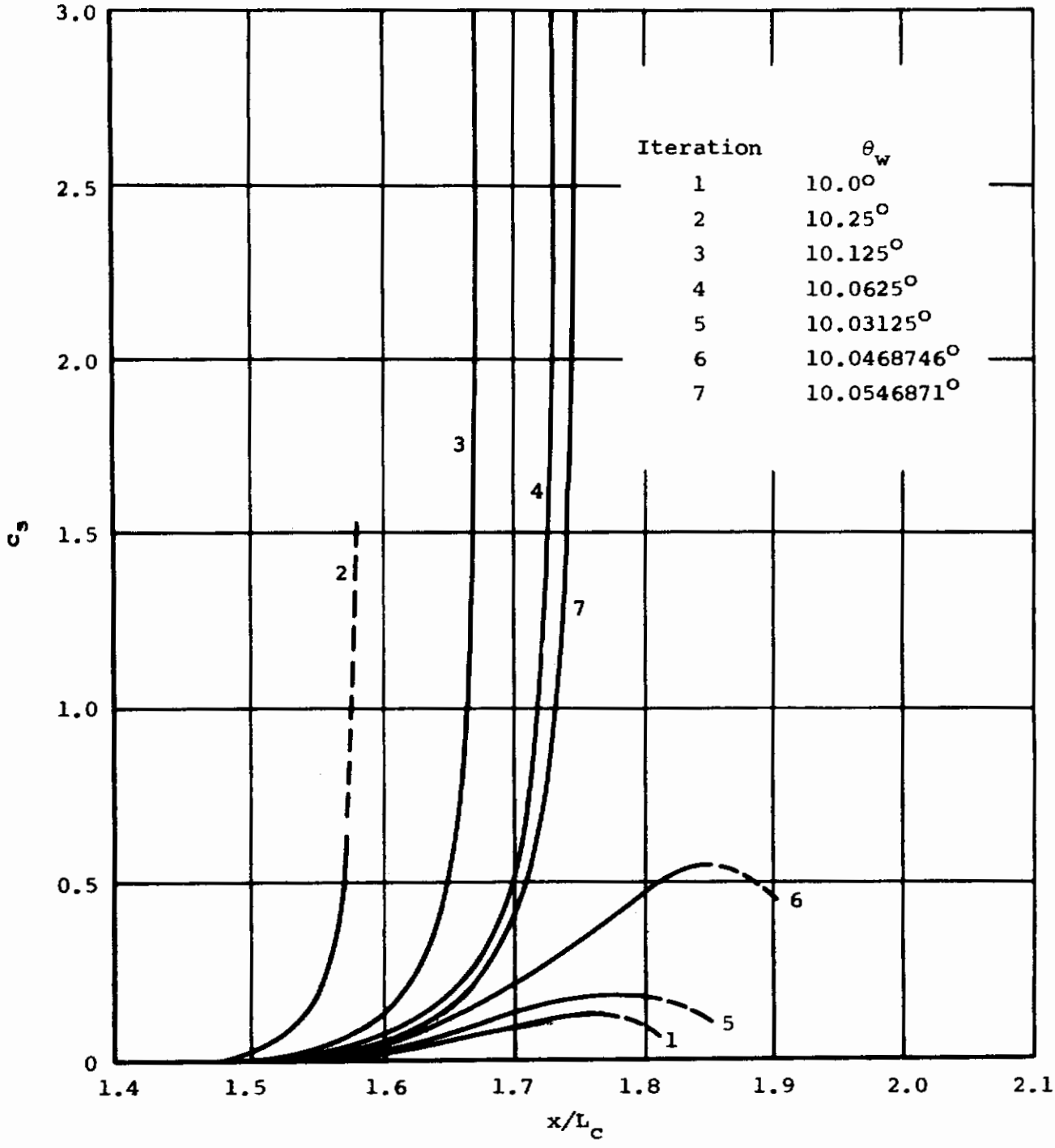

Figure 7.- Variation of velocity profile parameter, c_3, near downstream end of interaction region.

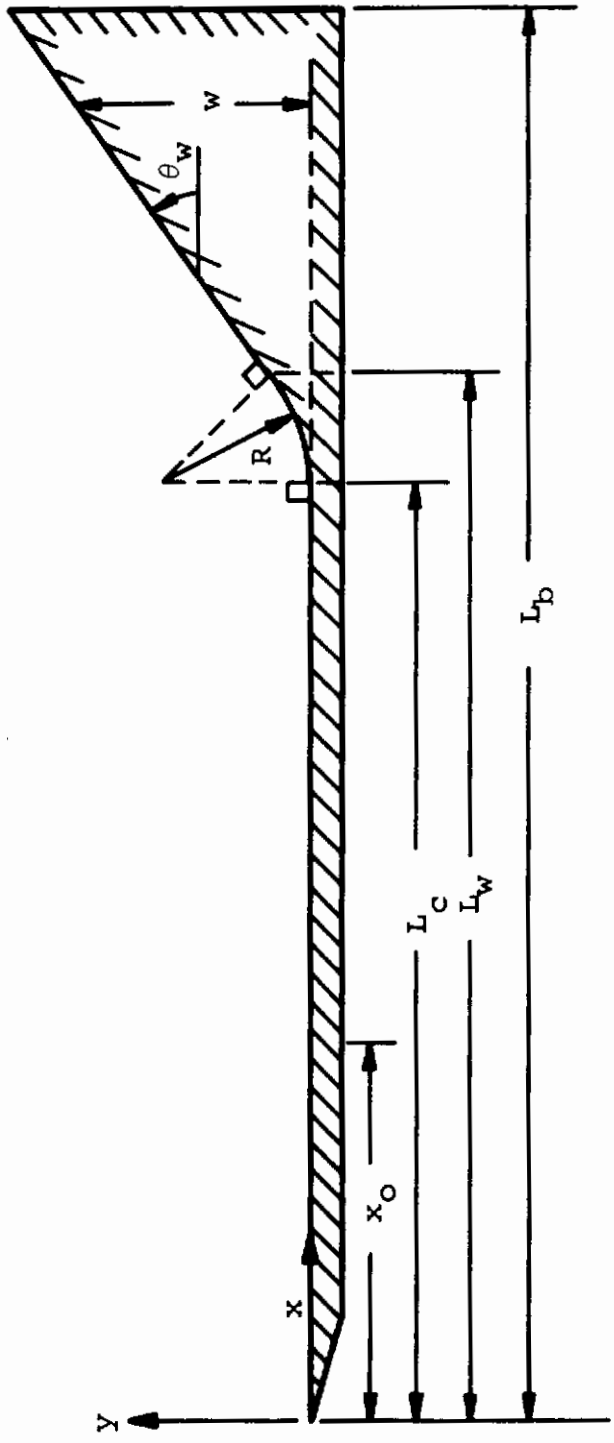

Figure 8.- Two-dimensional configuration handled by computer program.

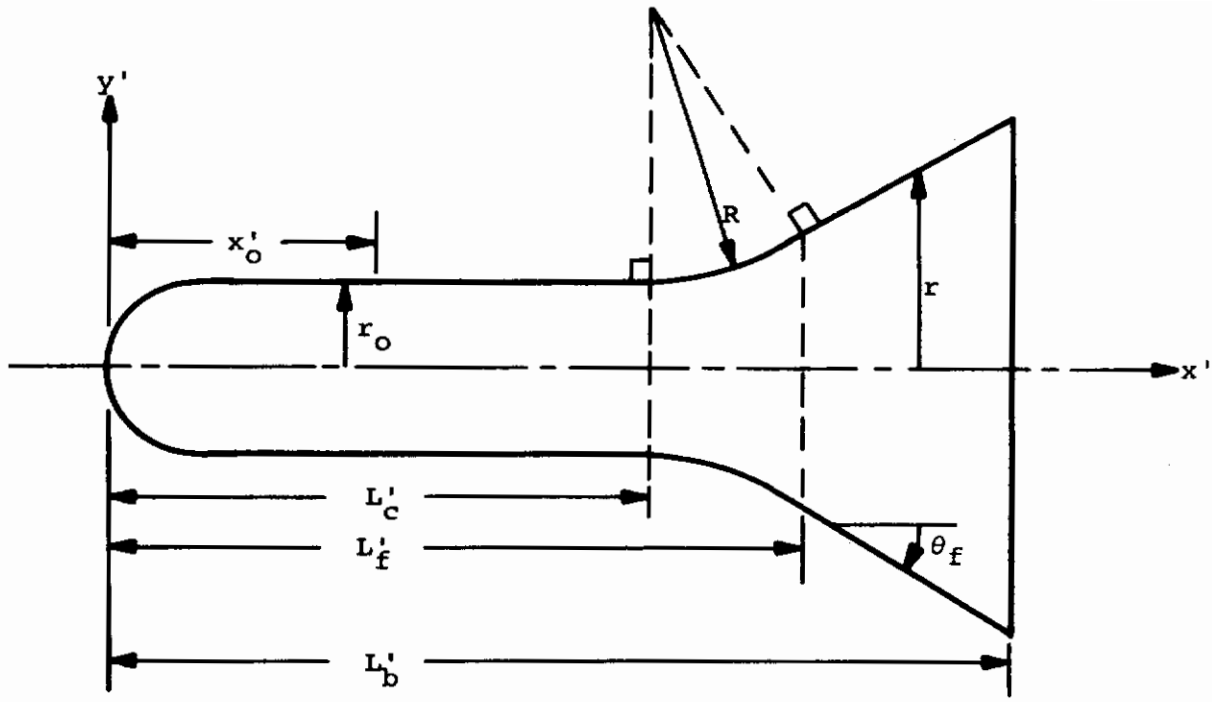

(a) Blunt axisymmetric body.

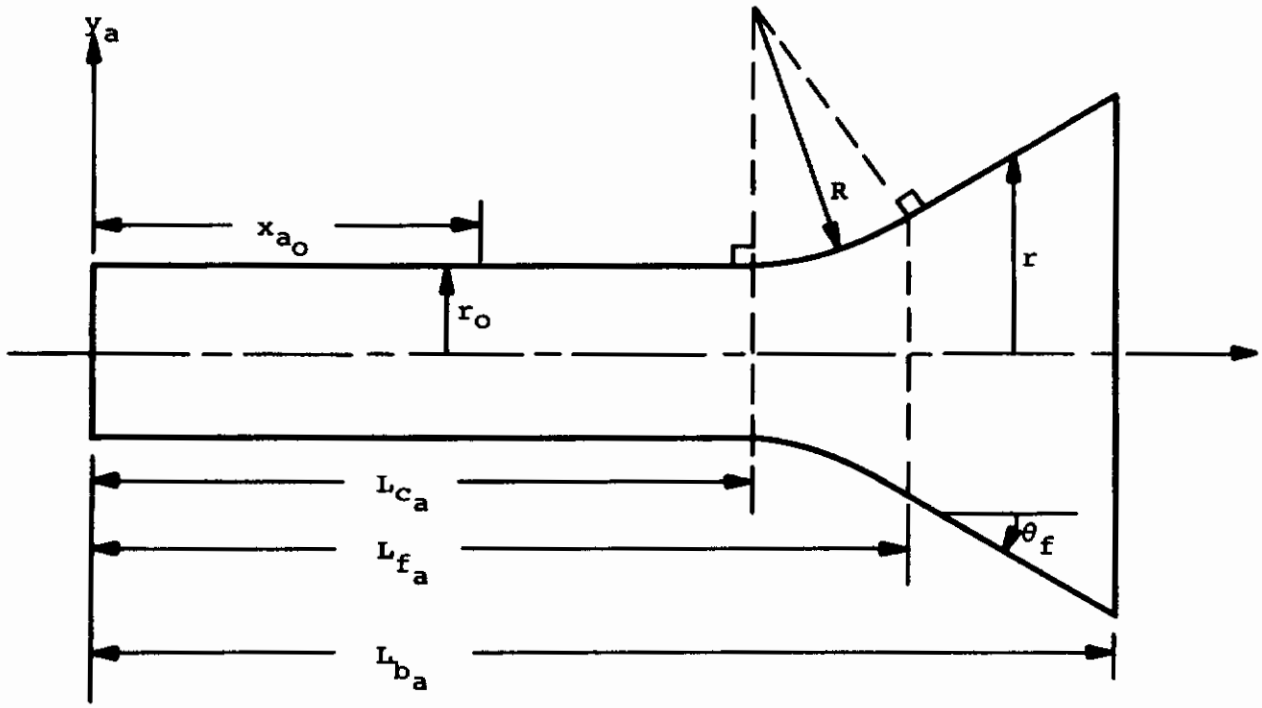

(b) Equivalent hollow axisymmetric body.

Figure 9.- Axisymmetric configuration handled by computer program.

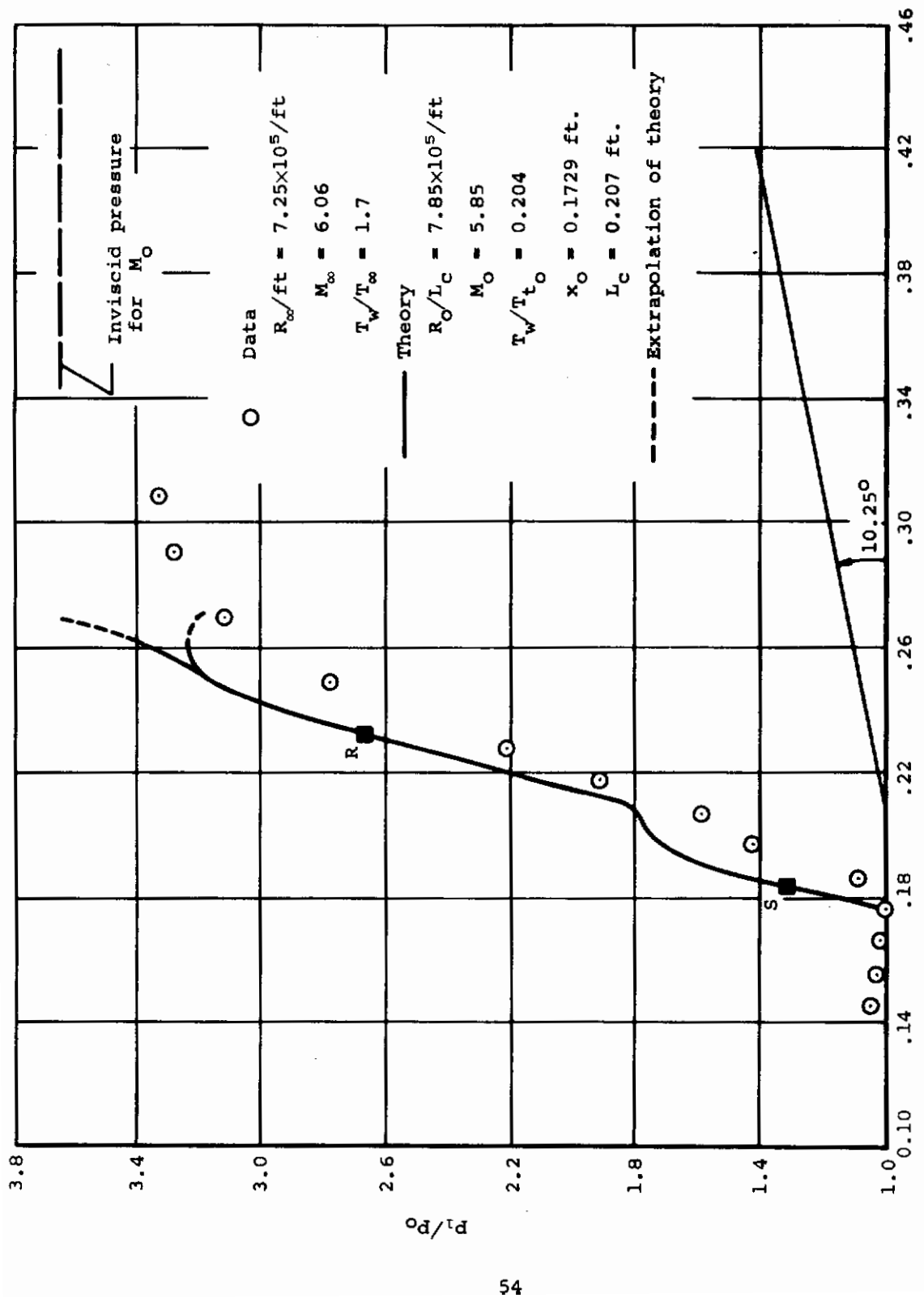

(a) Theory based on calculated flow conditions at beginning of interaction.

Figure 10.- Comparison of the theory with the highly cooled plate-wedge data of Lewis, Kubota, and Lees (ref. 8, fig. 19).

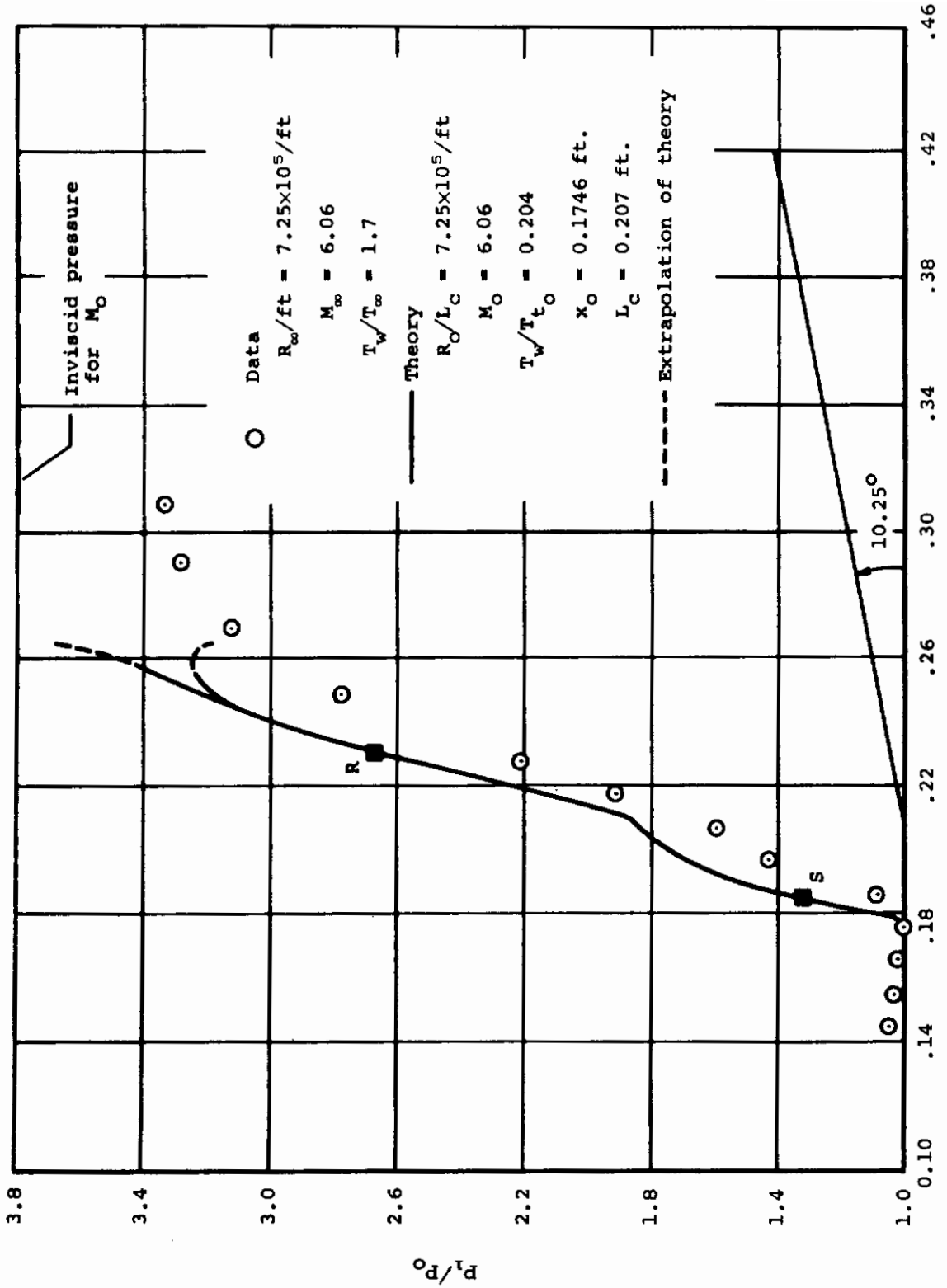

(b) Theory based on free-stream flow conditions.

Figure 10.- Concluded.

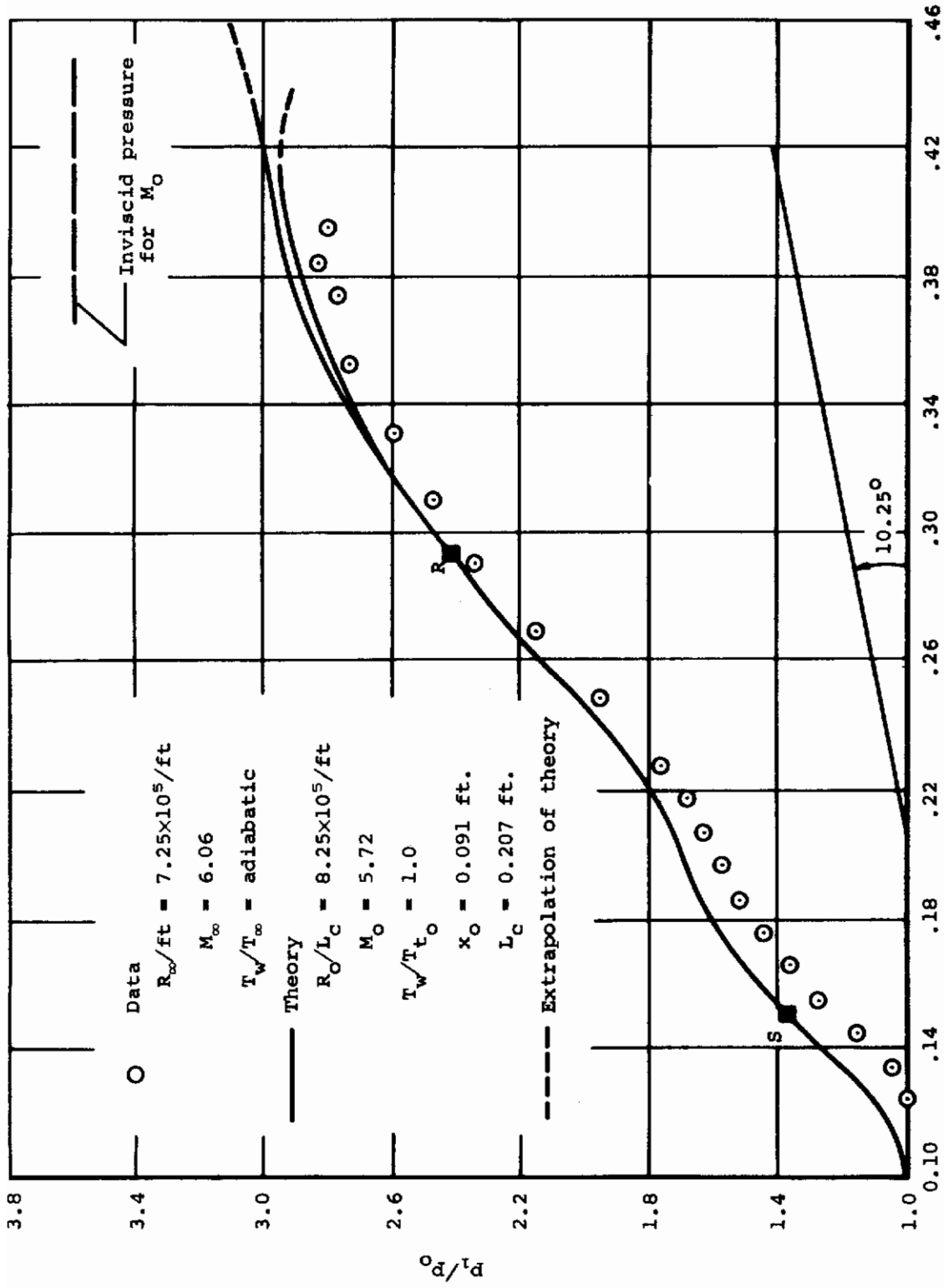

Figure 11.- Comparison of the theory with the adiabatic plate-wedge data of Lewis, Kubota, and Lees (ref. 8, fig. 17).

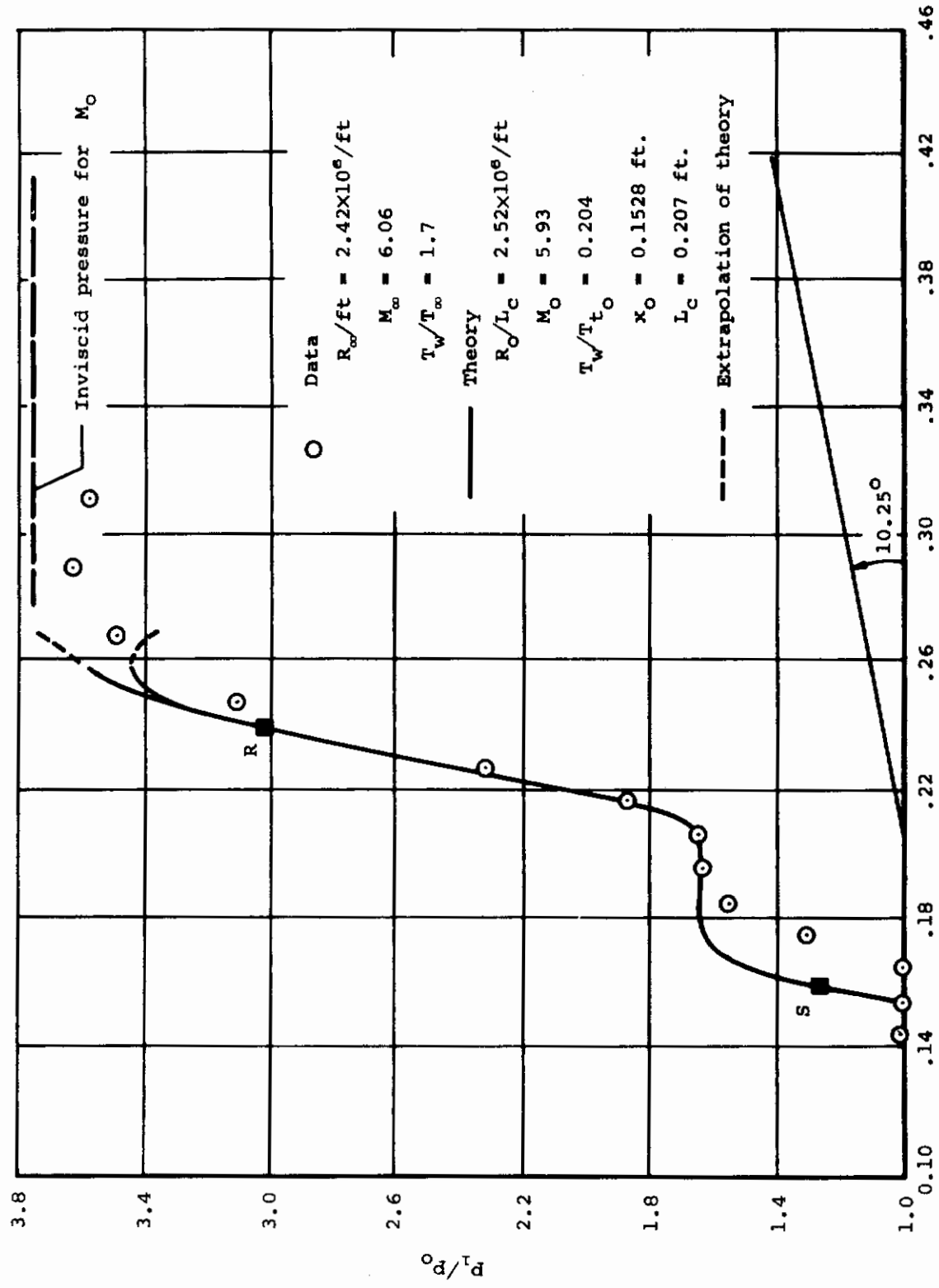

Figure 12.- Comparison of the theory with another set of highly cooled plate-wedge data from Lewis, Kubota, and Lees (ref. 8, fig. 19).

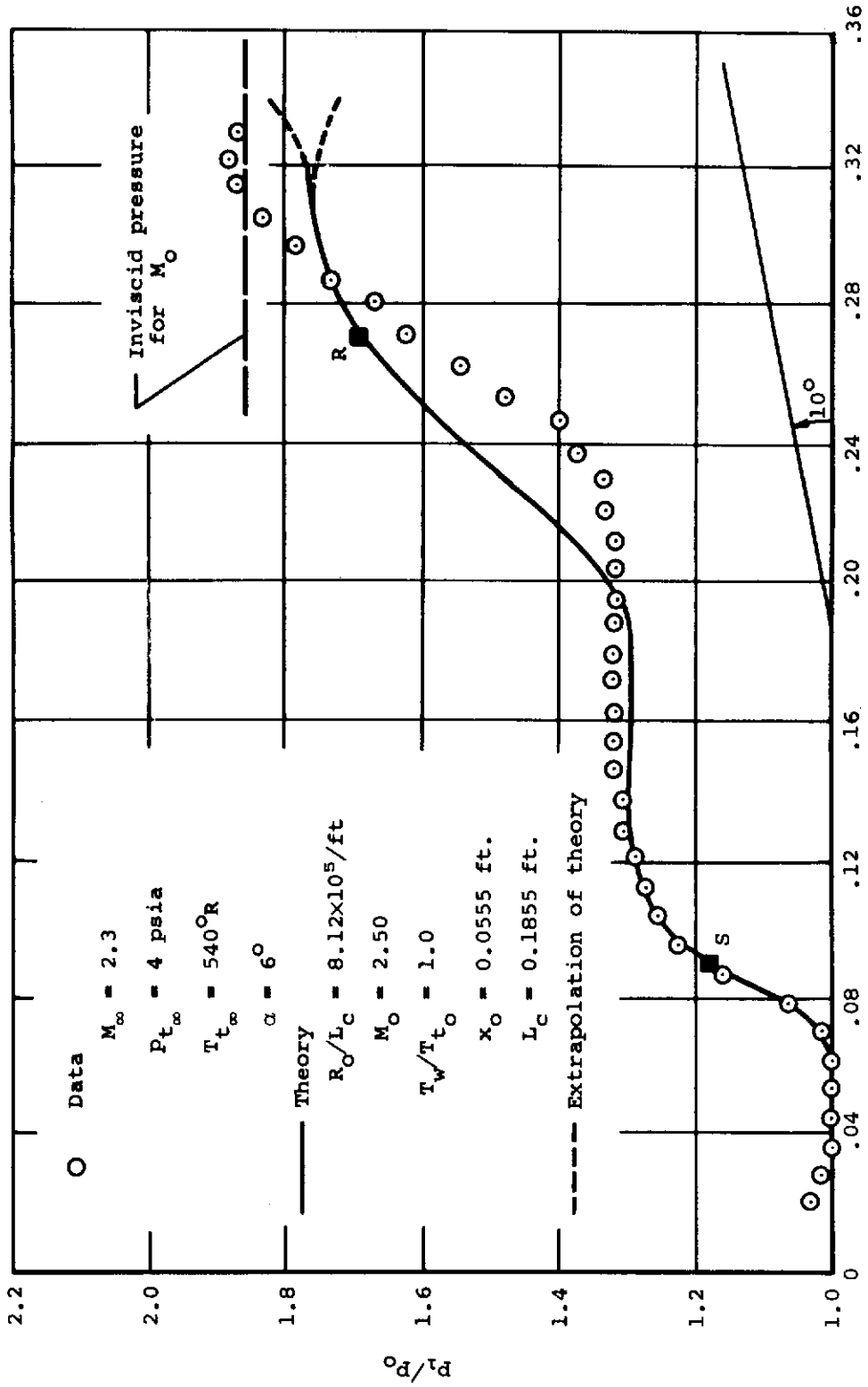

Figure 13.- Comparison of the theory with the adiabatic data of figure 21 of reference 1.

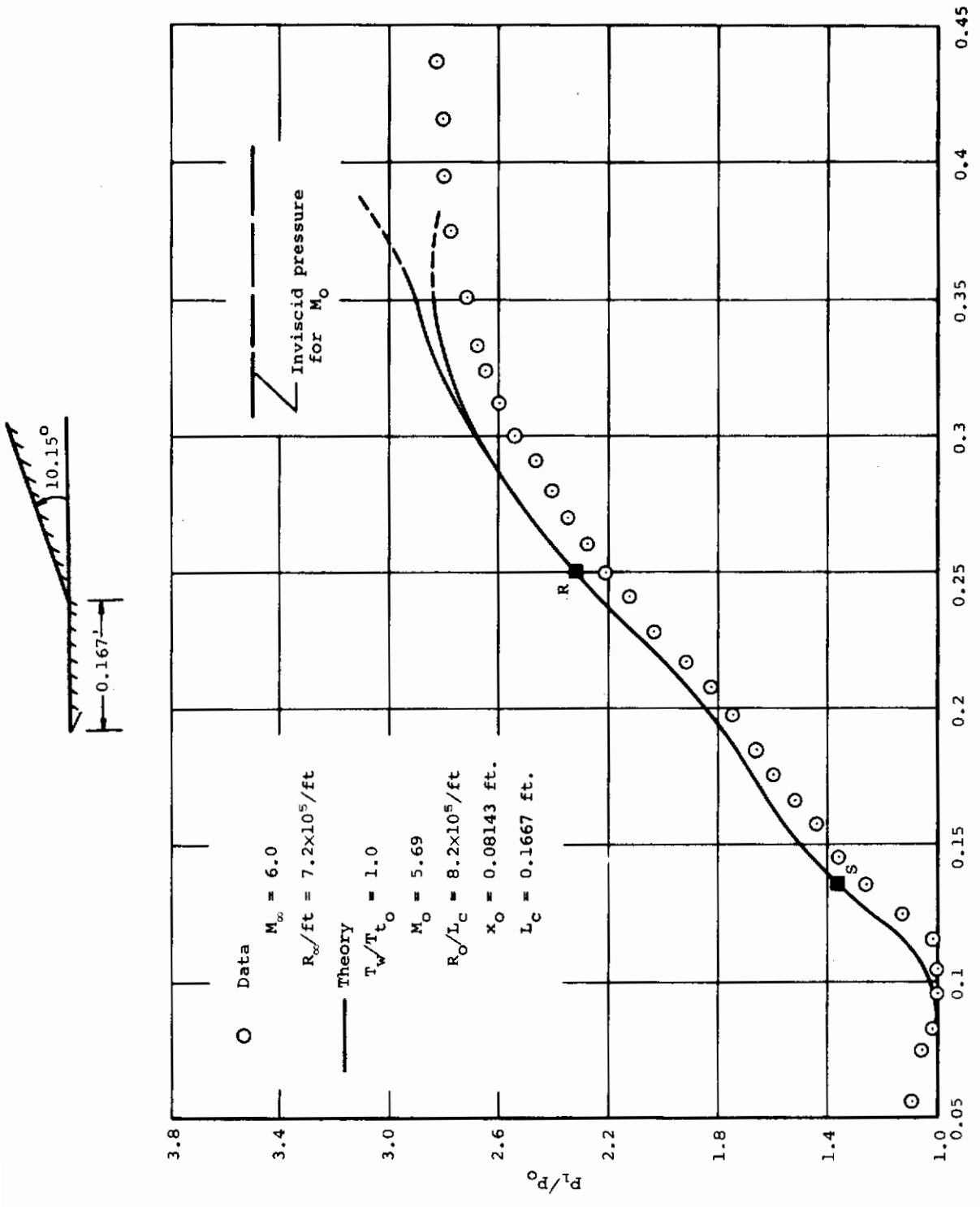

(a) Pressure distribution (ref. 9, fig. 3).

Figure 14.- Comparison of the theory with the adiabatic data of Ko and Kubota (ref. 9).

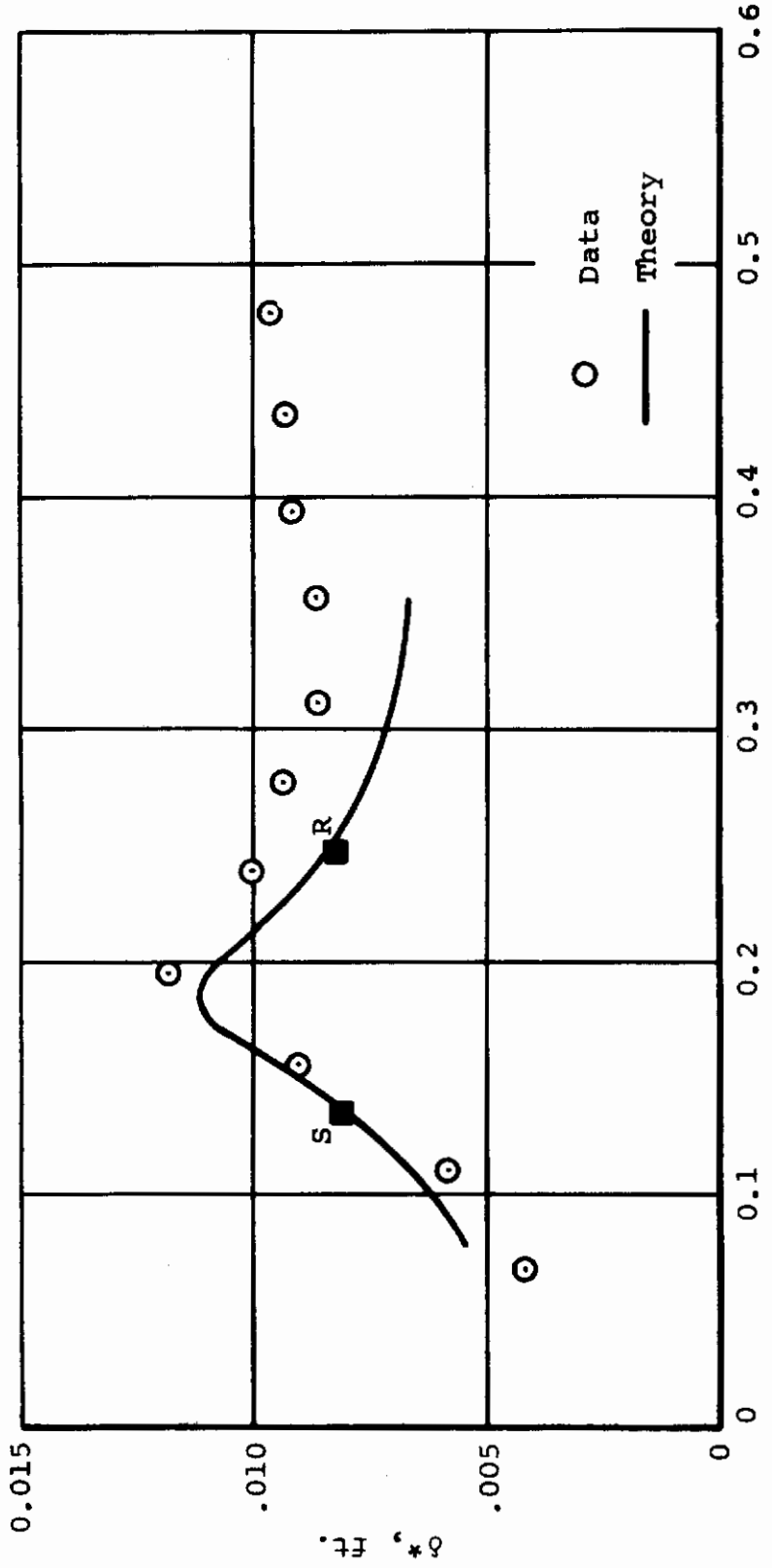

(b) Displacement thickness (ref. 9, fig. 5).

Figure 14.- Concluded.

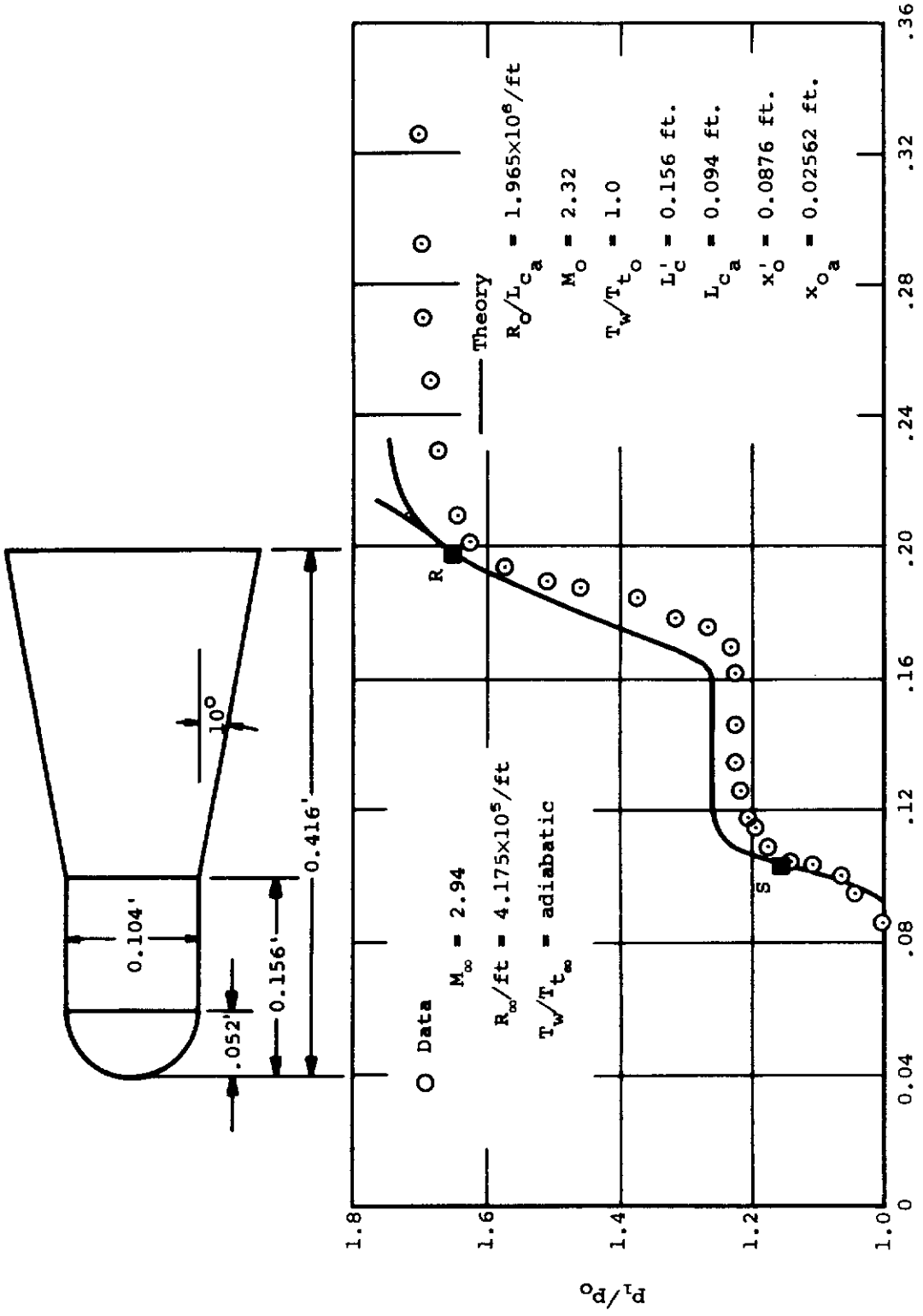

Figure 15.- Comparison of the theory with adiabatic data of Kuehn on a blunt-nosed cylinder-flare (ref. 10, fig. 6(a)).

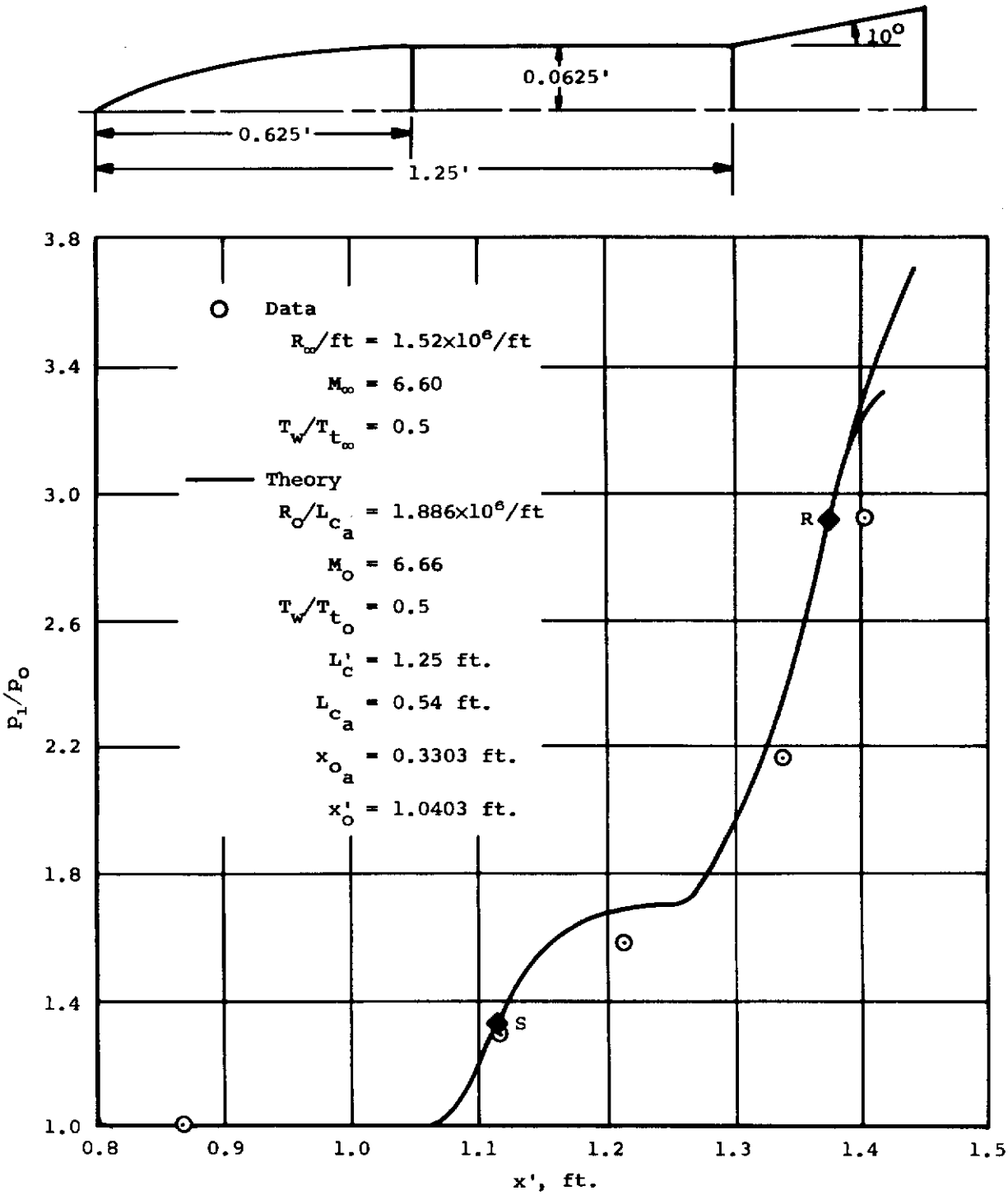

(a) Pressure distribution.

Figure 16.- Comparison of the theory with data of Becker and Korycinski (ref. 11, fig. 5(a)) on an ogive-cylinder-flare model.

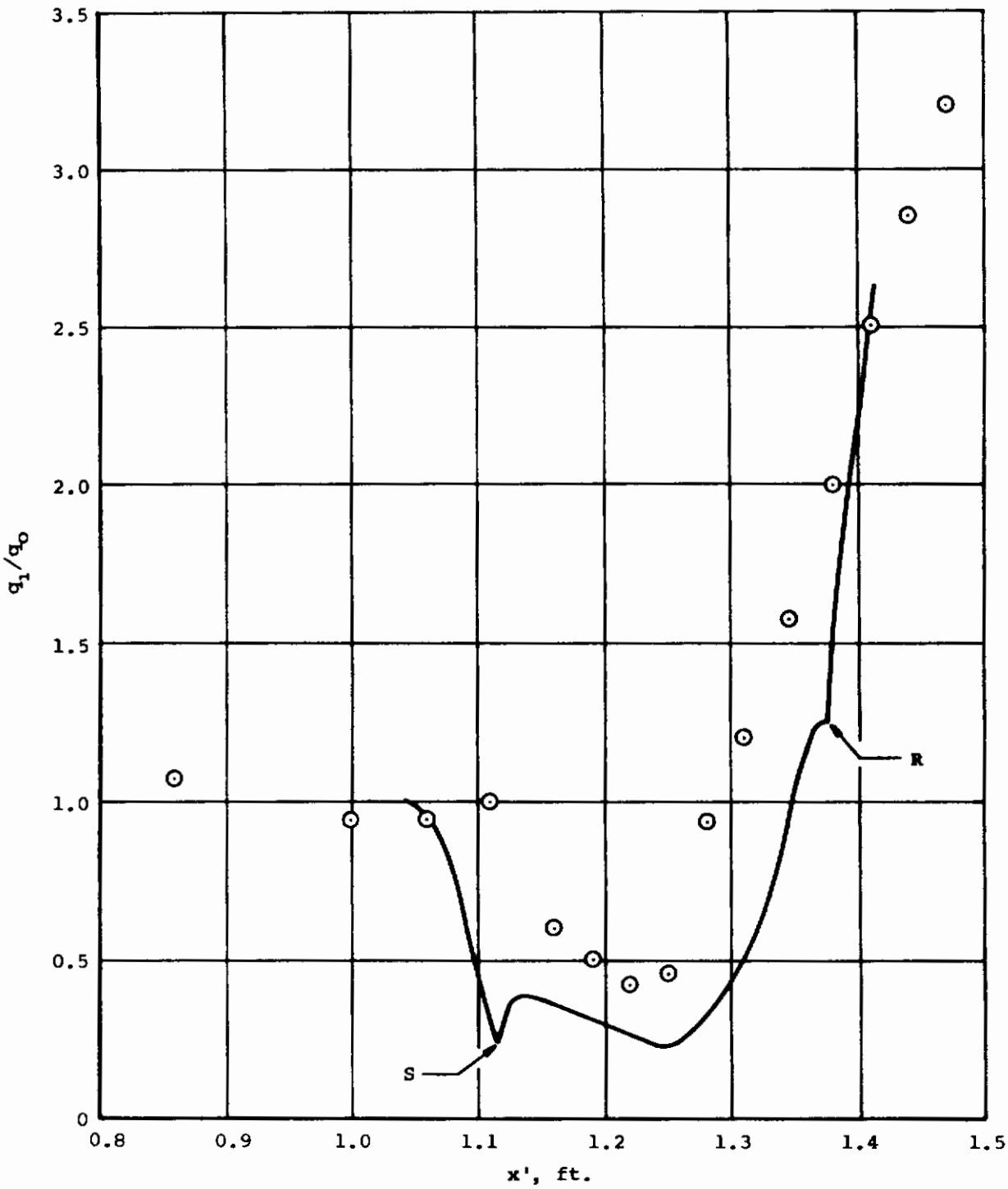

(b) Heat transfer distribution.

Figure 16.- Concluded.

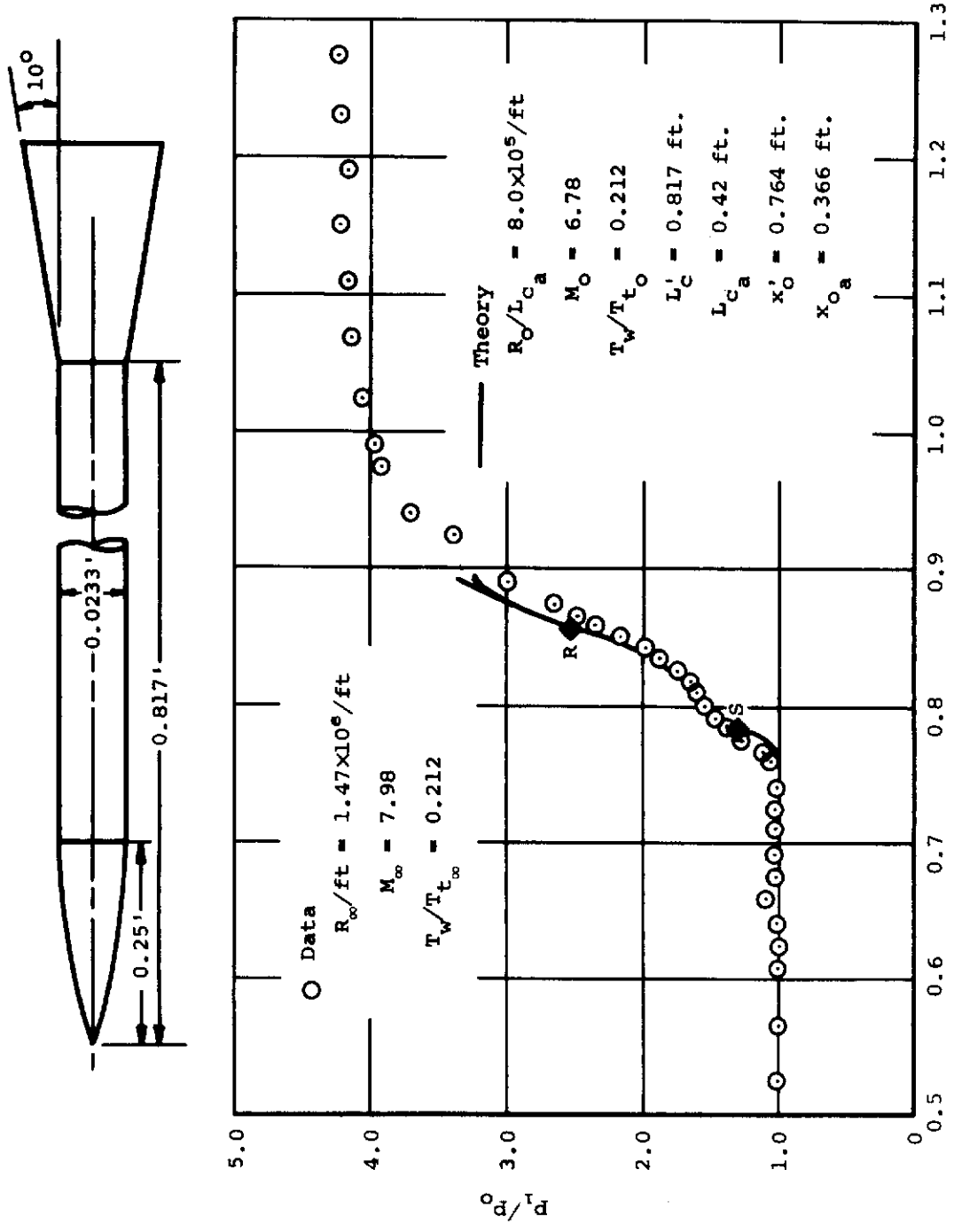

(a) R_∞/ft = 14.73×10⁵/ft, T_w/T_{t_∞} = 0.212.

Figure 17.- Comparison between experimental and theoretical pressure distributions for ogive-cylinder-cone model of reference 12.

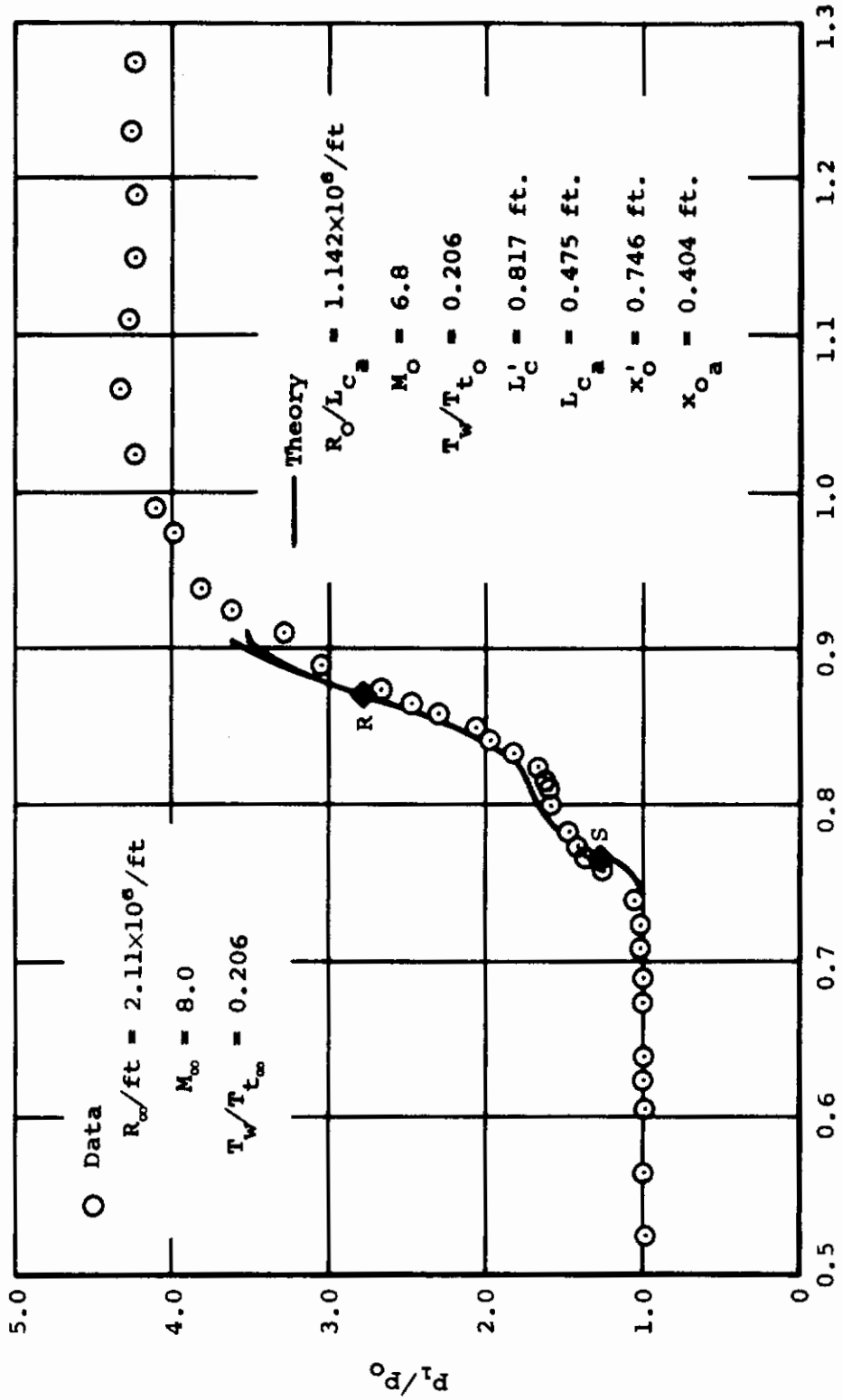

(b) R_∞/ft = 21.1×10⁵/ft, T_w/T_{t_∞} = 0.206.

Figure 17.- Continued.

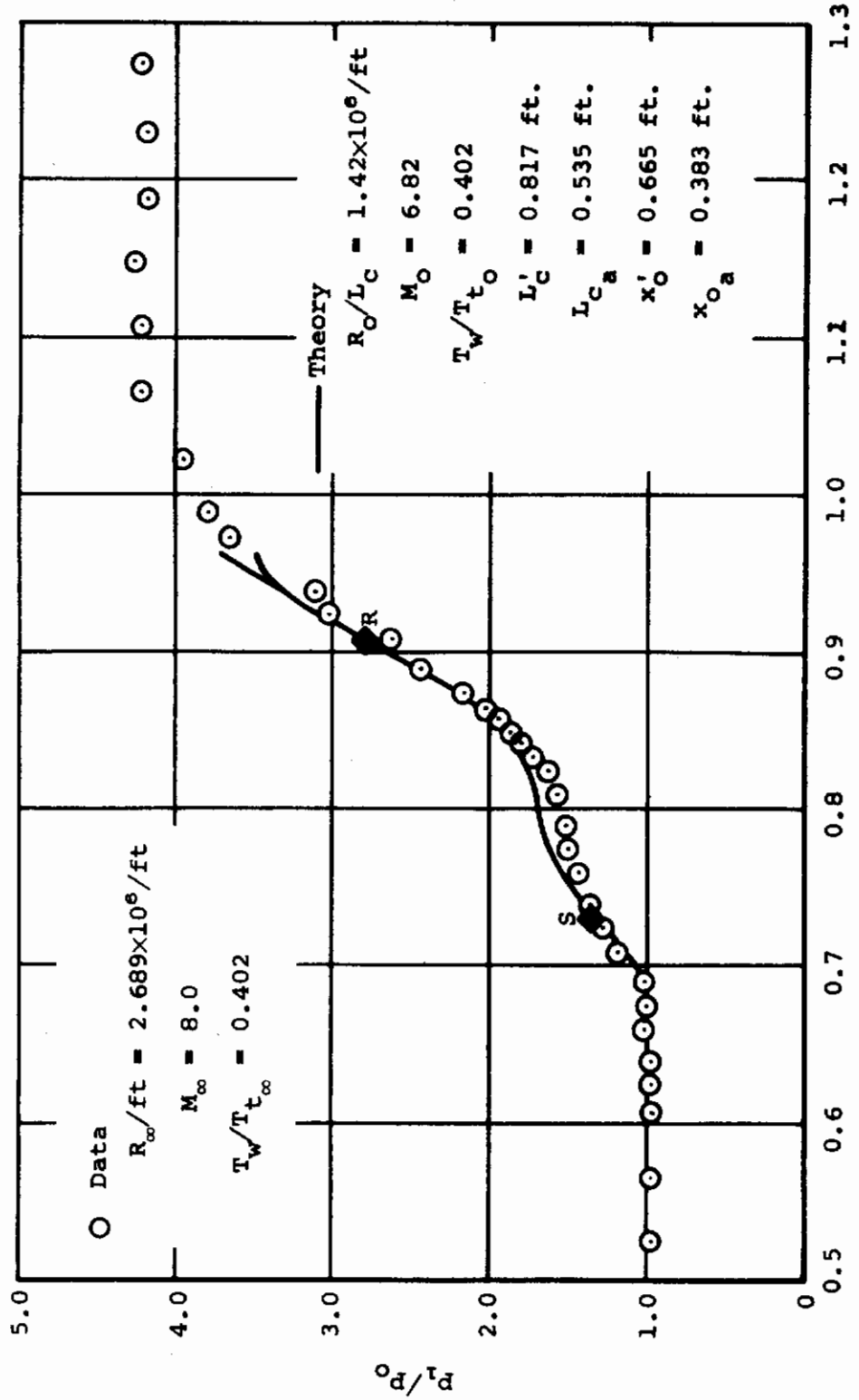

(c) R_∞/ft = 26.89×10⁵/ft, T_w/T_{t_∞} = 0.402.

Figure 17.- Concluded.

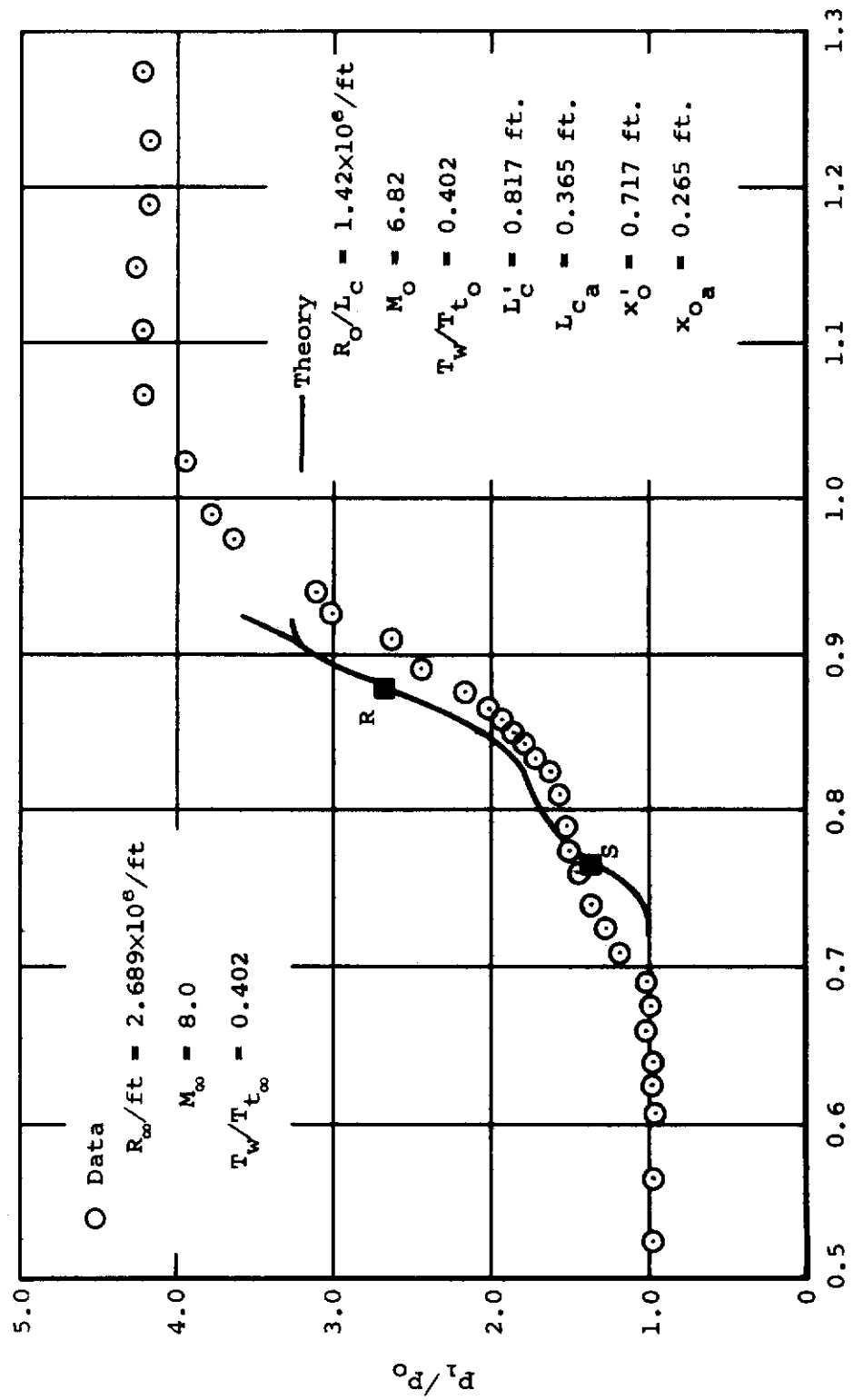

Figure 18.- Comparison of experimental and theoretical pressure distributions for ogive-cylinder-cone model of reference 12. Initial conditions from approximate method of reference 13.

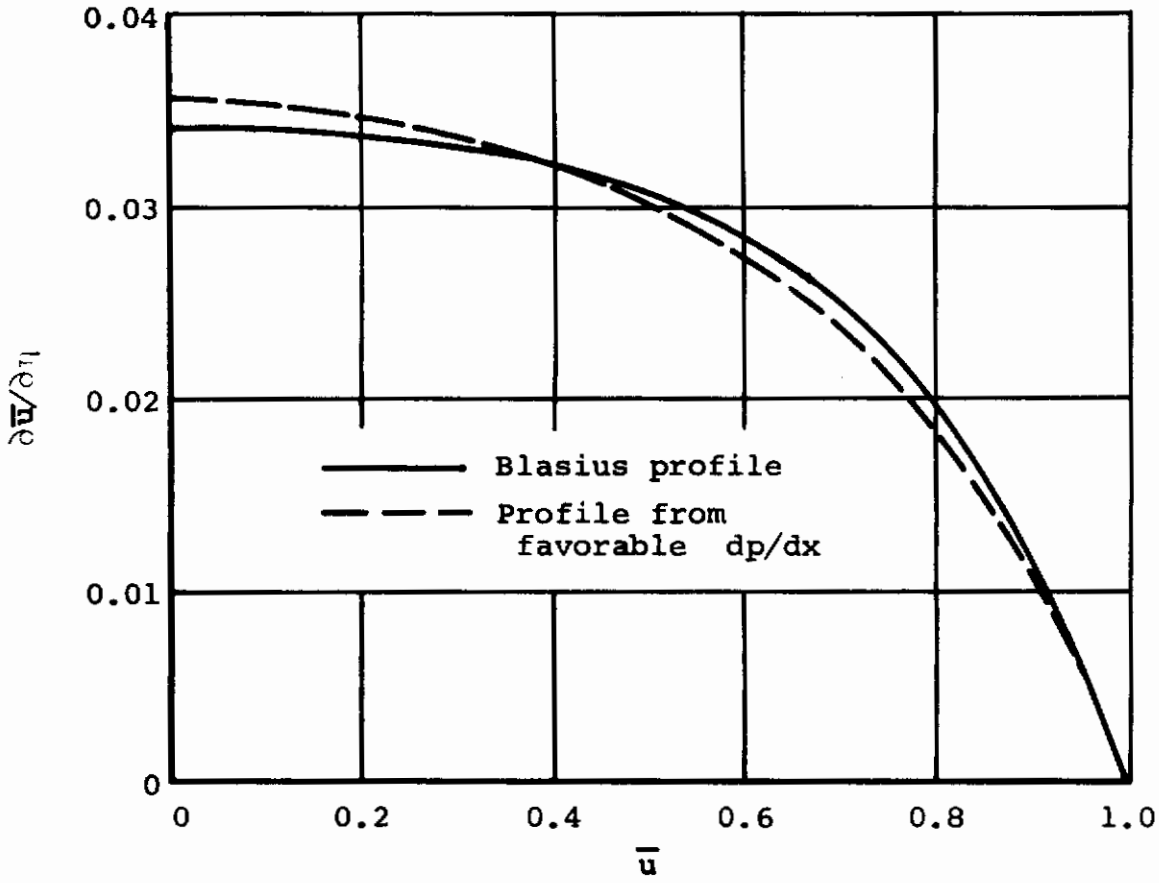

Figure 19.- Comparison of velocity gradient profile from accelerated flow with Blasius profile.

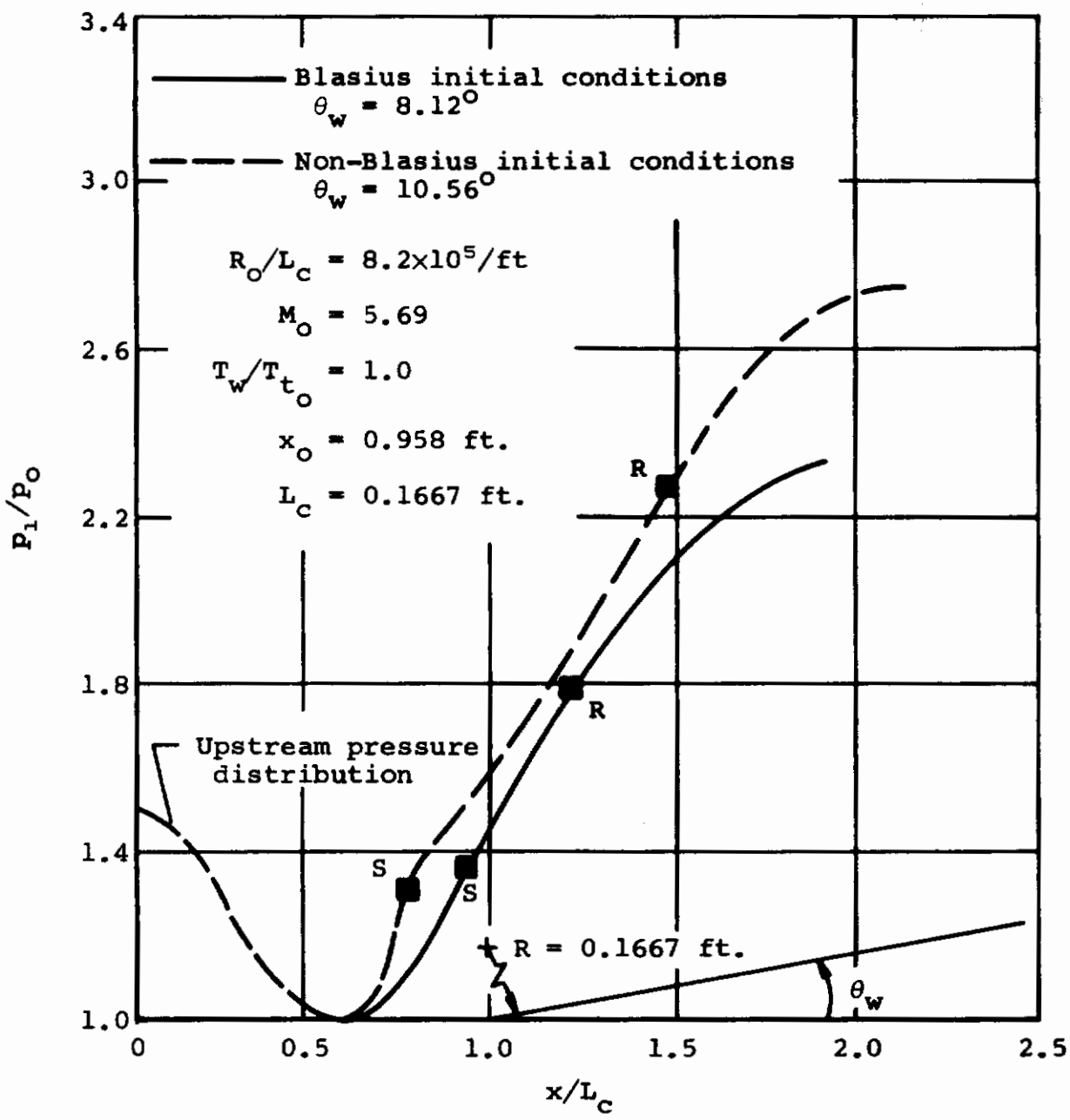

Figure 20.- Comparison of theoretical pressure distribution calculations for Blasius and non-Blasius initial conditions.

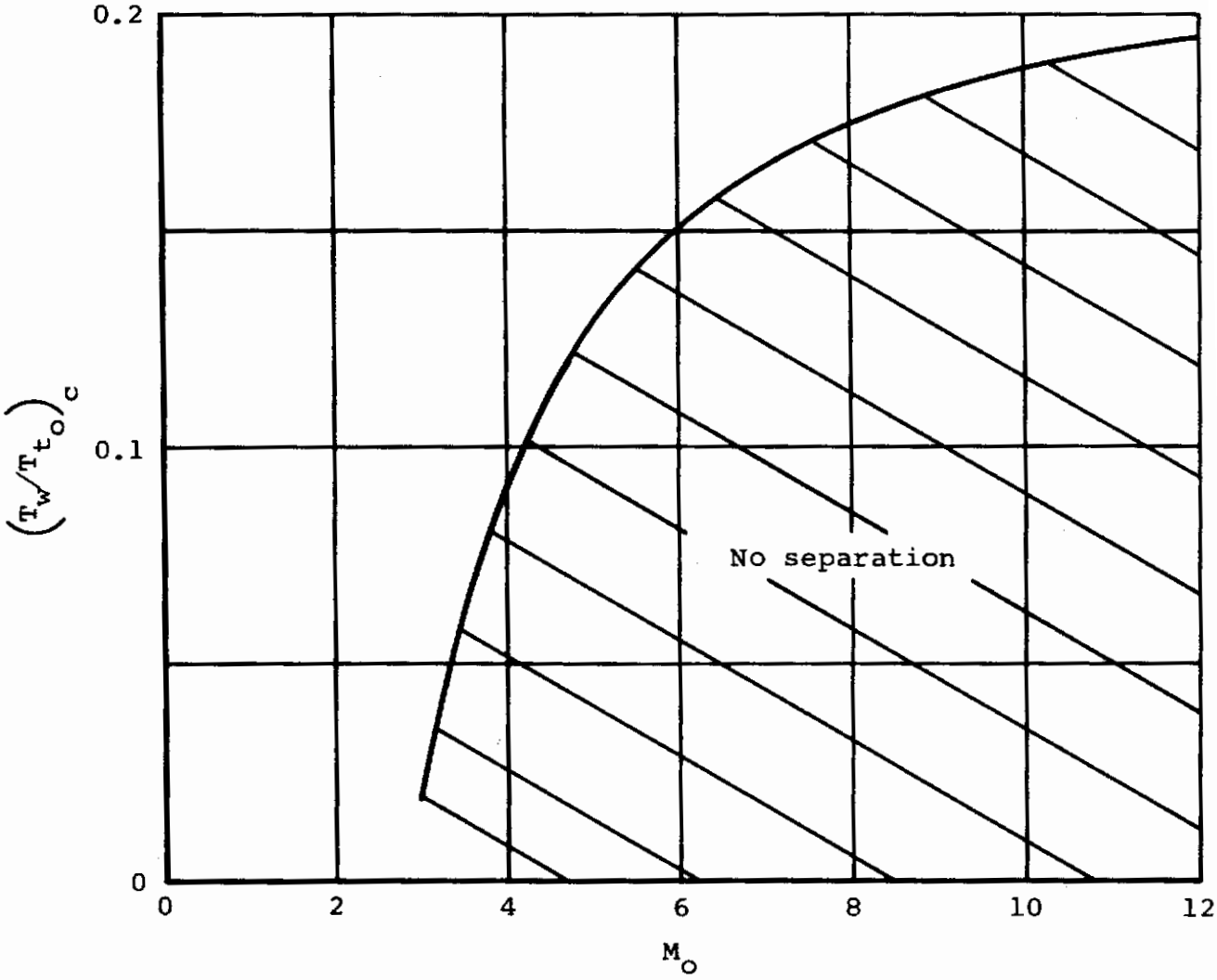

Figure 21.- Second-order coupling critical temperature ratio for laminar boundary layers.

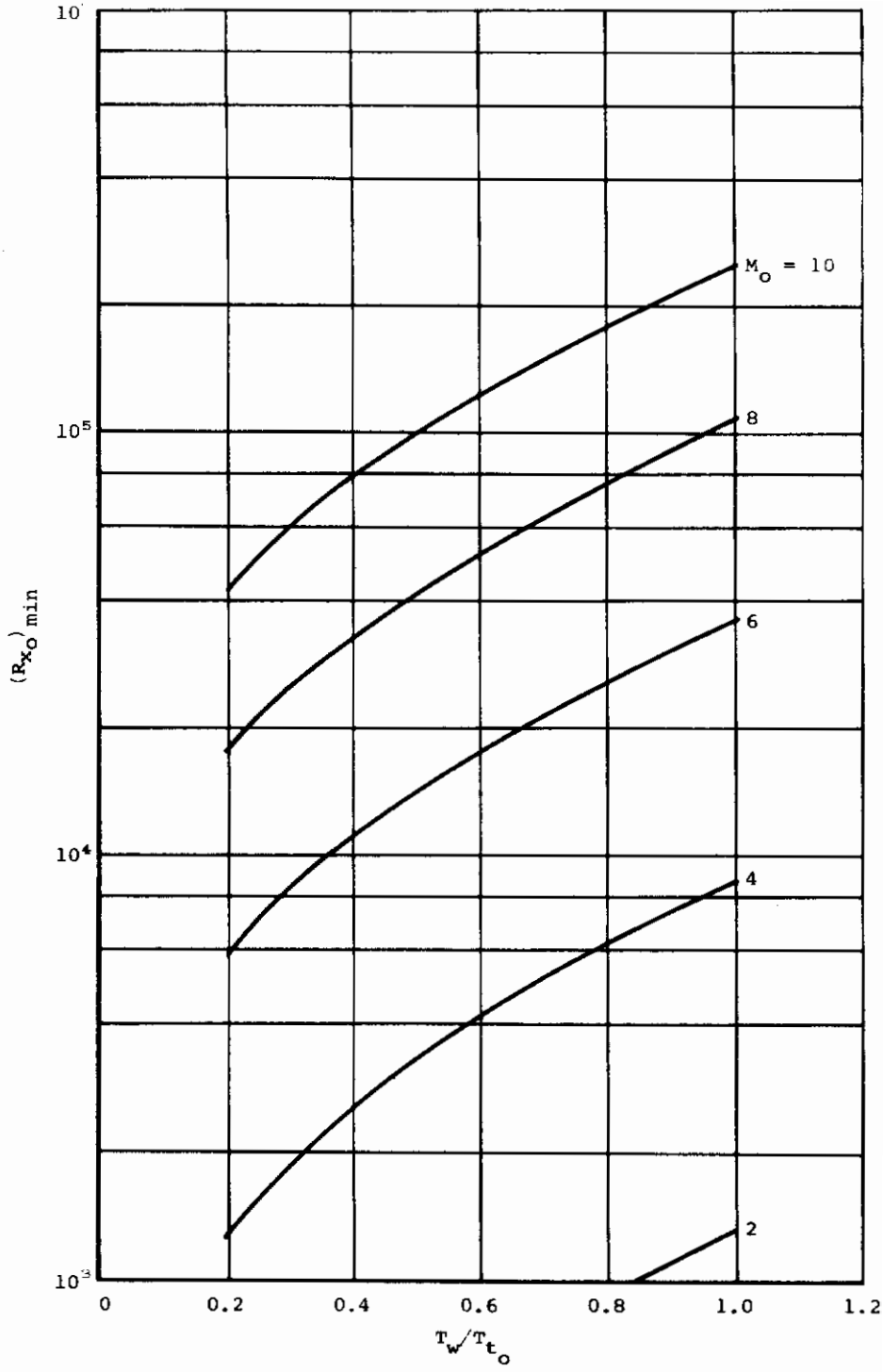

Figure 22.- Value of R_{x_o} at which $(\delta^*/x)_o = 0.1$.

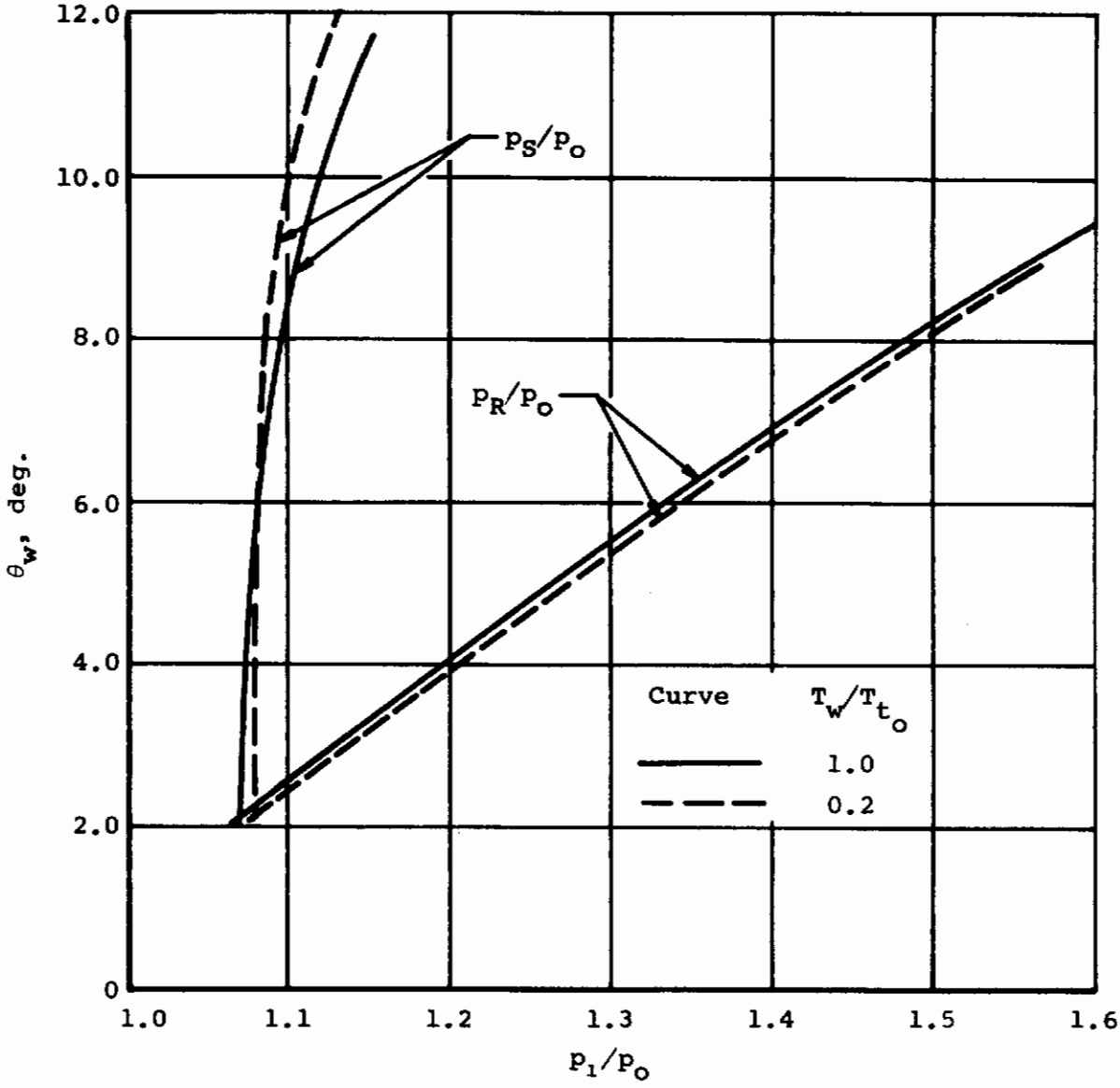

Figure 23.- Variation of separation and reattachment pressure with wedge angle. $M_o = 2.0$, $R_o = 10^6$.

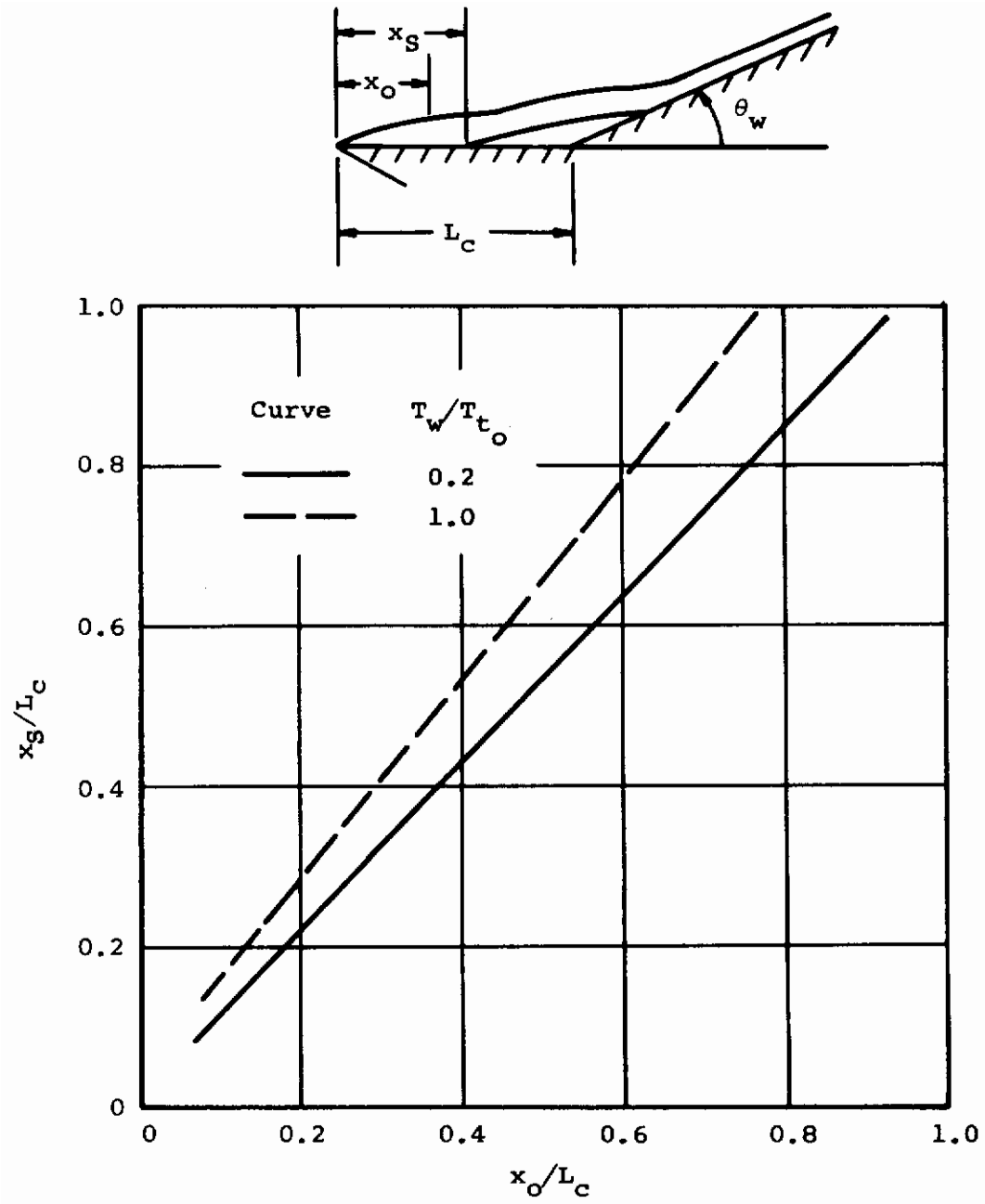

Figure 24.- Variation of separation point location with location of beginning of interaction. $M_o = 2.0$, $R_o = 10^6$.

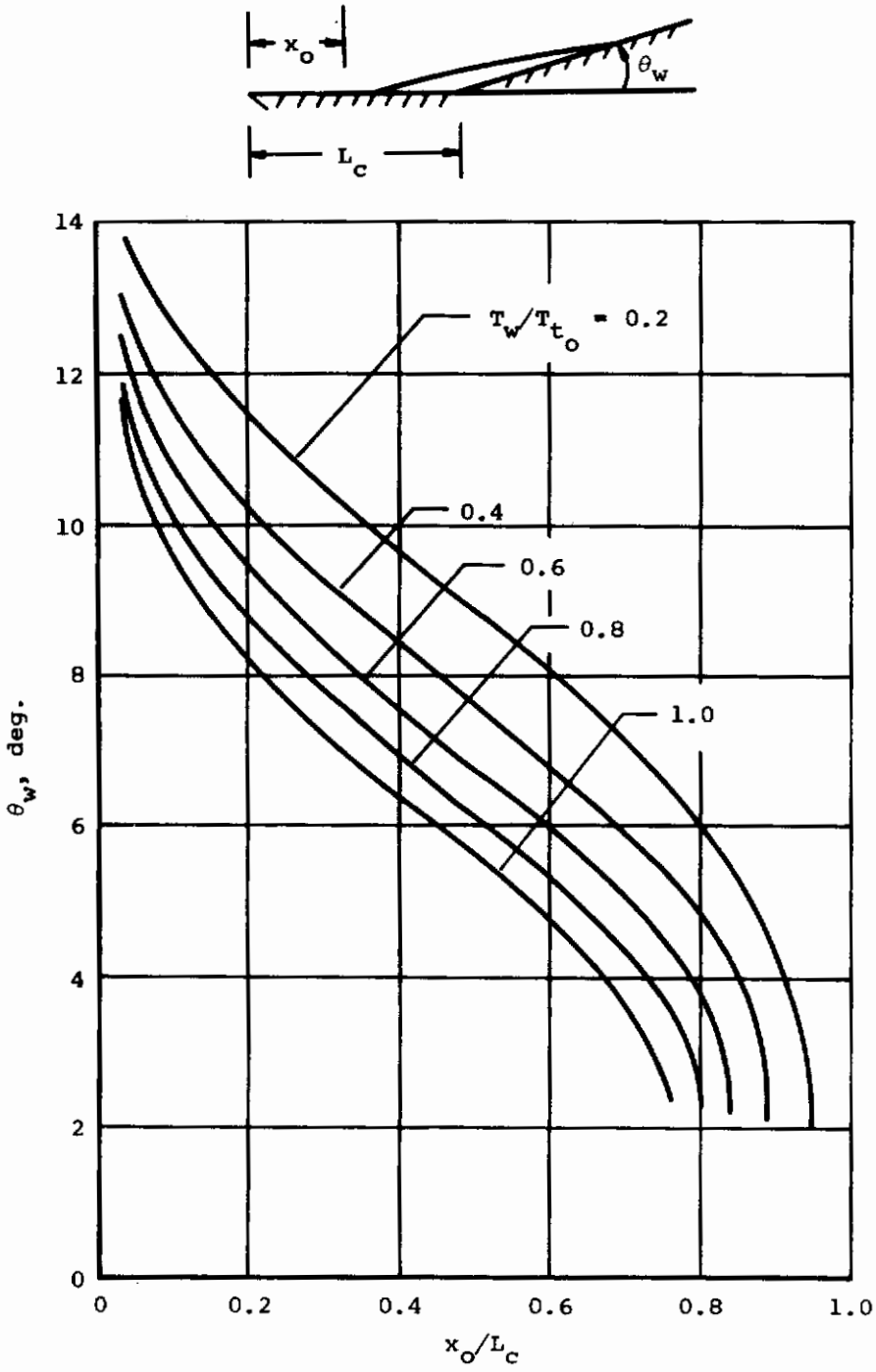

(a) Effect of wall temperature. $M_o = 2.0$, $R_o = 10^6$.

Figure 25.- Relation of wedge angle to beginning of interaction.

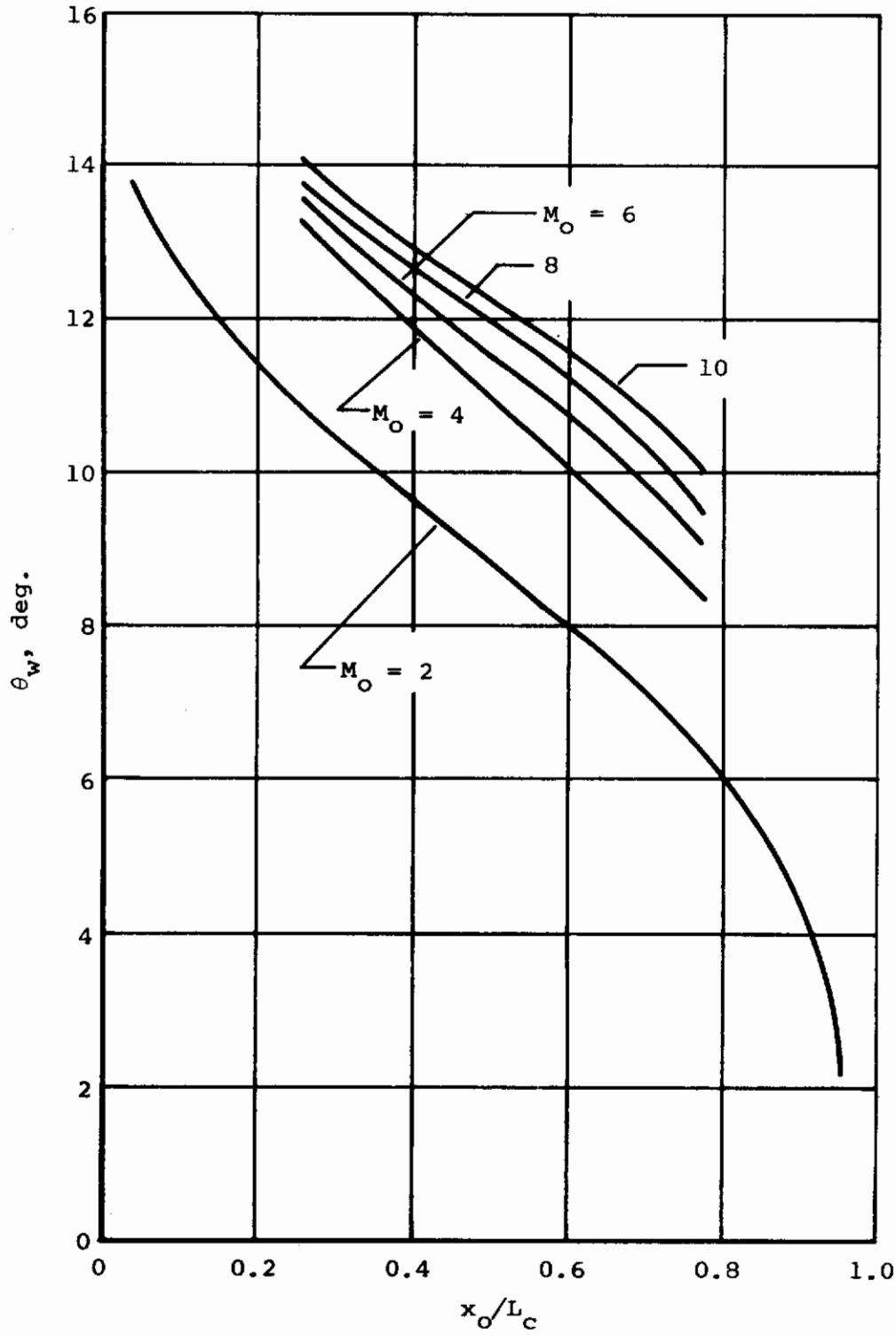

(b) Effect of Mach number. $R_o = 10^6$, $T_w/T_{t_o} = 0.2$.

Figure 25.- Continued.

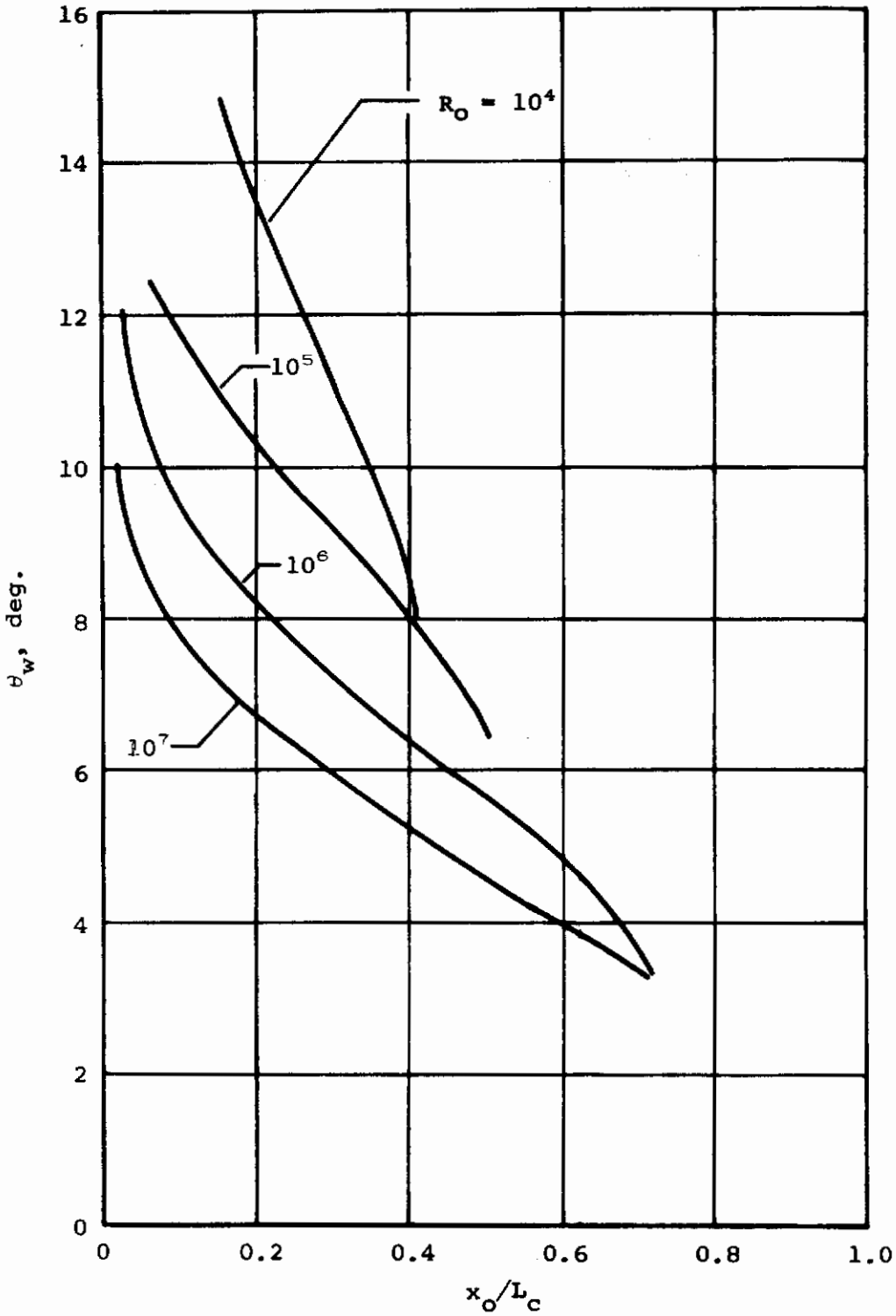

(c) Effect of Reynolds number. $M_o = 2.0$, $T_w/T_{t_o} = 1.0$.

Figure 25.- Concluded.

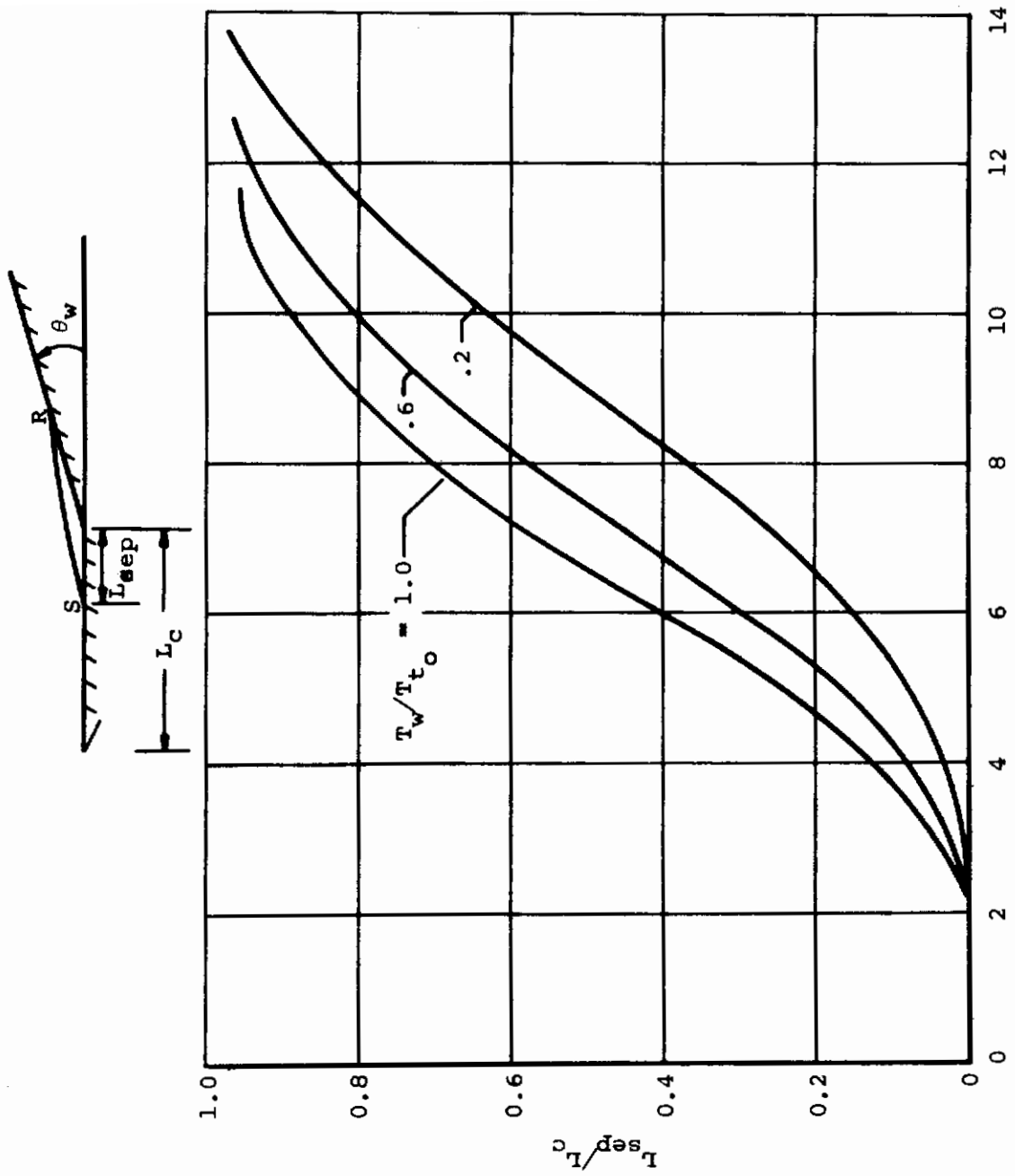

(a) Effect of wedge angle and temperature ratio. $M_o = 2.0$, $R_o = 10^6$.

Figure 26.- Effect of various parameters on upstream extent of separation.

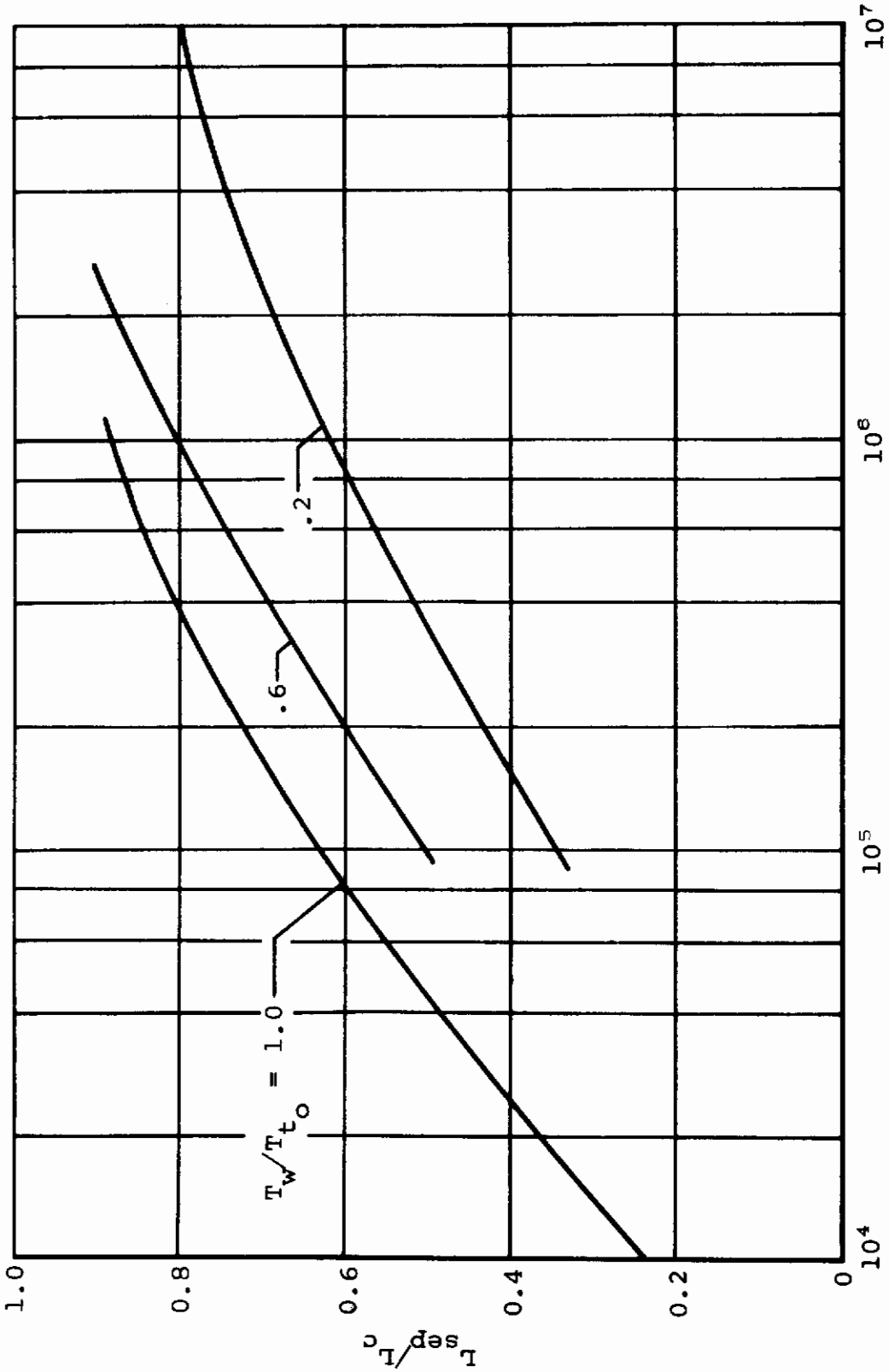

(b) Effect of Reynolds number and temperature ratio. $\theta_w = 10^o$, $M_o = 2.0$.

Figure 26.- Continued.

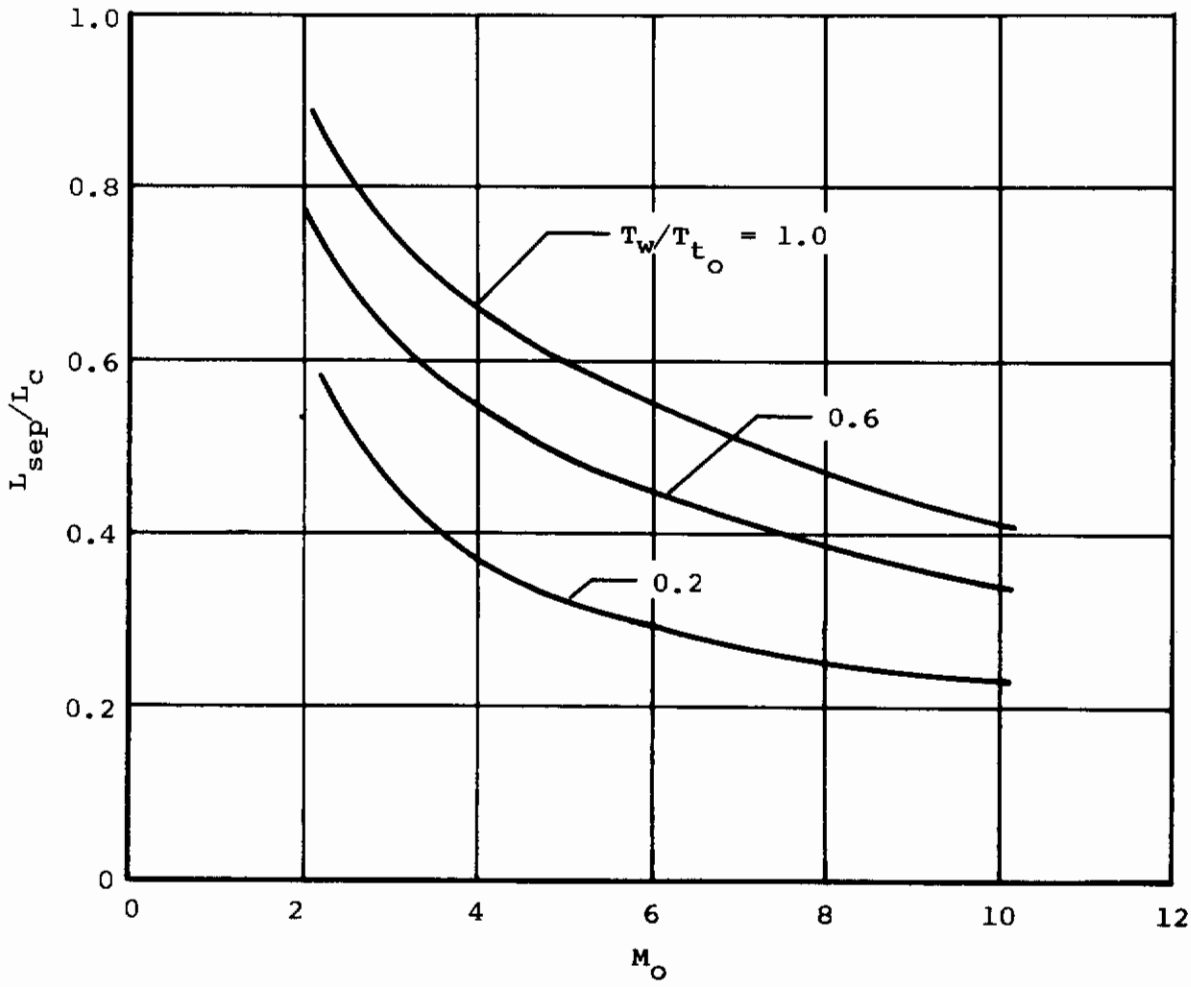

(c) Effect of Mach number and temperature ratio. $\theta_w = 10^o$, $R_o = 10^6$.

Figure 26.- Concluded.

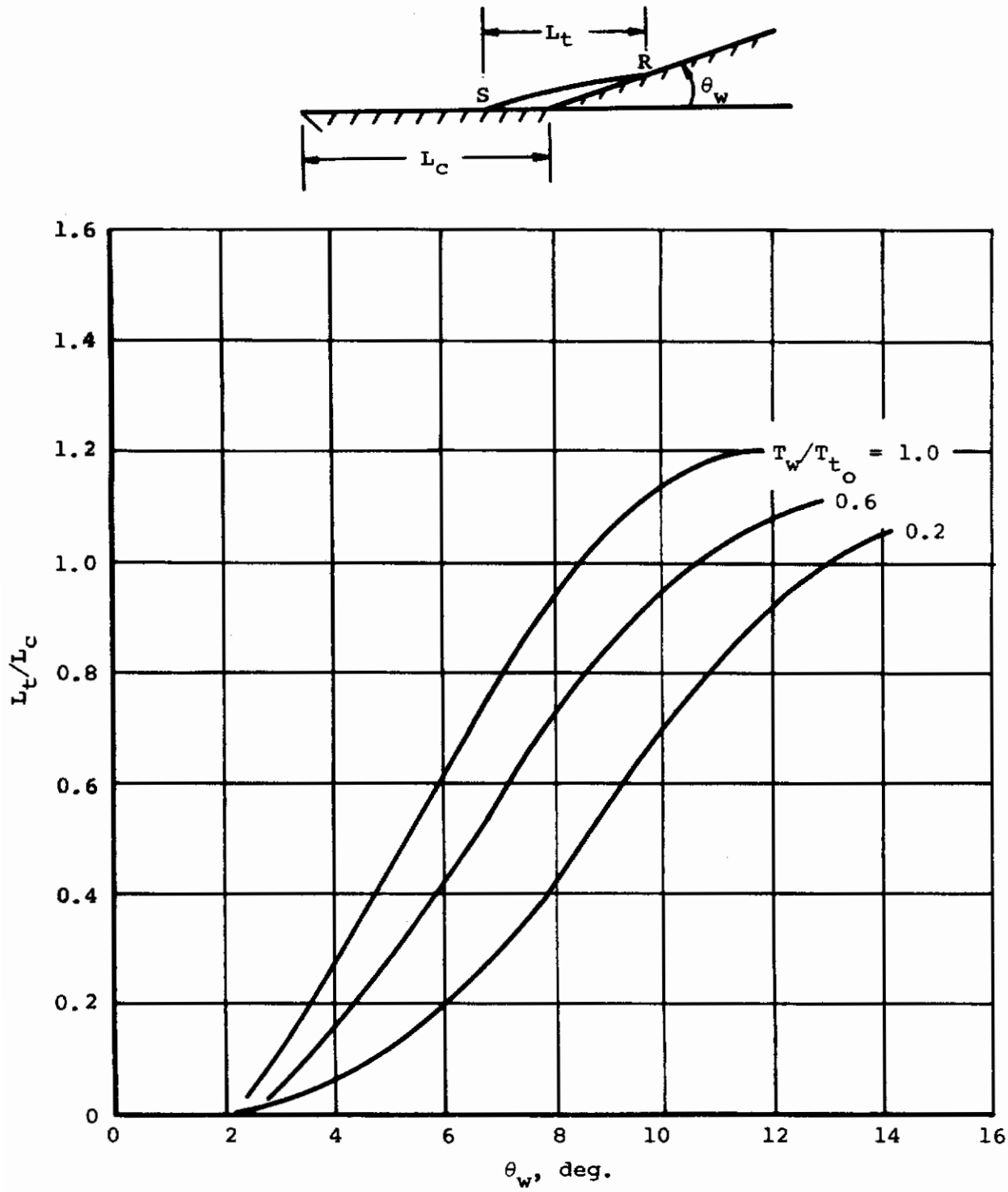

(a) Effect of wedge angle and temperature ratio. $M_o = 2.0$, $R_o = 10^6$.

Figure 27.- Effect of various parameters on total length of separated region.

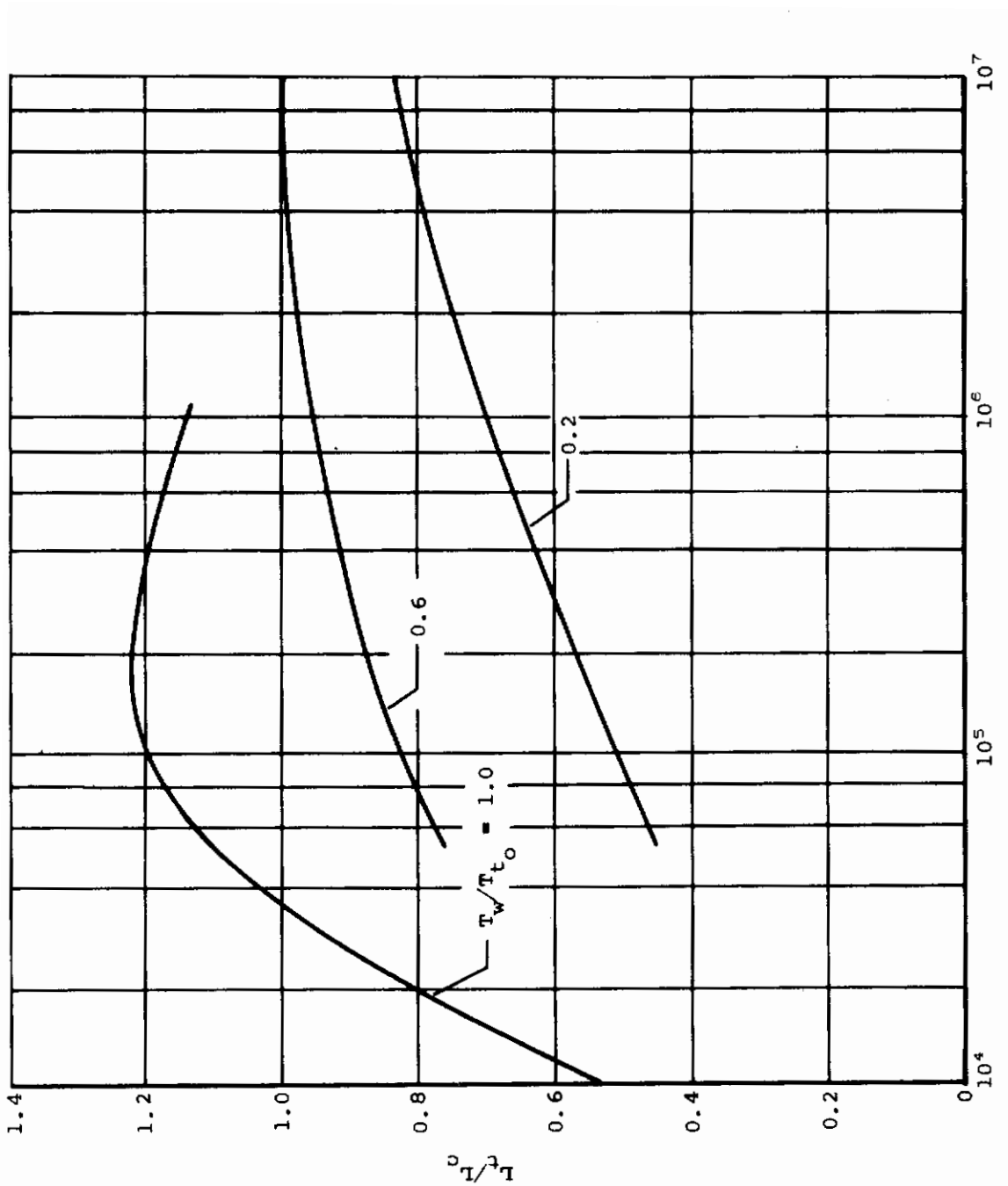

(b) Effect of Reynolds number and temperature ratio. $\theta_w = 10^o$, $M_o = 2.0$.

Figure 27.- Continued.

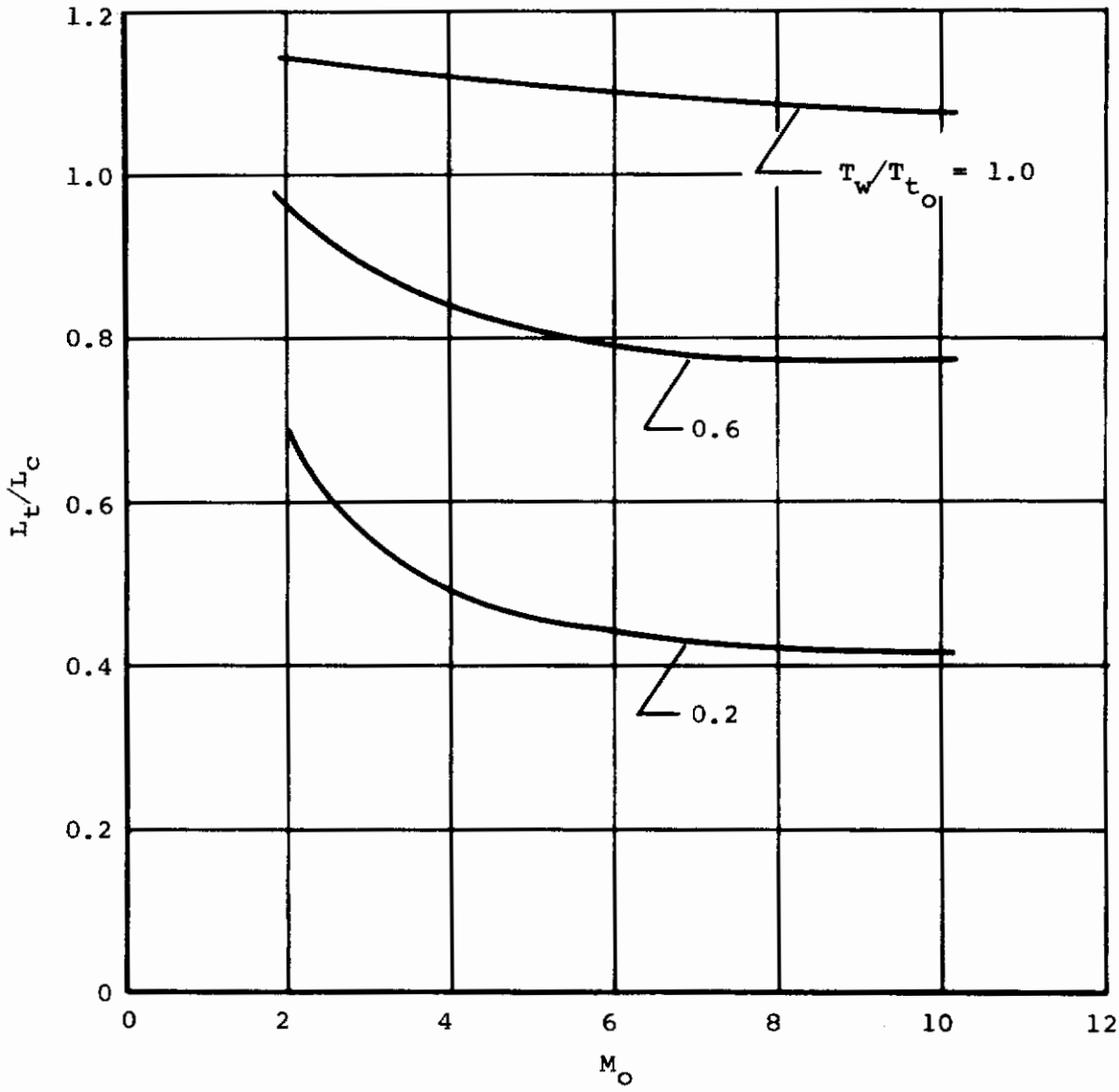

(c) Effect of Mach number and temperature ratio. $\theta_w = 10^o$, $R_o = 10^6$.

Figure 27.- Concluded.

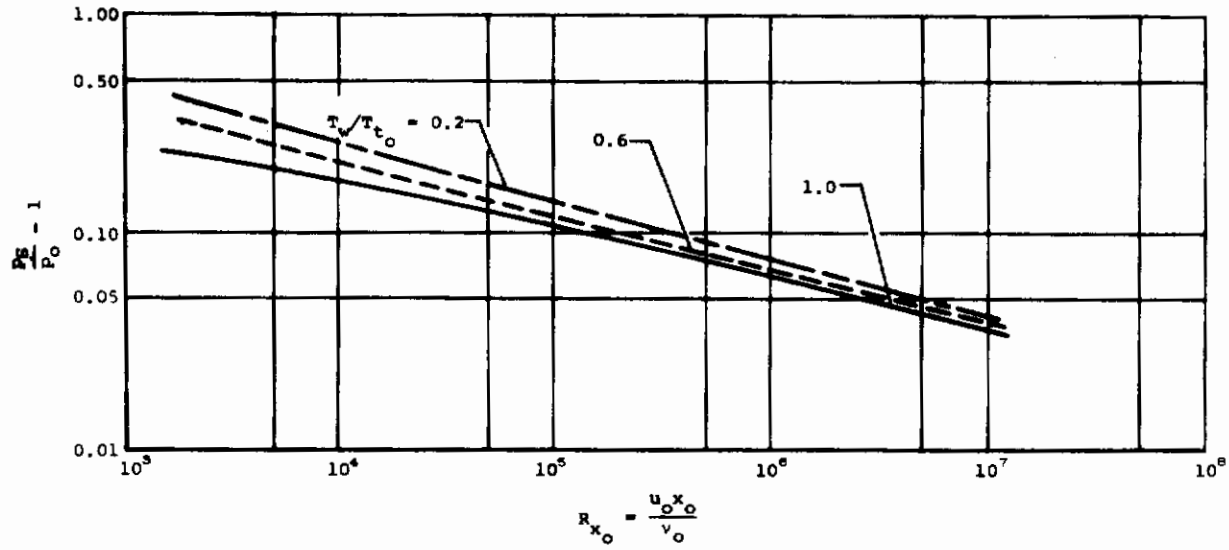

(a) Separation pressure for M_o = 2.0.

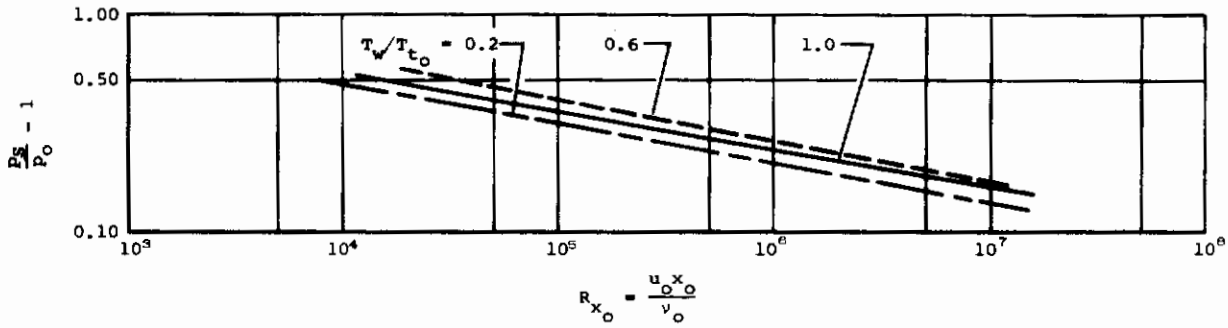

(b) Separation pressure for M_o = 6.0.

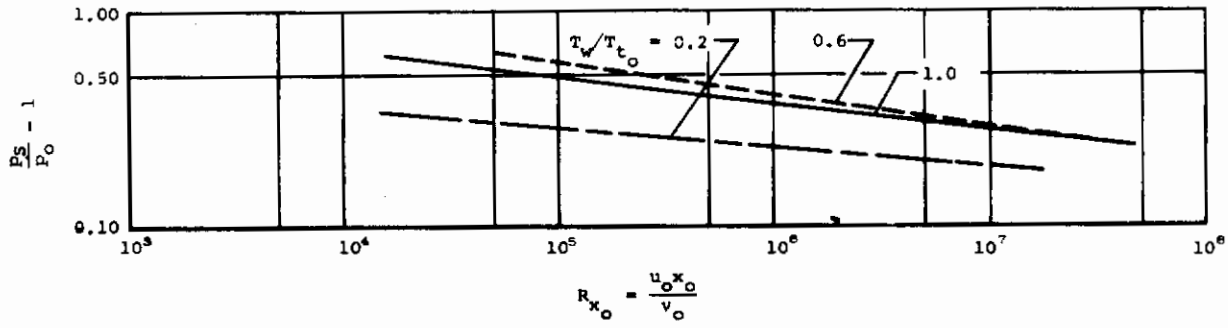

(c) Separation pressure for M_o = 10.0.

Figure 28.- Effect of Reynolds number and temperature ratio on separation pressure and plateau pressure.

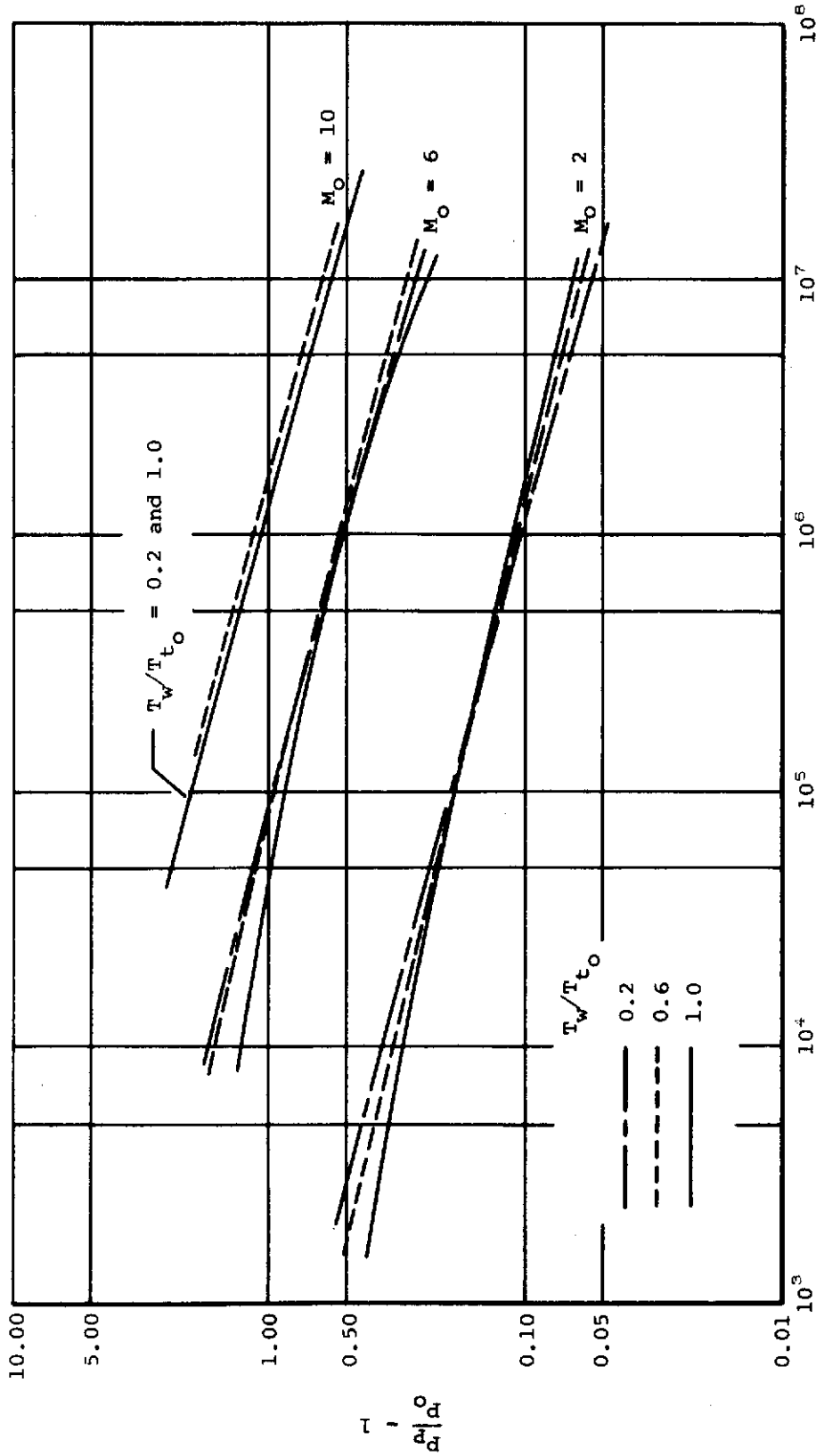

(d) Plateau pressures.

Figure 28.- Concluded.

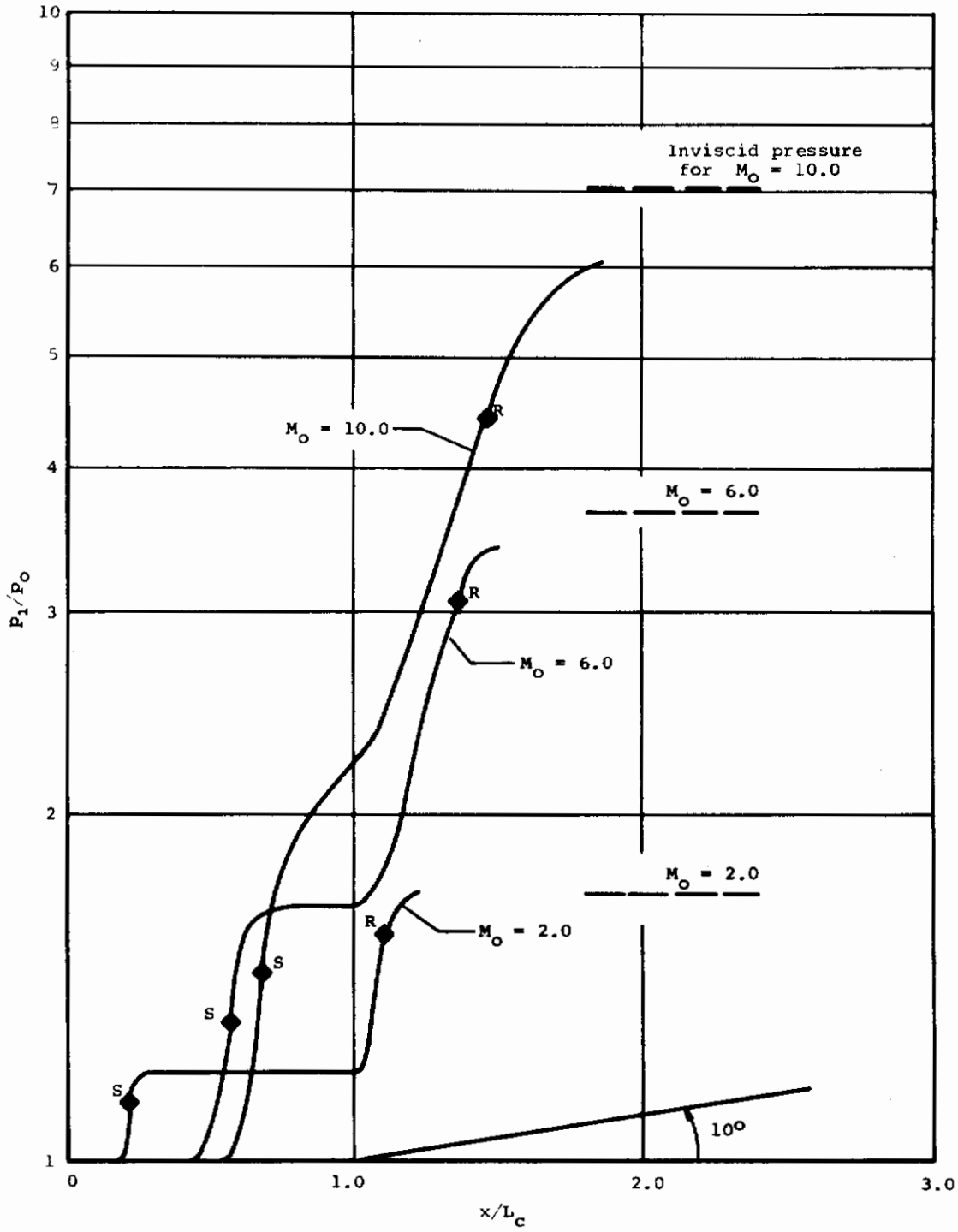

(a) Mach number effect. $\theta_w = 10^o$, $R_o = 10^6$, $T_w/T_{t_o} = 0.6$.

Figure 29.- Boundary-layer pressure distribution.

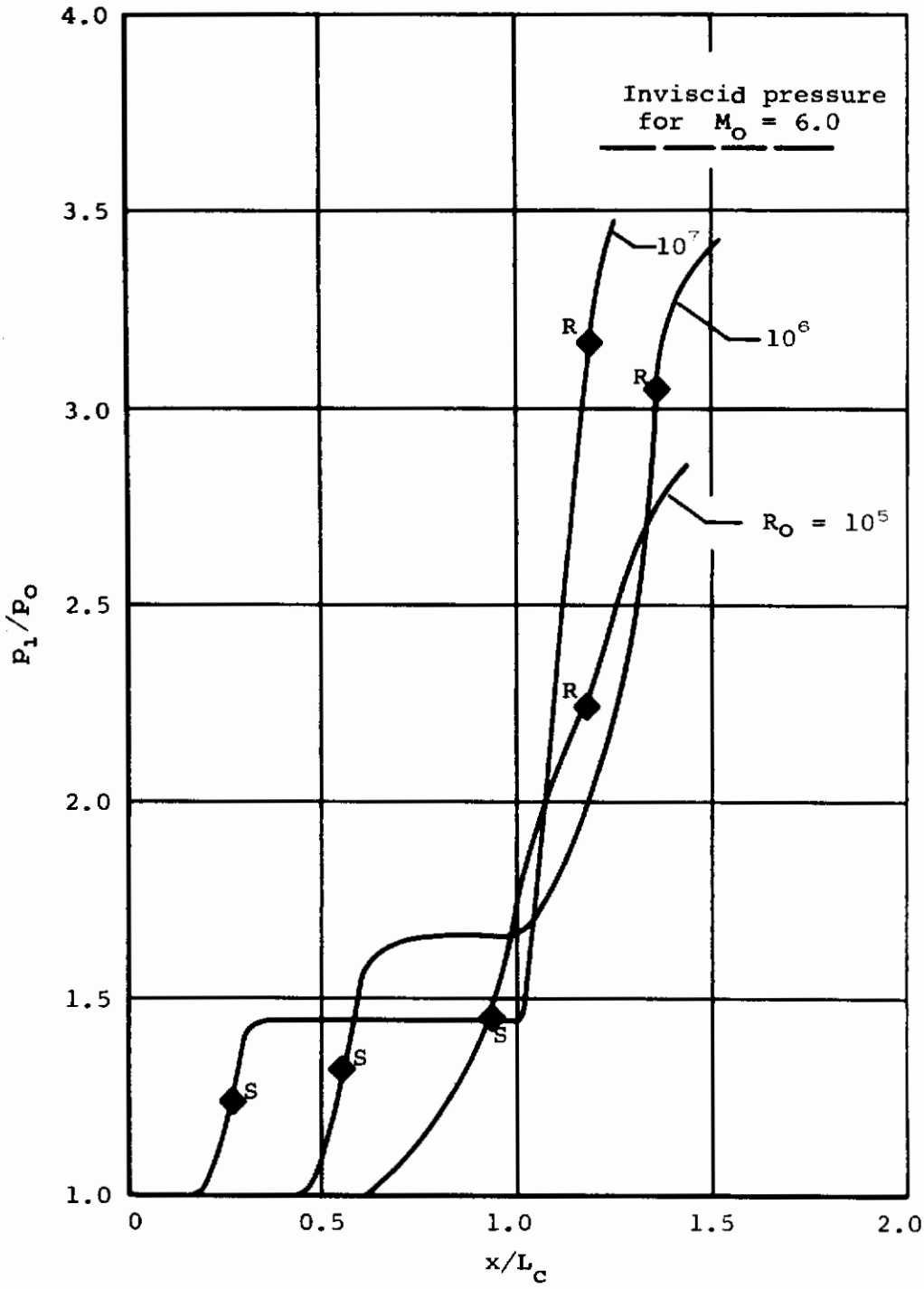

(b) Reynolds number effect. $\theta_w = 10^o$, $M_o = 6.0$, $T_w/T_{t_o} = 0.6$.

Figure 29.- Continued.

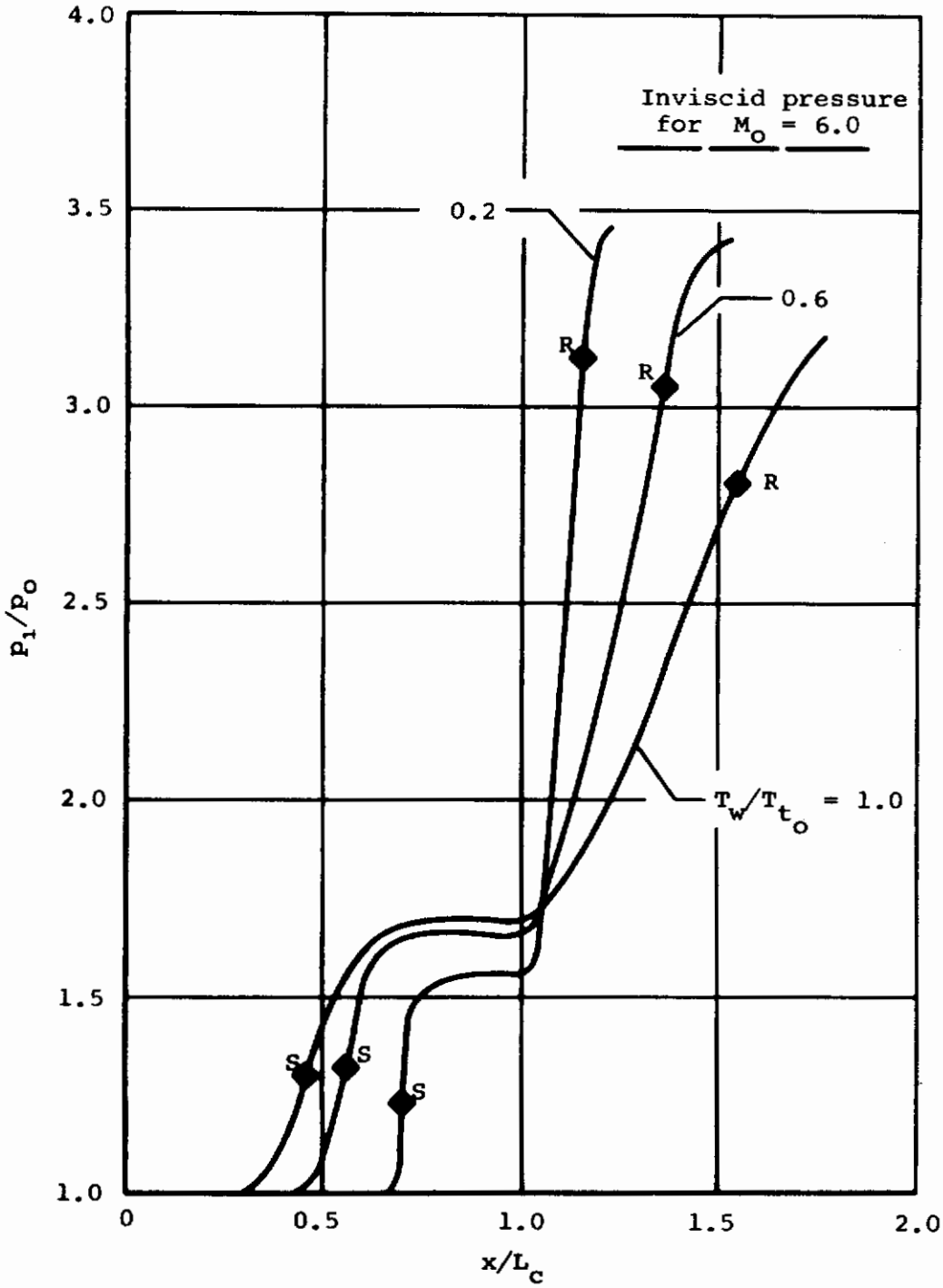

(c) Temperature ratio effect. $\theta_w = 10^o$, $M_o = 6.0$, $R_o = 10^6$.

Figure 29.- Concluded.

REFERENCES

1. Nielsen, J. N., Lynes, L. L., and Goodwin, F. K.: Calculation of Laminar Separation with Free Interaction by the Method of Integral Relations. Part I.- Two-Dimensional Supersonic Adiabatic Flows. Air Force Flight Dynamics Lab. Rep. AFFDL-TR-65-107, Oct. 1965.

2. Nielsen, J. N., Lynes, L. L., and Goodwin, F. K.: Calculation of Laminar Separation with Free Interaction by the Method of Integral Relations. Part II.- Two-Dimensional Supersonic Nonadiabatic Flow and Axisymmetric Supersonic Adiabatic and Nonadiabatic Flows. Air Force Flight Dynamics Lab. Rep. AFFDL-TR-65-107, Jan. 1966.

3. Nielsen, J. N., Lynes, L. L., and Goodwin, F. K.: "Theory of Laminar Separated Flows on Flared Surfaces Including Supersonic Flow with Heating and Cooling." AGARD Conf. Proc., no. 4, Part I, Proceedings of AGARD Fluid Dynamics Panel held in Rhode-Saint-Genése, Belgium, 10-13 May 1966.

4. Goodwin, F. K., Nielsen, J. N., and Lynes, L. L.: Inhibition of Flow Separation at High Speed. Vol. II - Calculation of Nonadiabatic Laminar Boundary Layers. Air Force Flight Dynamics Lab. Rep. AFFDL-TR-68-119, Vol. II, Oct. 1968.

5. Dorodnitsyn, A. A.: "General Method of Integral Relations and Its Application to Boundary-Layer Theory." Advances in Aero. Sci., vol. 3, von Kármán Ed., 1962.

6. Goodwin, F. K., Nielsen, J. N., and Lynes, L. L.: Recent Applications of the Method of Integral Relations to Laminar Boundary-Layer Problems. AIAA Paper No. 68-738, AIAA Fluid and Plasma Dynamics Conference, Los Angeles, Calif., June 24-26, 1968.

7. Reyhner, T. A. and Flügge-Lotz, I.: The Interaction of a Shock Wave with a Laminar Boundary Layer. Tech. Rep. No. 163, Div. of Eng. Mech., Stanford Univ., Stanford, Calif., Nov. 1966.

8. Lewis, J. E., Kubota, T., and Lees, L.: Experimental Investigation of a Supersonic Laminar, Two-Dimensional Boundary-Layer Separation in a Compression Corner With and Without Cooling. AIAA Paper No. 67-191, presented at AIAA 5th Aerospace Sciences Meeting, New York, N. Y., Jan. 23-26, 1967.

9. Ko, D. R. S., and Kubota, T.: Supersonic Laminar Boundary Layer Along a Two-Dimensional Adiabatic Curved Ramp. AIAA Paper No. 68-109, presented at AIAA 6th Aerospace Sciences Meeting, New York, N. Y., Jan. 22-24, 1968.

10. Kuehn, D. M.: Laminar Boundary Layer Separation Induced by Flares on Cylinders at Zero Angle of Attack. NASA TR R-146, 1962.

11. Becker, J. V., and Korycinski, P. F.: Heat Transfer and Pressure Distribution at a Mach number of 6.8 on Bodies with Conical Flares and Extensive Flow Separation. NASA TN D-1260, Apr. 1962.

12. Nielsen, J. N., Lynes, L. L., and Goodwin, F. K.: Inhibition of Flow Separation at High Speed. Vol. III - Experimental Results for Laminar Boundary Layers. Air Force Flight Dynamics Lab. Rep. AFFDL-TR-68-119, Vol. III, Sept. 1968.

13. Abbott, D. E., Holt, M., and Nielsen, J. N.: Investigation of Hypersonic Flow Separation and Its Effects on Aerodynamic Control Characteristics. ASD-TDR-62-963, Nov. 1962.

14. Bethel, H. E.: On the GKD Multi-Moment Method for Laminar Boundary Layers. Paper presented at the 10th Midwestern Mechanics Conference, Colorado State Univ., Aug. 21-23, 1967.

15. Lynes, L. L., Nielsen, J. N., and Kuhn, G. D.: Calculation of Compressible Turbulent Boundary Layers with Pressure Gradients and Heat Transfer. NASA CR-1303, Mar. 1969.

16. Klineberg, J. M. and Lees, L.: Theory of Laminar Viscous-Inviscid Interactions in Supersonic Flow. AIAA Paper No. 69-7, presented at AIAA 7th Aerospace Sciences Meeting, New York, N. Y., Jan. 20-22, 1969.

17. Needham, D. A. and Stollery, J. L.: Boundary Layer Separation in Hypersonic Flow. AIAA Paper No. 66-455, presented at AIAA 4th Aerospace Sciences Meeting, Los Angeles, Calif., June 27-29, 1966.

18. Chapman, D. R., Kuehn, D. M., and Larson, H. K.: Investigation of Separated Flows in Supersonic and Subsonic Streams with Emphasis on the Effect of Transition. NACA TN 3869, Mar. 1957.

UNCLASSIFIED
Security Classification

DOCUMENT CONTROL DATA - R & D
(Security classification of title, body of abstract and indexing annotation must be entered when the overall report is classified)

1. ORIGINATING ACTIVITY (Corporate author)	2a. REPORT SECURITY CLASSIFICATION
Nielsen Engineering & Research, Inc. 850 Maude Avenue Mountain View, California 94040	Unclassified
	2b. GROUP N/A

3. REPORT TITLE

Prediction of Supersonic Laminar Flow Separation by the Method of Integral Relations with Free Interaction

4. DESCRIPTIVE NOTES (Type of report and inclusive dates)

Technical Documentary Report - May 1968 to July 1969

5. AUTHOR(S) (First name, middle initial, last name)

Gary D. Kuhn, Frederick K. Goodwin, and Jack N. Nielsen

6. REPORT DATE	7a. TOTAL NO. OF PAGES	7b. NO. OF REFS
January 1970	100	18

8a. CONTRACT OR GRANT NO.	9a. ORIGINATOR'S REPORT NUMBER(S)
F33615-68-C-1499 b. PROJECT NO. 8219 c. Task No. 821902 d.	AFFDL-TR-69-87 9b. OTHER REPORT NO(S) (Any other numbers that may be assigned this report) NEAR Report TR 17

10. DISTRIBUTION STATEMENT

This document has been approved for public release and sale; its distribution is unlimited.

11. SUPPLEMENTARY NOTES	12. SPONSORING MILITARY ACTIVITY
None	Air Force Flight Dynamics Lab. Wright-Patterson Air Force Base, Ohio 45433

13. ABSTRACT

This report describes the development of a predictive method for calculating separated laminar boundary layers on flat-plate-wedge and cylinder-flare configurations in supersonic flow and the application of the method to predicting the effects of Mach number, Reynolds number, and temperature ratio on the properties of the boundary layer. The purpose of this report is to extend previous analytical work employing the method of integral relations to the region downstream of reattachment and to describe an iterative technique developed to produce a unique solution. The theory is shown to produce good comparisons with pressure data on flat-plate-wedge configurations for both adiabatic and cold walls. Accounting for non-Blasius initial velocity profiles produced by favorable pressure gradients upstream of the beginning of interaction was shown to decrease the predicted extent of separation. For axisymmetric configurations the length of an equivalent cylinder must be calculated by an auxiliary method. Good to fair comparisons with experimental pressure distributions were produced by adjusting the equivalent cylinder length. Fair comparison was produced between the theory and experimental heat-transfer rate data on an ogive-cylinder-flare configuration. The theory is shown to predict an incipient separation wedge angle which agrees reasonably well with experimental results.

DD FORM 1 NOV 68 1473 REPLACES DD FORM 1473, 1 JAN 64, WHICH IS OBSOLETE FOR ARMY USE.

UNCLASSIFIED
Security Classification

14. KEY WORDS	LINK A		LINK B		LINK C	
	ROLE	WT	ROLE	WT	ROLE	WT
Laminar Boundary Layer Separated Flow Supersonic Flow Aerodynamics Integral Relations Free Interaction						